



2013

STRUCTURAL AND FUNCTIONAL CHARACTERIZATION OF MULTIDRUG RESISTANCE TRANSPORTER AND REGULATOR

Linliang Yu

University of Kentucky, lyu4@g.uky.edu

[Right click to open a feedback form in a new tab to let us know how this document benefits you.](#)

Recommended Citation

Yu, Linliang, "STRUCTURAL AND FUNCTIONAL CHARACTERIZATION OF MULTIDRUG RESISTANCE TRANSPORTER AND REGULATOR" (2013). *Theses and Dissertations--Chemistry*. 19.
https://uknowledge.uky.edu/chemistry_etds/19

This Doctoral Dissertation is brought to you for free and open access by the Chemistry at UKnowledge. It has been accepted for inclusion in Theses and Dissertations--Chemistry by an authorized administrator of UKnowledge. For more information, please contact UKnowledge@lsv.uky.edu.

STUDENT AGREEMENT:

I represent that my thesis or dissertation and abstract are my original work. Proper attribution has been given to all outside sources. I understand that I am solely responsible for obtaining any needed copyright permissions. I have obtained and attached hereto needed written permission statements(s) from the owner(s) of each third-party copyrighted matter to be included in my work, allowing electronic distribution (if such use is not permitted by the fair use doctrine).

I hereby grant to The University of Kentucky and its agents the non-exclusive license to archive and make accessible my work in whole or in part in all forms of media, now or hereafter known. I agree that the document mentioned above may be made available immediately for worldwide access unless a preapproved embargo applies.

I retain all other ownership rights to the copyright of my work. I also retain the right to use in future works (such as articles or books) all or part of my work. I understand that I am free to register the copyright to my work.

REVIEW, APPROVAL AND ACCEPTANCE

The document mentioned above has been reviewed and accepted by the student's advisor, on behalf of the advisory committee, and by the Director of Graduate Studies (DGS), on behalf of the program; we verify that this is the final, approved version of the student's dissertation including all changes required by the advisory committee. The undersigned agree to abide by the statements above.

Linliang Yu, Student

Dr. Yinan Wei, Major Professor

Dr. John Anthony, Director of Graduate Studies

STRUCTURAL AND FUNCTIONAL CHARACTERIZATION OF MULTIDRUG
RESISTANCE TRANSPORTER AND REGULATOR

ABSTRACT OF DISSERTATION

A dissertation submitted in partial fulfillment of the
requirements for the degree of Doctor of Philosophy in the
College of Arts and Sciences
at the University of Kentucky

By
Linliang Yu

Lexington, Kentucky

Director: Dr. Yinan Wei, Department of Chemistry

Lexington, Kentucky

Copyright © Linliang Yu 2013

ABSTRACT OF DISSERTATION

STRUCTURAL AND FUNCTIONAL CHARACTERIZATION OF MULTIDRUG RESISTANCE TRANSPORTER AND REGULATOR

Drug resistant bacteria pathogen poses a severe threat to human health. Bacterial drug efflux pumps are transporter proteins involved in the export of antibiotics out of cells. Efflux by transporters is one of the major drug resistant mechanisms. Multidrug efflux pumps can transport multiple classes of antibiotics and are associated with bacteria multiple drug resistance (MDR). Overproduction of these pumps reduces susceptibility of bacteria to a variety of antibiotics. MDR regulators are cytoplasmic proteins that control the expression level of MDR transporters in response to the cellular concentration of antibiotics. This thesis research focuses on three main directions in the area of bacteria drug resistance: the structural and functional study of a MDR transporter, the characterization of a novel MDR regulator protein, and the development of a sensing method for the detection of glycopeptide antibiotics.

Acriflavine resistance protein B (AcrB) in *Escherichia coli* belongs to resistance nodulation division (RND) superfamily of efflux transporters. It plays an important role in conferring multidrug resistance in Gram-negative bacteria. The functional unit of AcrB is a trimer *in vivo*. However, the relationship between AcrB trimer stability and functionality remains elusive. In chapter 2, a residue that is critical for AcrB trimerization, Pro 223, was identified. The replacement of Pro 223 by other residues destabilized AcrB trimer, and thus decreased its activity. The loss of transport activity could be partially recovered when the AcrB trimer was stabilized by the introduction of a pair of inter-subunit disulfide bond. In chapter 3, a systematically alanine-scanning study of the producing loop (amino acid residues 211-240) was conducted. Five residues in the loop were found to be important for AcrB activity. These residues form a collar or belt in the loop close to the tip. These mutation studies revealed new insight into the conformation of the loop during AcrB trimerization. In chapter 4, residue Arg 780 was identified to be crucial for the pump function of AcrB. The study results indicated that Pro 223 serves as a “wedge” and Arg 780 as a “lock” via hydrogen bonding between the backbone carbonyl oxygen of Pro 223 and side chain

of Arg780. Similar as Pro 223, replacement of Arg 780 by other residues drastically decreased the activity of AcrB. Dissociation of the AcrB trimer also contributed to the decrease of activity. However, the introduction of inter-subunit disulfide bond could not restore the function of the mutant, indicating that Arg 780 plays multiples roles in the operation of AcrB.

In chapter 5, a MDR regulator ST1710 from the archaeon *Sulfolobus tokodaii*, homologous to the multiple-antibiotic resistance repressor (MarR) family bacterial regulators, was characterized *in vitro*. The binding affinities of ligands and double strand (ds) DNA for ST1710 were measured. The presence of substrates suppressed the interaction between ST1710 and dsDNA, which indicated that ST1710 functioned as a repressor *in vivo*.

Finally, in chapter 6, a direct fluorescence polarization based method for the detection of glycopeptide antibiotics is developed. Briefly, the acetylated tripeptide L-Lys-D-Ala-D-Ala was labeled with a fluorophore (fluorescein isothiocyanate or AlexaFluor 680) to create a peptide probe. The fluorescence polarization signal of the peptide probe increased upon binding with glycopeptide antibiotics in a concentration dependent manner. The detection is highly selective toward glycopeptide antibiotics. The designed method is expected it to have broad applications in both research and clinical settings.

KEY WORDS: MDR transporter, AcrB, oligomerization, MDR regulator, glycopeptide antibiotics

Linliang Yu

02-10-2013

STRUCTURAL AND FUNCTIONAL CHARACTERIZATION OF MULTIDRUG
RESISTANCE TRANSPORTER AND REGULATOR

by

Linliang Yu

Dr. Yinan Wei

Director of Dissertation

Dr. John Anthony

Director of Graduate Studies

May 2, 2013

Date

Dedicated to my beloved family

ACKNOWLEDGEMENTS

Working on a Ph.D. degree is a wonderful and overwhelming experience for my whole life. For the completion of my Ph.D. thesis, I really appreciate many people for their help those years.

First and foremost, I am deeply grateful to my advisor Dr Yinan Wei. Working with her is a greatly pleasure and excitement. She is always supportive, patient and encouraging throughout my Ph.D. study. Her office door is always open where we could discuss my ideas and thoughts. Her key insights guided me through the difficult research problems. Her nice nature of personality will set as an example for my life. Also, I admire her ability to balance research and personal life. Above all, she made me feel like a friend, which I appreciate from my heart.

Second, I would like to thank my committee member: Dr. Stephen Testa, Dr. Dongsheng Yang and Dr. Brian Rymond for insightful suggestions and comments.

Third, I would like to thank all the members of Yinan lab, both past and present: Dr Jun Fang, Dr Wei Lu, Meng Zhong, Brent Ferell, Geng Shen, Ye Cui, Qian Chai and Maria Wu. I had a pleasant time working with them.

Fourth, I would like to thank National Science Foundation for financial support (1158036) of my graduate research.

Last but not least, I appreciate my family for their support, trust and love especially for my wife—Xiaonan Mei. Her sacrifice, inspiration, and encouragement shaped me as a better man, husband and father.

Table of Contents

Chapter 1 Introduction	1
1.1 Oligomerization is Dominant Feature among Bacterial Membrane Protein.....	1
1.2 Biogenesis of Membrane Proteins	4
1.3 Function Roles of Helix Bundle Membrane Protein Oligomerization.....	9
1.4 Why Membrane Proteins Form Homo-oligomers.....	20
1.5 Major Multidrug Resistant Transporter Families.....	22
1.6 Introduction of AcrB	29
Chapter 2 An Invariable Residue P223 Is Critical for AcrB Stability and Function..	45
2.1 Introduction	45
2.2 Materials and Methods	47
2.3 Results	53
2.4 Discussion and Conclusion	67
Chapter 3 Alanine-Scanning Study of the Protruding Loop of AcrB.....	70
3.1 Introduction	70
3.2 Materials and Methods	72
3.3 Results	75
3.4 Discussions.....	83
Chapter 4 Role of R780 for the Stability and Functionality of AcrB	86
4.1. Introduction	86
4.2 Materials and Methods	88
4.3 Results	96
4.4 Discussion and Conclusion	113
Chapter 5 Characterization of Ligand Binding of a Putative Archaeal Regulator Protein ST1710	116

5.1 Introduction	116
5.2 Material and Methods.....	120
5.3 Results and Discussion.....	125
Chapter 6 Development of a Direct Fluorescence Polarization Assay for the Detection of Glycopeptide Antibiotics	144
6.1 Introduction	144
6.2 Materials and Methods	148
6.3 Results and Discussions	152
Reference.....	162
VITA.....	179

LISTS OF FIGURES

Figure 1.1 The statistical data about crystal structures of bacterial obligate homo-oligomeric α -helices bundles membrane proteins in the data bank	3
Figure 1.2 A biogenesis process of bacterial membrane protein	5
Figure 1.3 The oligomerization steps of globular proteins	7
Figure 1.4 Oligomer of ClC-ec	11
Figure 1.5 Oligomer of NhaA	13
Figure 1.6 Oligomer of BetP	15
Figure 1.7 Oligomer of GlpF	17
Figure 1.8 Oligomer of KcsA	19
Figure 1.9 Five major families of multi-drug resistant transporter	23
Figure 1.10 EmrD monomer	25
Figure 1.11 Two dimeric forms (parallel and antiparallel) of EmrE	26
Figure 1.12 Structure of Norm	27
Figure 1.13 Structure of Sav 1866	28
Figure 1.14 The surface structures of AcrA, AcrB and TolC and their locations in the cell	30
Figure 1.15 Selected substrates of AcrAB-TolC efflux system	31
Figure 1.16 Structure of AcrB	32
Figure 1.17 Rotation mechanism of AcrB	34
Figure 1.18 The proposed drug pathways	37
Figure 1.19 Phenylalanines cluster region of binding pocket	38
Figure 2.1 Subunit interaction of AcrB	46
Figure 2.2 Sequence alignments of loop region of AcrB homologues	53

Figure 2.3 Crystal structure of AcrB.....	54
Figure 2.4 Comparison of the expression levels of wild type AcrB and AcrB _{P223G} ...	57
Figure 2.5 Circular Dichroism (CD) characterization of wild type and the mutant ..	59
Figure 2.6 Limited trypsin digestion of purified wild type AcrB (A) and AcrB _{P223G} (B)	60
Figure 2.7 The disulfide trapping method.....	62
Figure 2.8 BN-PAGE and western-blot analysis of AcrB _{P223G/A225C/V777C}	65
Figure 3.1 The structure and amino acid composition of loop	71
Figure 3.2 The strategy to construct chimeric AMA gene using overlapping PCR ...	73
Figure 3.3 Expression levels of loop mutants and BN-PAGE analysis of AcrB _{L230A}	79
Figure 3.4 Structural characterization of AMA	82
Figure 4.1 The proposed binding pocket of P223.....	95
Figure 4.2 Comparison of the expression levels of wild type AcrB and the other mutants.....	97
Figure 4.3 Real-time measurement of ethidium bromide accumulation for the intact BW25113 Δ acrB with different AcrB mutant	100
Figure 4.4 Circular Dichroism (CD) characterization of wild type and the mutant	101
Figure 4.5 Disulfide trapping analysis of AcrB tertiary structure	102
Figure 4.6 Quaternary structure analysis of the mutant AcrB _{R780A}	104
Figure 4.7 Cross-linking characterization of the AcrB _{R780A/V225C/A777C}	104
Figure 4.8 Fluorescent substrate labeling assay.....	107
Figure 4.9 <i>In vivo</i> chemical cross-linking of the AcrAB-TolC efflux pump.....	109
Figure 4.10 The view of direct interaction between AcrB and TolC.....	111
Figure 4.11 <i>In vivo</i> disulfide cross-linking between AcrB and TolC	112
Figure 4.12 The overlook picture of asymmetric AcrB.....	115

Figure 5.1 Structure of ST1710 and its ligands.	119
Figure 5.2 Binding of ethidium with ST1710.	126
Figure 5.3 Circular Dichroism characterization of ST1710.	127
Figure 5.4 Circular Dichroism characterization of ST1710 conformation change...	130
Figure 5.5 Effect of ethidium binding on the Trp fluorescence emission	131
Figure 5.6 Binding study of CCCP and ST1710 with CD spectroscopy	135
Figure 5.7 Effect of temperature on the binding between ST1710 and ST1	139
Figure 5.8 Effects of small molecule ligands salicylate (A), CCCP (B) and Tyr (C) on ST1710-DNA binding.....	141
Figure 6.1 The mechanism of fluorescence polarization immunoassay	145
Figure 6.2 Calibration curves of two different peptide probes (FITC-peptide-diamond and AF680-peptide-squares) with vancomycin, teicoplanin, and telavancin in PBS buffer.....	155
Figure 6.3 The free fluorephores do not interact with vancomycin and teicoplanin	156
Figure 6.4 Selectivity of the assay	158
Figure 6.5 Calibration curves of detection for vancomycin, teicoplanin and telavancin in FBS	159

LIST OF TABLES

Table 2.1 MIC of BW25113 Δ <i>acrB</i> containing plasmid encoding the indicated AcrB constructs.	56
Table 2.2 MIC of BW25113 Δ <i>acrB</i> containing plasmid encoded AcrB measured in the presence or absence of DTT.	66
Table 3.1 Drug resistance of BW25113 Δ <i>acrB</i> expressing plasmids and mutations... ..	77
Table 3.2 The surface area of residues in the loop, the calculated area is based on the server (PDBePISA)	85
Table 4.1 Drug resistance of BW25113 Δ <i>acrB</i> expressing plasmids and mutations.	98
Table 5.1 Fitting parameters of binding property between ST1710 and its ligands.	136
Table 6.1 Fitting parameters of labeled peptide and drug interaction	153
Table 6.2 The recovery of teicoplanin with designed method and commercial kit.. ..	160

Chapter 1 Introduction

1.1 Oligomerization is a Dominant Feature of Bacterial Membrane Protein

A genome-wide analysis shows that 20-30% of all genes code for membrane protein both in prokaryotic and eukaryotic organisms.¹ As for *Escherichia coli*, about 20-30% of its proteome are inner-membrane proteins and about 2% are outer membrane proteins.^{2, 3}

Membrane proteins contain trans-membrane domains that are embedded in a lipid bilayer and extra-membrane regions exposed to an aqueous environment. They facilitate communication across cellular membrane, and are essential for cellular function.

Based on the structure, membrane proteins can be categorized into two general classes: α -helix bundles and β -barrels. Most bacterial outer membrane proteins are β -barrels. Compared with α -helix bundles, β -barrels are less common. Recently, Meng et al. have summarized the latest studies on oligomerization of bacterial outer membrane proteins.⁴ Therefore, outer-membrane proteins would not be discussed in my thesis.

The inherent difficulty of expression and purification of membrane proteins has been an obstacle for studies of those crucial components. However, in the past decade, with the efforts of many research groups and novel crystallization methodology, more and more high-resolution crystal structures of membrane protein were reported. The availability of an increasing number of protein structures has made it possible to study those critical cellular players from a structure-based view. Oligomerization is a general feature of membrane proteins whose structures are known. Oligomers containing the multi-copies of the same or different subunits are called homo or hetero-oligomers. Statistically, more than half of proteins exist as dimers or higher-order oligomers either in prokaryotes or

eukaryotes and homo-oligomers appear more frequent than hetero-oligomers.⁵ The oligomeric state of α -helix membrane protein is summarized in the figure 1.1 for all bacterial membrane proteins with known structures (<http://blanco.biomol.uci.edu/mpstruc/listAll/list>). As of October of 2012, there are about 95 unique crystal structures of bacterial homo-oligomeric α -helices bundles membrane proteins in the data bank. Out of these proteins (Figure 1.1), 22 structures are monomers, 27 dimers, 19 trimers, 12 tetramers, 10 pentamers, 1 hexamer, 1 heptamer, 1 octomer, 1 decamer, and 1 dodecamer. Dimeric state occurs more frequent than other oligomeric state. Oligomer state containing more than 6 subunits was much less prevalent. These statistics from crystal structures further emphasized the importance of oligomerization for membrane proteins.

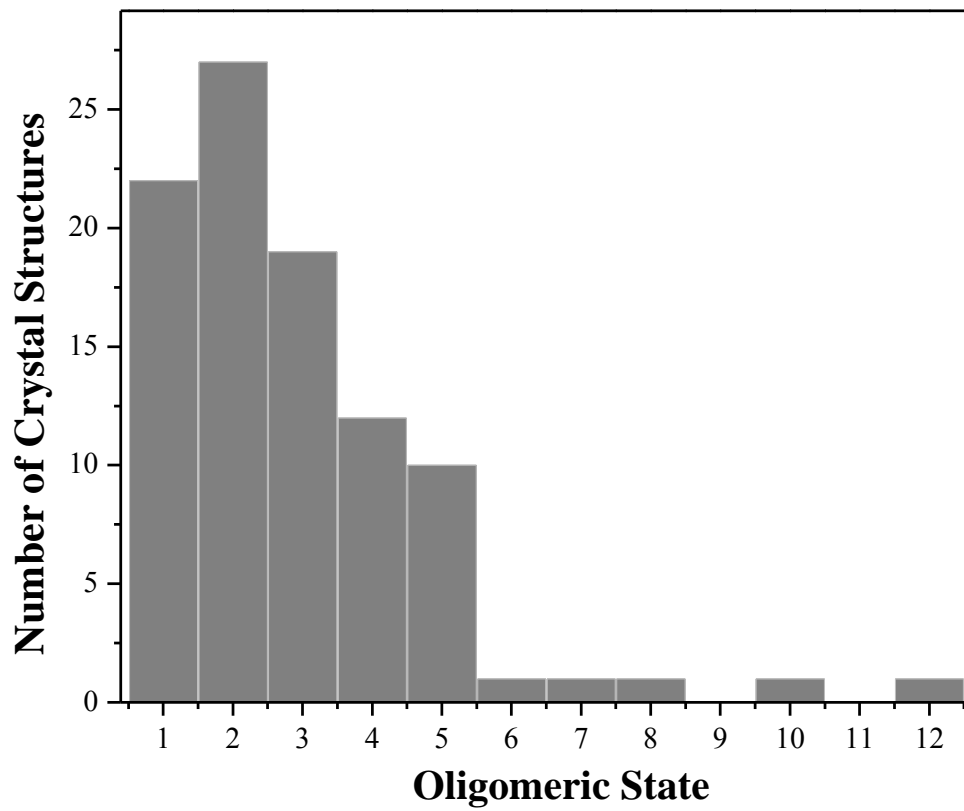


Figure 1.1 Oligomeric state of crystal structures of bacterial homo-oligomeric α -helices bundles membrane proteins in the data bank. Only a small percentage of membrane proteins exist as monomers.

1.2 Biogenesis of Membrane Proteins

Synthesis of membrane protein is more complicated than soluble proteins. Understanding of membrane protein biogenesis is crucial for the study of their oligomerization process. An important step of membrane protein biogenesis is insertion of the nascent polypeptide chains from the ribosome into the membrane. There are three biochemical steps for bacterial membrane protein insertion (Figure 1.2): the nascent polypeptide targeted to the membrane, the co-translational lateral insertion of the apolar region of polypeptide into the membrane, and membrane protein folding.

In step 1, the translation of bacterial membrane protein is initiated in the cytoplasm. The first hydrophobic region of the nascent chain emerges from the ribosome exit tunnel and binds to a signal recognition particle (SRP), which guides the entire complex (the nascent membrane-ribosome-mRNA) to the SRP receptor located on the surface of the membrane.⁶ In *Escherichia coli*, SRP is composed of SRP54 ortholog (Ffh) and small RNA (4.5S RNA). It binds to the exit site of the ribosome when the hydrophobic signal sequence of membrane protein emerges.⁷ The SRP receptor (FtsY) is anchored in membrane and also associated with the SecYEG translocase. The interaction between SRP and FtsY is driven by the hydrolysis of GTP, leading to the releases of the SPR and insertion of the nascent membrane protein forward to Sec translocase. The dissociated SRP was recycled for another round of membrane targeting.⁸⁻¹⁰

In step 2, the protein membrane insertion is facilitated by the Sec translocase. The Sec translocase is made of a core component-SecYEG translocon, SecDF complex and SecA ATPase. SecYEG is an integral membrane heterotrimeric complex and provides a conduction pore through which the newly synthesized membrane protein enters into the

membrane.^{11, 12} SecDF is another membrane-integrated complex. It associates with Sec YEG and makes membrane protein translocation and insertion more efficient.^{13, 14} SecA functions as a molecular motor for the translocation process. The hydrolysis of ATP by SecA mediates the inserting of the polypeptide through the Sec YEG channel.^{15, 16} For a small selection of proteins, YidC insertase plays an important role for membrane insertion in a Sec-dependent or Sec-independent manner.^{17, 18}

In step 3, the inserted polypeptide folds and assembles into functional unit or complex. A two-stage model for membrane protein folding has been proposed by Popot and Engelman.¹⁹ The model simplifies the α -helix membrane protein folding into two distinguished stages. In the first stage, transmembrane helices form independently; in the second stage, transmembrane helices interact with each other to form the higher order of interaction. The tertiary and quaternary structures are built on the second stage.

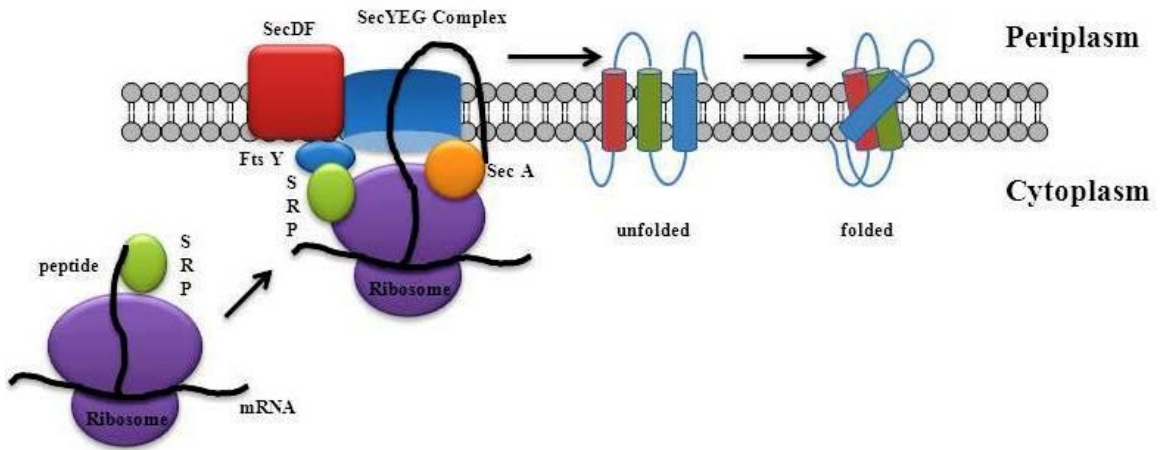


Figure 1.2 A biogenesis process of bacterial membrane protein.

The three steps are essential for the biogenesis of membrane proteins. However, it is still elusive how membrane proteins form quaternary structures in the plasma membrane of a cell. Several models have been proposed through the studies of assemblies of hetero-oligomeric membrane protein complexes. In one model, the assemblies of hetero-oligomeric membrane proteins are sequential. Each subunit of the complex interacts in an ordered manner to form intermediates, and then is organized into a functional complex. For example, Green and Claudio studied the assembly of the acetylcholine receptor, and found that the folding and assembly of the hetero-pentameric $\alpha_2\beta\gamma\delta$ complex are sequential.²⁰ The intermediate trimer $\alpha\beta\gamma$ forms first, followed the second intermediate $\alpha\beta\gamma\delta$ tetramer and finally the $\alpha_2\beta\gamma\delta$ pentamer. During the process, several subunits folding occur during or between these oligomerization steps and contributed to subunit recognition site formation during assembly. In the other model, the subunit assembly is not sequential. There are no specific intermediate complexes formed during the process. For example, *Escherichia coli* maltose transporter complex MalFGK₂, is composed of two membrane subunits MalF and MalG, and a dimer MalK₂ in the cytoplasm for ATP-binding. First, the MalK forms a dimer in the absence of MalF and MalG.²¹ The MalF or MalG is synthesized, inserted into the membrane and folded independently.²² The isolation of stable complexes-MalFG, MalFK₂, and MalGK₂ indicated that the formation of tetrameric complex MalFGK₂ are not necessarily sequential.²³

It is a different story in the case of obligate homo-oligomers. Obligate oligomers exist and function predominantly in one specific aggregation state. No monomeric or intermediate oligomeric states can be isolated from the cell membrane. Studies of homo-oligomeric soluble proteins reveal that oligomerization may occur via a two-step or a

three-step pathway (Figure 1.3).²⁴ In the two-step pathway, individual monomers remain largely unfolded prior to oligomerization and there is no well-folded monomer as an intermediate. Folding and oligomerization occur simultaneously. In the three-step pathway, individual monomers first fold independently into a structure that may or may not be the same as the final structure in the complex, which then assemble into an oligomer.

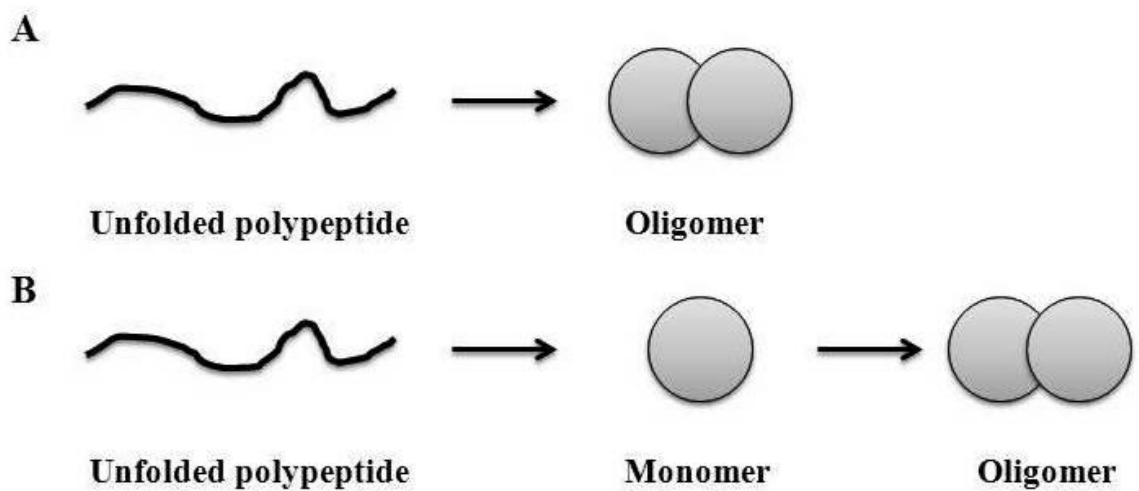


Figure 1.3 Protein oligomerization process. A. Subunit folding is coupled with oligomerization. B. Subunit folding precedes oligomerization.

Study of membrane protein oligomerization is a challenging task. The expression level of membrane proteins is usually much lower than the expression level of soluble proteins, limiting the quantity and quality of protein samples that could be obtained for analysis. In addition, purification of membrane protein involves the extraction of the protein from cell membrane using detergent, which could dissociate membrane protein oligomers. Another obstacle is the scarcity of suitable experimental techniques. Structures obtained via x-ray

crystallography do not always faithfully reflect the biologically relevant quaternary structure. And membrane proteins of the same family in different species may have different oligomeric state. For example, the tetracycline transporter TetA from *Escherichia coli* is a trimer,²⁵ while a related tetracycline transporter TetL from *Bacillus subtilis* is a dimer.²⁶ In addition to x-ray crystallography, the combinations of other methods including chemical cross-linking, 2D-electron microscopy, analytical ultracentrifugation, blue-native PAGE, and electron spin resonance (EPR) have been used to determine the oligomeric state of membrane proteins.²⁷ Most of these methods need purified protein samples dissolved in detergent micelles, which may not reflect the actual oligomeric state of the protein in cell membrane. More recently, methods that reveal the oligomeric state of proteins in lipid bilayer or even *in vivo* are emerging, including steric trap, fluorescence resonance energy transfer (FRET), TOXCAT, and GALLEX.²⁸⁻³¹ Finally, obtaining of the monomeric form of an otherwise stable oligomer without affecting the tertiary folding is also challenging. Despite of these difficulties, the assembly process and functional role of oligomerization have been investigated for several α -helical membrane proteins.

1.3 Function Roles of Helix Bundle Membrane Protein Oligomerization

1.3.1 Chloride Channel

Chloride channels (ClC) play important roles in many cellular functions including the regulation of cellular excitability, cell volume, transepithelial transport, and acidification of intracellular organelles.³² In mammals, there are nine known ClCs distributed in different tissues. Clinical studies have shown that mutations of ClC channels are correlated with many human inherited diseases.³³ ClC genes have also been identified in prokaryotic cells. Based on the mechanism of its function, ClC family proteins could be categorized into two subclasses--ion channels and exchange transporters.³⁴ In ion channels, free chloride ion could diffuse through the center pore down the electrochemical gradient. In exchange transporters, the proton gradient across the cell membrane is exploited by the protein to move chloride against its electrochemical gradient. Both channels and transporters share similar structure organization.

The sequence conservation among ClC family proteins is low, but their structural architectures are similar. Compared with eukaryotic ClCs, the bacterial homologues lack the large C-terminal domain but maintain the minimal functional unit of a ClC protein. The ClC transporter from *Escherichia coli* (ClC-ec) has been purified and reconstituted into lipid bilayers.^{35, 36} The projection structure of ClC-ec has been obtained from cryo-electron microscopy in 2001, which reveals a dimeric complex.³⁶ The first crystal structure of the chloride channel from *S. typhimurium* (ClC-st) and *Escherichia coli* (ClC-ec) were reported by Raimund et al. shortly after.³⁷ The structure of ClC-ec is essentially the same as that of the ClC-st, although their primary sequences only have 20% similarity. Each subunit of ClC-ec contains 18-helices and crosses the membrane with a

titled angle (Figure 1.4A). Each subunit contains its own chloride binding site and ion translocation pathway. The dimer interface is approximately 1200 Å². Interaction between Leu and Ile side chains is the major stabilizing force for dimerization. No hydrogen bond or salt bridge has been observed at the dimer interface.

In an effort to create CIC monomers, Robertson et al. developed a “warts and hooks” strategy to destabilize the dimeric structure.³⁸ They introduced Trp mutations on the subunit interface near the position of the lipid head groups. Trp is usually found at the extracellular or intracellular ends of transmembrane α -helices, and therefore has been assumed to serve as floats to anchor the helices into the membrane. By replacing Leu and Ile with Trp, the authors expected to disrupt the dimer structure while stabilize the resultant monomer. Among the mutants created, a double mutant (I201W/I422W, denoted as WW), completely dissociated into monomer (Figure 1.4B). WW is partially functional. The Cl⁻/H⁺ exchange stoichiometry of transport conducted by WW is the same as that conducted by the wild type protein, while the Cl⁻ efflux rate of WW reduces to half of the wild type level. The crystal structure of WW mutant has been obtained, which is very similar to the structure of individual subunit in a WT dimer.

Mutations in CIC at the dimer interface lead to several diseases. To date, 148 CIC-5 mutations have been reported in patients with Dent’s disease.³⁹ The majority of these mutations have been located at the dimer interface.⁴⁰ Effects of these mutations include defective or delayed protein processing and decreased stability of the mature protein.⁴¹ Interestingly, several mutations without apparent defect in processing or stability lead to altered chloride conduction. Although the quaternary structure of these mutants CIC-5 is

unknown, it is tempting to speculate that the mutation could have led to dimer dissociation and affected channel regulation. Similarly, many of mutations that alter the function of ClC-1 have been located to the dimer interface, which lead to a dramatic shift in the voltage dependence of channel activation.⁴² Mutations introduced at the subunit interface in ClC-0 also lead to altered gating.⁴³

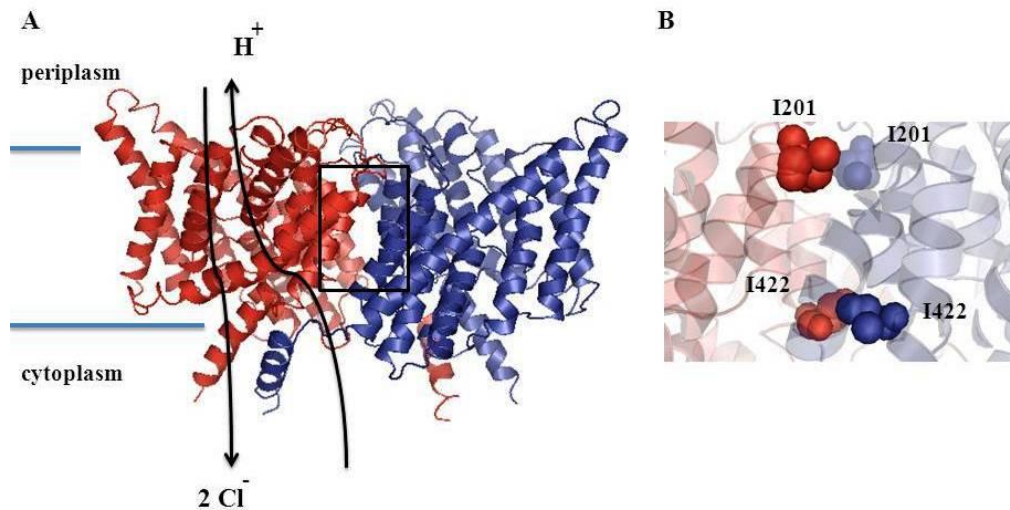


Figure 1.4 A. Structure of ClC-ec dimer (Protein Data Bank ID 1KPK).³⁷ B. Zoom in view of the dimer interface of ClC-ec (box in A) with residues I201 and I422 highlighted. The structure was generated using PYMOL.

1.3.2 Na⁺/H⁺ Channel

Na⁺/H⁺ channels are a large family of integral membrane proteins which allow the diffusion of monovalent cations H⁺ and Na⁺ across biological membranes. They regulate the intracellular pH, Na⁺ concentration, and volume of cells.⁴⁴ Two subfamilies of Na⁺/H⁺ channel, NHE (Na⁺-H⁺ exchanger) and NHA (Na⁺-H⁺ antiporter), spread widely in all kingdoms of life, ranging from bacterial to human cells. In mammalian cells, NHE family

has nine isoforms (NHE1-9) presenting in different tissues.⁴⁵ Among them, NHE1 is the most widely expressed in the cytoplasmic membrane. It exchanges an intracellular H^+ for an extracellular Na^+ to control intracellular pH. Dysfunction of NHE1 has been associated with health issues including cancer, heart failure, and kidney disease.⁴⁴ In plant cells, the deletion of Na^+/H^+ antiporter gene decreases the plant's salt tolerance while over-expression of these transporters yields salt resistant plants.⁴⁶ In bacteria, function of the Na^+/H^+ antiporters is critical for their growth at alkaline pH and high salt condition.⁴⁷

Escherichia coli NhaA is the most extensively studied protein in this family. The activity of NhaA is pH dependent. It has maximum activity at pH 8.5 and no activity at pH 6.5. It plays an essential role for the homeostasis of Na^+ and H^+ in *Escherichia coli*. The crystal structure of NhaA at pH 4.0 was obtained in 2005.⁴⁸ The protein contains 12 transmembrane helices, with both N and C-termini facing the periplasm (Figure 1.5A). NhaA exists as a monomer in the crystal. However, several other studies of NhaA in 2D crystals and reconstituted proteoliposomes indicate that NhaA is a dimer.⁴⁹⁻⁵¹ Finally, a high-resolution structure of NhaA dimer is obtained through an electron paramagnetic resonance study, which reveals two points of contact between two subunits in a dimer (Figure 1.5B).⁵² NhaA contains a double-stranded β hairpin loop close to the level of lipid bilayer head groups at the periplasmic side, far away from the active site. The deletion of the β -hairpin leads to a monomeric mutant $\Delta P45-N58$.⁵³ When reconstituted in proteoliposomes, the $\Delta P45-N58$ mutant and the wild type NhaA have similar transport activity and response to pH regulation, which indicates that monomeric NhaA is the functional unit. Defect in the function of the monomeric mutant was only apparent under

the extreme stress condition, at which point the growth of the cells with monomeric NhaA is greatly reduced while the cells containing wild type dimeric NhaA is not affected. Furthermore, apparent K_m for Na^+ of $\Delta(\text{P45-N58})$ increased 50-fold as compared with the wild type protein, indicating that the affinity of a monomer to the substrate is much weaker.⁵⁴ Dimerization has been shown to greatly improve the thermostability of NhaA as compared to that of the monomer, suggesting that the increased stability might play certain roles in the observed functional difference between monomer and dimer under extreme stress conditions.

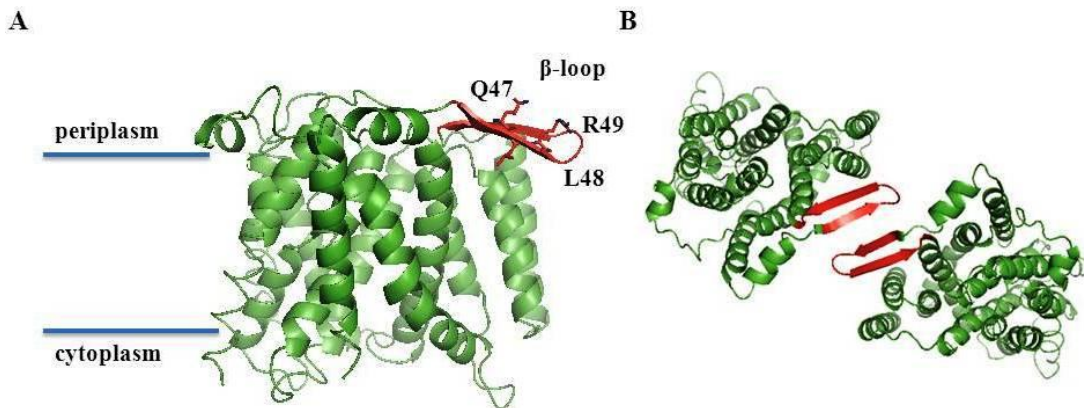


Figure 1.5 A. Structure of NhaA monomer (Protein Data Bank ID 1ZCD).⁴⁸ The β loop and residues critical for dimerization are shown in red. B. Structure of dimeric NhaA. The structure was generated using PYMOL.

Additional cysteine-scanning study of the β -hairpin revealed a stretch of three residues, Q47, L48, and R49, to be critical for the dimerization of NhaA.⁵⁴ Similarly, a cysteine-scanning study of the β -hairpin has also been conducted on NhaA from *Helicobacter pylori*.⁵⁵ The mutant Q58C in the β hairpin loop forms an intermolecular disulfide bond, which is expected to stabilize the dimer and increase the activity. However, the Q58C

mutant is nonfunctional under a non-reducing condition, and the activity can be restored under a reducing condition. This observation suggests that a flexible association between the two subunits in a dimer is necessary for NhaA to function.

1.3.3 Osmoregulated Transporters

Osmolytes are a class of highly polar organic compounds ubiquitously used by living organisms to maintain cell volume and fluid balance.⁵⁶ Osmolytes also stabilize intracellular proteins against denaturation.⁵⁷ Common osmolytes include betaine, taurine, sarcosine, and trimethylglycine. Among them, betaine is widely used for osmoregulation in bacteria, plant, and human cells. Many organisms can not synthesize osmolytes. Instead, they express highly efficient transporters to import osmolytes from the extracellular environment. The osmoregulated betaine transporter BetP from *Corynebacterium glutamicum* is a well-characterized model protein to investigate the osmolytes transport across cell membrane. Coupled with two Na⁺ ions, one molecule of betaine is specifically imported by BetP. BetP is activated specifically by a change of internal K⁺ concentration.

The first BetP crystal structure has been reported by Ressler et al.⁵⁸ It exists as a symmetric trimer, with twelve transmembrane helices and a curved helix 7 along the periplasm membrane surfaces (Figure 1.6A). The C-terminal domain of BetP contains a long α -helix, which acts as a sensor for the cytoplasmic K⁺ concentration and regulates the uptake of betaine. The interface of subunit interaction is composed of the transmembrane helix 2 and the amphipathic helix 7 on the periplasmic side. In a later study, BetP has been showed to exist as an asymmetric trimer in 2D crystals, suggesting a coupling interaction

between protomers in a trimer.⁵⁹ More recently BetP has been crystallized as asymmetric trimers in two different conformations, which reveals three distinct transport states.⁶⁰

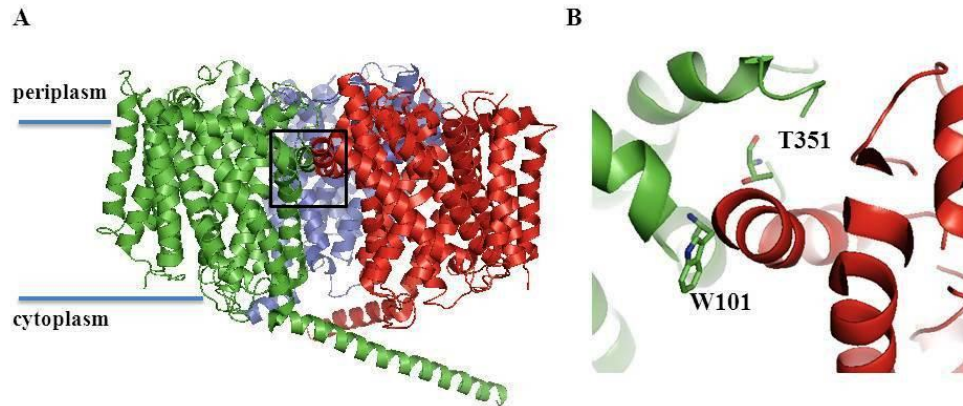


Figure 1.6 Oligomer of BetP. A. BetP trimer (Protein Data Bank ID 2W8A).⁵⁶ B. Zoom in picture of important interface residue W101 and T351. The structure was generated using PYMOL.

To probe the functional importance of trimerization, Camilo et al. created a well-folded monomeric BetP. The *in silico* alanine scanning has been used as a prediction method to investigate the association energy contributed from each residue on the subunits interfaces.⁶² Two residues were identified as making critical contributions to inter-subunit interaction, T351 and W101. T351 locates in transmembrane helix 7 and contributes to multiple hydrogen bonds and van der Waals interactions with residues from the neighboring subunit. W101 in transmembrane helix 2 makes hydrophobic contacts with residues in helix 7 from the adjacent subunit (Figure 1.6B). When mutated individually, both T351A and W101A are mostly trimers. However, the double mutation T351A/W101A drastically disrupts the trimerization of BetP. This monomeric mutant has similar apparent K_m as the wild type BetP and retains the ability to accumulate betaine.

However, it is no longer regulated, behaving similarly as a trimer formed from truncated BetP monomers lacking the C-terminal sensing domain.

1.3.4 Aquaglyceroporin

Aquaporins are a family of membrane proteins that regulate the flow of water across the cell membrane.⁶³ Aquaporins found in bacterial, plant and human are genetically conserved and structurally similar. Aquaglyceroporin are a subfamily of aquaporins that regulate the flow of glycerol, water and small uncharged organic molecules. Aquaglyceroporins-glycerol facilitator (GlpF) from *Escherichia coli* is an extensively studied example in this family. GlpF conducts urea, glycine, DL-glyceraldehyde and several other linear carbohydrates, but not cyclized carbohydrates. The first crystal structure of GlpF was determined by Fu et al.⁶⁴ It crystallized as a tetramer, with three glycerol molecules bound to each subunit (Figure 1.7A). Each subunit folds into an α -helical bundle, with a central channel surrounded by six transmembrane helices and two half-spanning helices. Two Mg^{2+} ions were identified in the center of the tetramer interface close to the periplasmic side. The coordination shell of Mg^{2+} includes water and residues E42 and W43 (Figure 1.7B).

Cymer and Schneider speculated that E42 or W43 were involved in the tetramerization of GlpF and created mutants in which E42 or W43 were replaced by different amino acids.⁶⁵ The oligomerization propensity of wild type and the mutated GlpFs were measured using an *in vivo* GALLEX assay developed by the Engelman group.³¹ The GALLEX assay couples the target protein oligomerization with a decrease of protein expression from the reporter gene (*lacZ*). The β -galactosidase activity is used as readout

of oligomerization propensity. With this method, Cymer and Schneider found that mutation of W43 had little effect on GlpF oligomerization.⁶⁵ However, the replacement of E42 with Ala, Thr, or Cys greatly reduces the tetramer propensity. Compared with wild type GlpF, the mutant GlpF_{E43A} has decreased transport activity and is degraded much faster in cell. Tetrameric GlpF is more active and stable *in vivo*. The authors suggest that cations such as Mg²⁺ coordinate with GlpF *in vivo* to stabilize the tetramer. Later *in vitro* studies revealed that the unfolding of tetrameric GlpF followed two stages: tetrameric GlpF first dissociated into dimeric units, followed by the dissociation into monomers.⁶⁶ These results suggest that dimer is an intermediate state in the process of GlpF tetramerization *in vivo*.

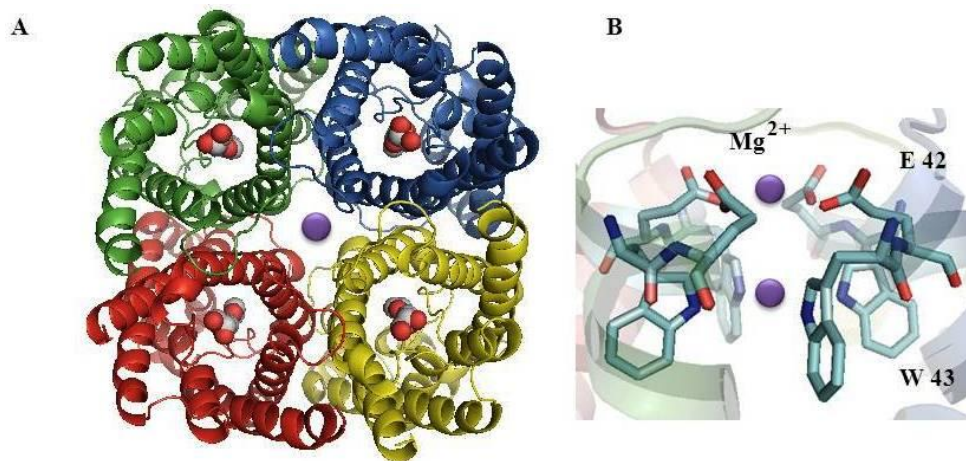


Figure 1.7 A. Structure of GlpF tetramer with glycerol bound. (Protein Data Bank ID 1FX8).⁶⁴ B. The zoom in picture of interface residues E42 and W43 coordinated with a magnesium cation. The structure was generated using PYMOL.

1.3.5 Potassium Channel

Potassium channels conduct the flow of K^+ with high specificity.⁶⁷ Much insight of the structure and function of this family protein has been obtained from studies on a bacterial potassium channel—KcsA from *Streptomyces lividans*. A truncated version of KcsA, with the fragments at the N-terminus (the first 22 residues) and C-terminus (the last 30 residues) removed, has been crystallized in the presence of 150 mM K^+ at pH 7.5.⁶⁸ Later EPR studies reveal that the C-terminal and N-terminal fragments form a bundle of α -helices in the cytoplasm.⁶⁹ KcsA is a tetramer and each subunit contains two transmembrane helices (Figure 1.8). The sequence connecting the two transmembrane helices is named P-loop, which forms the selection filter. The motif sequence TVGYG in the P-loop adopts an extended conformation and their backbone oxygen atoms face toward the pore center. K^+ ion is coordinated by these oxygen atoms while passing through the channel. The structure suggests that the coordination of potassium ion by the cation-oxygen interactions may contribute to the tetramer stability.

Krishnan et al. measured the effect of different cations on the thermal stability of KcsA tetramer using sodium dodecyl sulfate-polyacrylamide gel electrophoresis (SDS-PAGE).⁷⁰ The presence of substrate K^+ improves the thermal stability of KcsA tetramer, while non-substrate cations including Li^+ , Na^+ , and $Tris^+$ destabilizes the tetramer. In addition, a mutation of residues in the TVGYG motif also reduces the tetramer stability as well as compromising the potassium conducting activity.⁷¹ These results indicate that the interfacial pore at the four-fold axis of the tetramer is not only an important ion translocation pathway, but also involved in tetramerization. The KcsA tetramerization process has been monitored *in vivo* through a pulse chase experiment.⁷² The assembly of

membrane inserted KcsA monomers to tetramers has been shown to be a rapid and efficient process. Tetrameric species could be detected immediately after the 30 sec pulse labeling step at a monomer to tetramer ratio of 0.6, indicating that more than 60% of KcsA synthesized during the 30 sec window has already tetramerized. The monomer to tetramer ratio drops to 0.2 ten min after the chase and maintained stable afterward. Interestingly, the authors also discovered that the proton motive force is required for efficient KcsA tetramerization.⁷² More recently, Molina et al. found that the cytoplasmic C-terminal domain of KcsA plays an important role during the assembly of KcsA tetramer.⁷³ However, once assembled, the tetramer stability is not affected by the truncation of the C-terminal domain. Finally, KcsA without the C-terminal domain has been shown to tetramerize efficiently into lipid bilayers *in vitro*. These results indicate that the role of the C-terminal domain is to promote the initial subunit association during tetramerization *in vivo*.

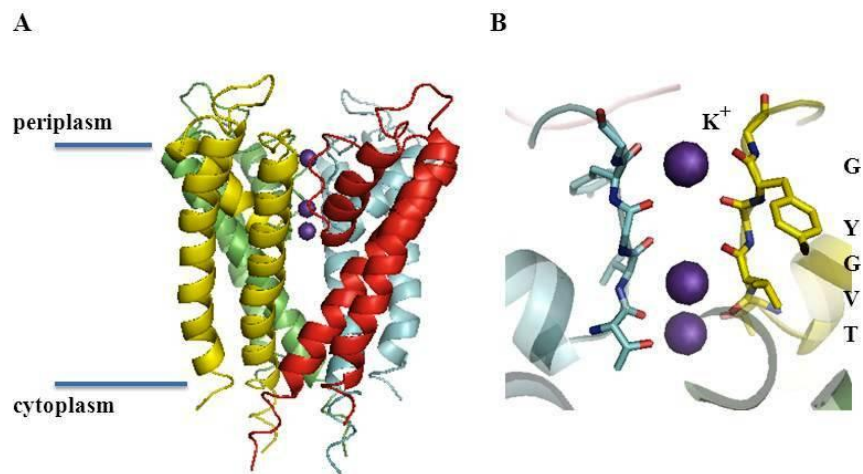


Figure 1.8 A. Structure of KcsA tetramer with bound potassium. (Protein Data Bank ID 1BL8).⁶⁸ B. The zoom in view of the TVGYG motif with bound potassium cation. The structure was generated using PYMOL.

1.4 Why Membrane Proteins Form Homo-oligomers

Why membrane proteins form homo-oligomers? Several functional roles of oligomerization have emerged from case studies of model systems. First, for certain proteins oligomerization is essential for the architectural purpose. The active sites or translocation pathway of the protein is located at the inter-subunit surface. The potassium channel KcsA is such an example—the translocation pathway of the channel is at the center of the tetramer. Second, oligomerization could provide increased structural stability against denaturation and degradation. Oligomerization reduces the specific surface area of a protein. Exposed protein surface is vulnerable to protease digestion and chemical modification. It is a common observation that protein oligomers are digested much slower than the corresponding monomers. In addition, the reduction of specific surface area decreases the amount of solvent molecules necessary to hydrate the protein, which is an important entropic factor for protein stability. Therefore, oligomers are usually thermodynamically more stable than the corresponding monomers. Third, oligomerization creates additional opportunities for allosteric regulation. Each subunit in a homo-oligomer may have an identical binding site for the ligands. The sequential binding and occupation of a site in one subunit may affect the binding of the neighboring subunit. For many secondary transporters such as CIC, NhaA, and BetP, while the functional unit is a monomer, the oligomeric organization is important for the regulation of protein function *in vivo*.

In summary, while membrane protein oligomerization remains a challenging field of study, immense progress has been made to elucidate the functional role and assembly progress of membrane protein oligomers. Based on a limited number of case studies,

oligomerization has been shown to play roles including architectural support, structure-stabilization, and allosteric regulation and activation.⁷⁴⁻⁷⁷ Proteins rarely function alone in biological systems. How protein subunits recognize and interact with each other is a fundamental question in protein science. The exploration of structure and functional mechanism of membrane proteins lags far behind those of soluble proteins. With the advance of experimental techniques and collective efforts of many research groups, new and exciting discoveries on how membrane proteins work are emerging at an unprecedented rate. The recent award of the Nobel Prize in Chemistry to Drs. Robert J. Lefkowitz and Brian K. Kobilka for their work on G-protein coupled receptors is a great recognition of the importance of membrane proteins. Without these amazing proteins, cells would be isolated islands that could not survive and adapt to the ever changing environment.

1.5 Major Multidrug Resistant Transporter Families

The emergence of bacterial infection involving drug-resistant strains is a serious issue for human health. The wide spread drug resistance among pathogens drastically reduced the efficacy of current therapeutic treatments. One of the resistance mechanisms is the expression of efflux pumps to export antibiotic out of bacteria. Multidrug resistant (MDR) transporters are one kind of the efflux pumps. It can actively recognize and extrude a broad spectrum of structurally diverse chemical compounds. Over-expression of those MDR pumps by bacteria has been observed in multidrug resistance infections, and thus presents serious health problems.

Based on structures, bacterial multidrug efflux transporters can be divided into five major families (Figure 1.9): (1) Resistance nodulation cell division (RND), (2) Major facilitator superfamily (MFS), (3) Small multidrug resistance (SMR), (4) Multidrug and toxic compound extrusion (MATE) and (5) ATP-binding cassette (ABC) family. The functions of first three families of transporters (RND, MFS and SMR) are driven by the proton gradient across the inner membrane. MATE family transporters are powered by the sodium gradient. ATP- binding cassette family transporters hydrolyze ATP as an energy source.⁷⁸

Each family has their respective energy source and selection of substrates. A single organism can express MDR transporters from more than one family. Different MDR transporters belonging to the same family could also be expressed in one organism. For example, *Escherichia coli* expresses AcrAB-TolC (one type of RND family), EmrE (one type of SMR family) and MacAB-TolC (one type of ABC family) simultaneously; AcrEF-TolC (belongs to RND family) is also expressed in *Escherichia coli*.

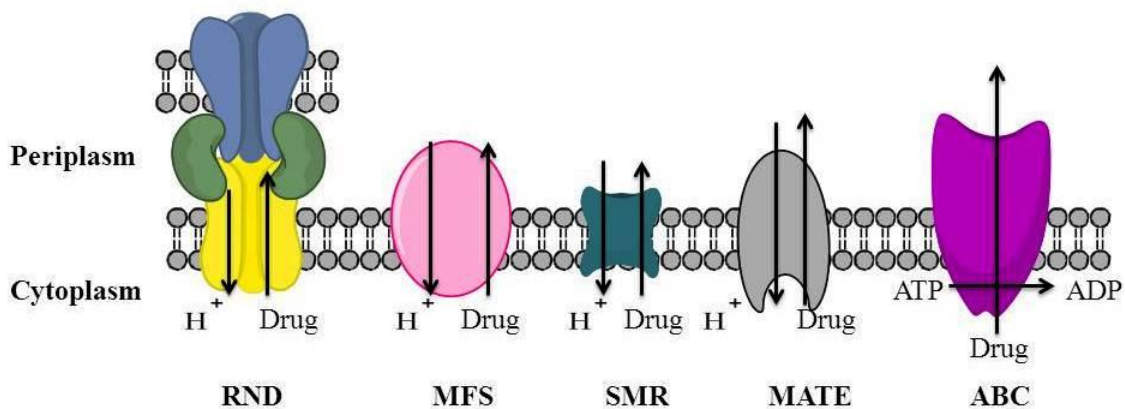


Figure 1.9 Five major families of multi-drug resistant transporter.

1.5.1 RND family

RND family multidrug resistant pumps are prevalent among Gram-negative species and major contributors for MDR drug resistance. The functional MDR complex is composed of three proteins: an inner membrane protein, an outer membrane protein and a membrane fusion protein in the periplasm (Figure 1.9). The inner membrane protein captures drugs and provides energy for the entire system, the outer membrane protein interacts with inner membrane protein in the periplasm and helps to extrude drugs out of cells, and the membrane fusion protein assists with the docking and interaction between the inner and outer membrane proteins. Each of the three components is essential for drug efflux, and absence of one component makes the system nonfunctional. The tripartite complex allows the direct efflux of drug outside of cell. The AcrAB-TolC system in *Escherichia coli* and MexAB-OprM in *Pseudomonas aeruginosa* are the representative examples of this family.⁷⁹ Except for efflux of antibiotics, RND family like MexAB-OprM in *Pseudomonas aeruginosa* could export virulence determinants which allowed

bacteria to be invasive and cause infection⁸⁰; AcrAB-TolC system in *Escherichia coli* has also been found to export signal molecules for bacterial quorum sensing (communication between bacterial cells), which stimulated the bacterial growth density.⁸¹ In addition, some types of RND transporter protect gram-negative bacteria against toxic heavy metal. Efflux system CusCBA in *Escherichia coli* is responsible for extruding of Cu(I) and Ag(I) ions.⁸²

1.5.2 MFS family

The MFS family transporters exist in both Gram-positive and Gram-negative bacteria. The QacA from *Staphylococcus aureus* is the first identified example in this family.⁸³ Other examples include NorA from *Staphylococcus aureus*, LmrP from *Lactococcus lactis*, MdfA and EmrD from *Escherichia coli*, and Bmr from *Bacillus subtilis*. Those pumps actively extrude monocationic biocides and dyes, such as benzalkonium chloride, cetyltrimethylammonium bromide, and ethidium bromide.⁸⁴ Among MFS transporters, the crystal structure of EmrD from *Escherichia coli* has been solved, which reveals the structural-based transport mechanism of this family.⁸⁵ It crystallized as a monomer with 12 transmembrane helices (Figure 1.10). It was suggested that drugs could be facilitated through the hydrophobic internal cavity of EmrD from the cytoplasm coupled with proton antiport.

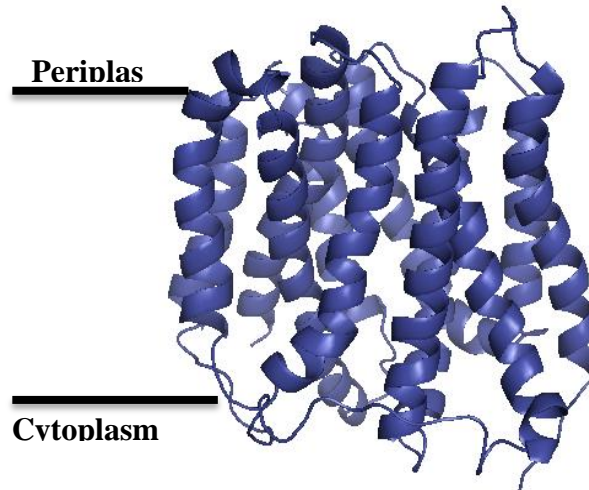


Figure 1.10 EmrD monomer (Protein Data Bank ID 2GFP)⁸⁵.

1.5.3 SMR family

The SMR family, one of the smallest transporters in nature (amino acid length ranged from 100-140) also exists in both Gram-positive and Gram-negative bacteria. The substrates of this family include cetylpridinium, tetraphenyl phosphonium, ethidium, methyl vilogen and benzalkonium.⁸⁶ EmrE from *Escherichia coli* is the model protein from this family. EmrE forms a dimer in the inner membrane and can cooperate with AcrAB-TolC to remove toxic compounds.⁸⁷ Toxic compound such as ethidium is extruded from the cytoplasm to periplasm by EmrE. AcrAB-TolC captures those compounds in the periplasm and extrudes it out of the cell. Based on the structure of EmrE, there is one charged residues E14 in the EmrE transmembrane domain, which is proposed to bind with protons, or stabilize the positive charge of polyaromatic cation substrate in the deprotonated state. The crystal structure of apo and substrate bound EmrE was solved by Chen et al.⁸⁸ However, the active form *in vivo* (parallel dimer or antiparaller dimer) of the protein is still under debate (Figure 1.11). Recently, Morrison et

al. conducted solution NMR and FRET experiments to study substrate-bound EmrE in micelles *in vitro*. They revealed that the monomers in dimeric EmrE were antiparallel and functional residues in the active site were asymmetric.⁸⁹ Pilar et al. found that the antiparallel dimeric EmrE was more stable than the parallel one, which suggested that antiparallel dimer might be the functional form of the protein.⁹⁰

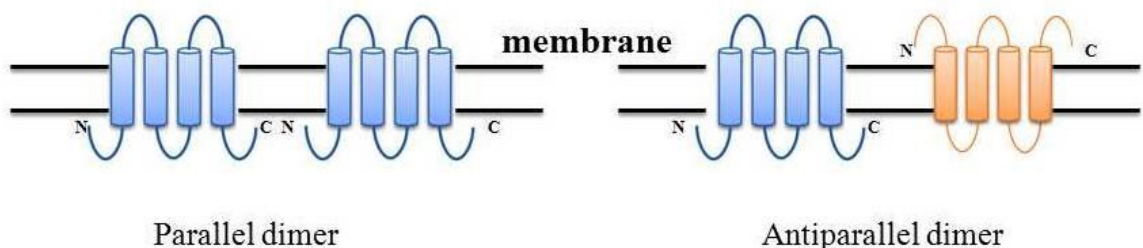


Figure 1.11 Two dimeric forms (parallel and antiparallel) of EmrE.

1.5.4 MATE family

The MATE is the most recently established among the five major families. NorM from *Vibrio parahaemolyticus* is the first multidrug resistant transporter categorized in the MATE family.⁹¹ The crystal structure of NorM from *Vibrio cholerae* was determined by He et al.⁹² It consists of 12 trans-membrane helices and an Rb^+ binding site is identified in the structure (Figure 1.12). It adopts an outward-facing conformation open to the outer-leaflet of the membrane. A substrate transport mechanism has been proposed based on this structure: cation binds in the conserved pocket in the outward facing conformation, which induces a structural change to the inward-facing conformation suitable for capturing the substrate. Substrate binding will change NorM back to outward-facing conformation followed by the export of the substrate to the medium.

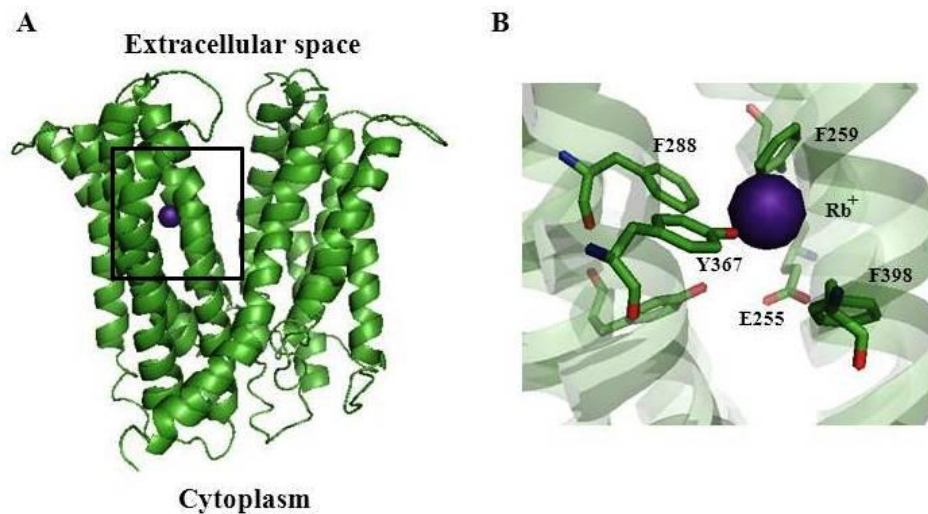


Figure 1.12 Structure of Norm. A. Norm Monomer (Protein Data Bank ID 3MKU)⁹² B. Zoom in picture of cation binding domain. The structure was generated with PYMOL.

1.5.5 ABC family

ABC transporters are a large family. Approximately 5% of the entire *Escherichia coli* genome encodes ABC transporters.⁹³ In mammalian cells, ABC multidrug transporter like P-glycoprotein in cancer cells extrudes anti-tumor drugs during chemotherapy.⁹⁴ Established role of bacterial ABC multidrug transporter is limited.⁸⁴ LmrA from gram-positive bacteria *Lactococcus lactis* was the first identified bacterial ABC-type MDR transporter.⁹⁵ LmrA conferred a broad spectrum of antibiotics resistance when it was expressed in *Escherichia coli*.⁹⁶ Sav 1866 from *Staphylococcus aureus* is the first bacterial multidrug ABC transporter crystallized.⁹⁷ The protein is crystallized as a homodimer with an outward-facing conformation and with bound ADP. Like most ABC transporters, Sav 1866 consists of two trans-membrane domains which provide a substrate translocation pathway, and two cytoplasm nucleotide-binding domains which

hydrolyze ATP to drive the pump (Figure 1.13). Based on the structure, drug transport was proposed to invoke two stages: the drug binds to the protein from the cell interior in an inward-facing conformation; the energy from hydrolysis of ATP drives the protein to an outward-facing conformation and extrude the drug to the external medium. Next, ATP binding returns the protein conformation to an inward-facing conformation. MacAB-TolC efflux system is an ABC-type transporter in gram-negative bacteria. Similar to AcrAB-TolC from RND family, MacB is the inner membrane protein, MacA a membrane fusion protein and TolC an out-membrane component. Experiments showed that the ATP binding to MacB stimulated the association between MacB and MacA, and assembly of MacAB stabilized the ATP-bound conformation of MacB.^{98,99}

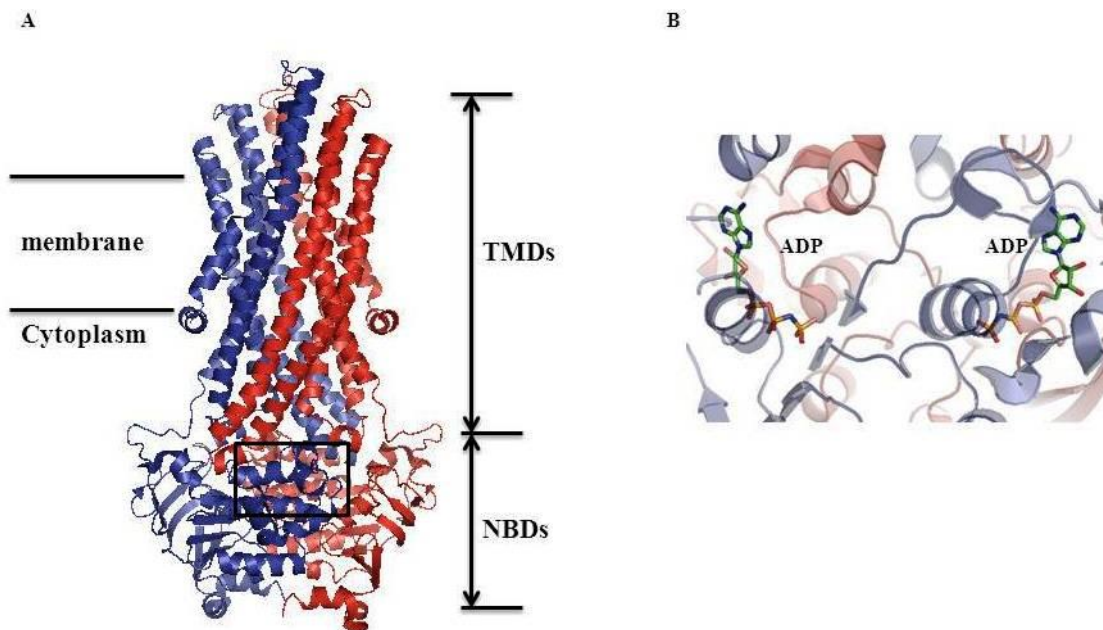


Figure 1.13 Structure of Sav 1866 A. Sav 1866 Dimer (Protein Data Bank ID 2ONJ),⁹⁷ TMDs stands trans-membrane domains; NBDs for nucleotide binding domains. B. Zoom in picture of ADP binding domain. The structure was generated with PYMOL.

1.6 Introduction of AcrB

AcrAB-TolC is one of the most well characterized RND efflux transporter systems in Gram-negative bacteria (Figure 1.14). AcrB is an inner membrane protein, AcrA a membrane fusion protein and TolC an outer membrane protein. AcrA was the first protein in the complex that drew researchers' attention. The mutation of gene *acrA* of *Escherichia coli* was firstly identified to make the host strain hyper-susceptible to acridine dyes.¹⁰⁰ Further studies showed that mutations at this locus also make the strain susceptible to other basic dyes, detergents, and certain antibiotics.¹⁰¹ Ma et al. first cloned and characterized *acrB* (formerly called *acrE*) gene of *Escherichia coli*, a neighbor gene to *acrA*.¹⁰² Primary protein sequence aligned with a known toxic metal cation efflux transporter EnvD, AcrB was predicted as a transmembrane protein and involved in the drug susceptibilities. Over-expression of AcrAB increased levels of bacterial resistance to a number of chemical agents, which demonstrated that the *acrAB* gene codes for the multi-drug resistant pump.¹⁰³ In light of the structure of the hemolysin transporter system HlyBD-TolC (AcrB is the homologue of transmembrane protein HlyB; AcrA is the homologue of putative accessory protein HlyD), TolC was late proved to be required for the function of AcrAB efflux pump.¹⁰⁴ AcrAB-TolC pump complex has a wide a range of substrate specificity (Figure 1.15), such as dyes (acriflavine, rhodamine 6G and ethidium bromide), antibiotics (β -lactams, tetracyclines, novobiocin and erythromycin but not aminoglycosieds), detergents (SDS and Trition X-100), other organic chemicals (tetraphenylphosphonium and hydroxylated polychlorinated biphenyl) and even organic solvent (cyclohexane, hexane, heptanes octane and nonane).^{105, 106}

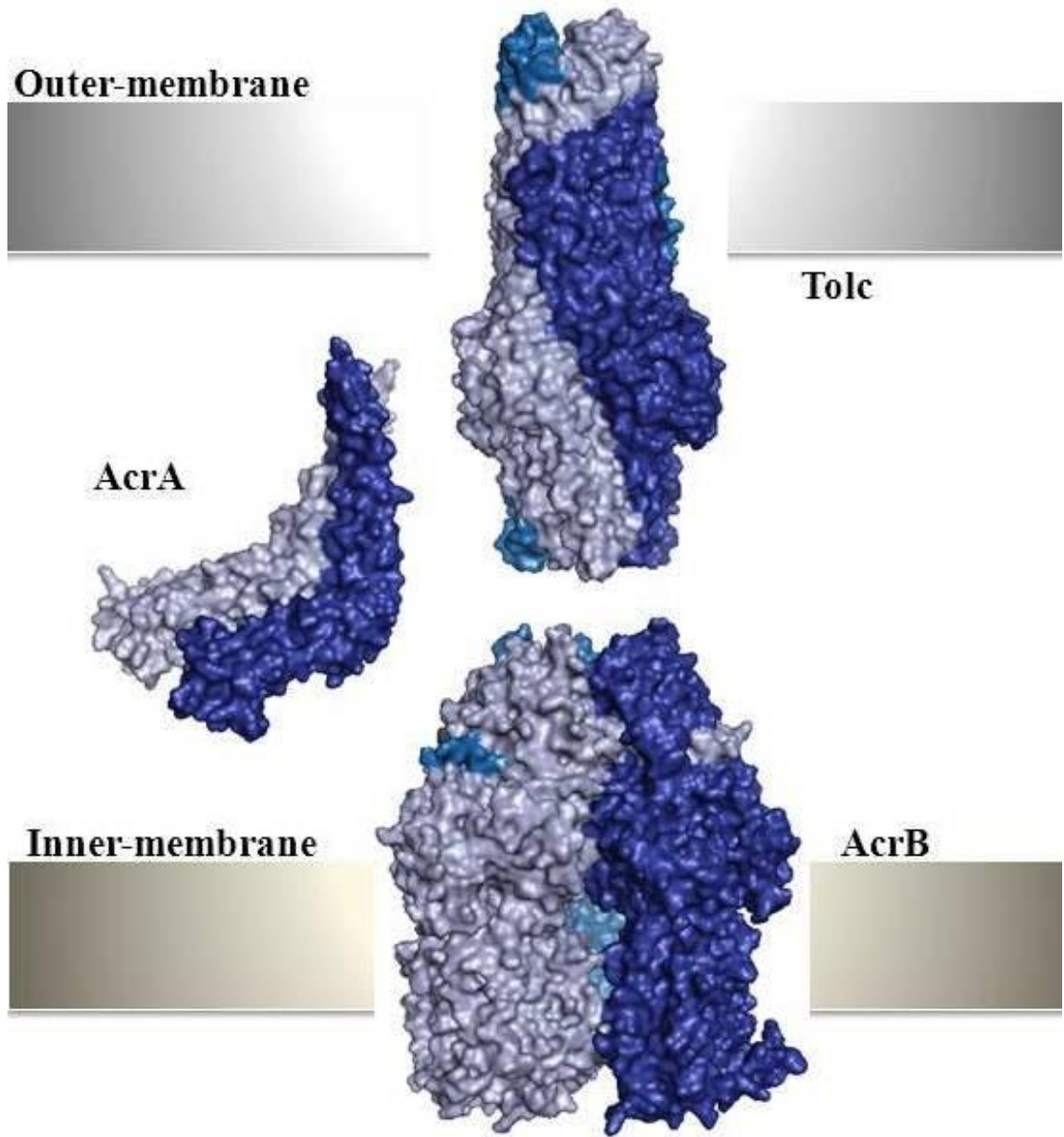


Figure 1.14 The surface structures of AcrA, AcrB and TolC and their locations in the cell. (Protein Data Bank ID: AcrA 1F1M, AcrB 2DHH, and TolC 1EK9). The structure was generated with PYMOL.

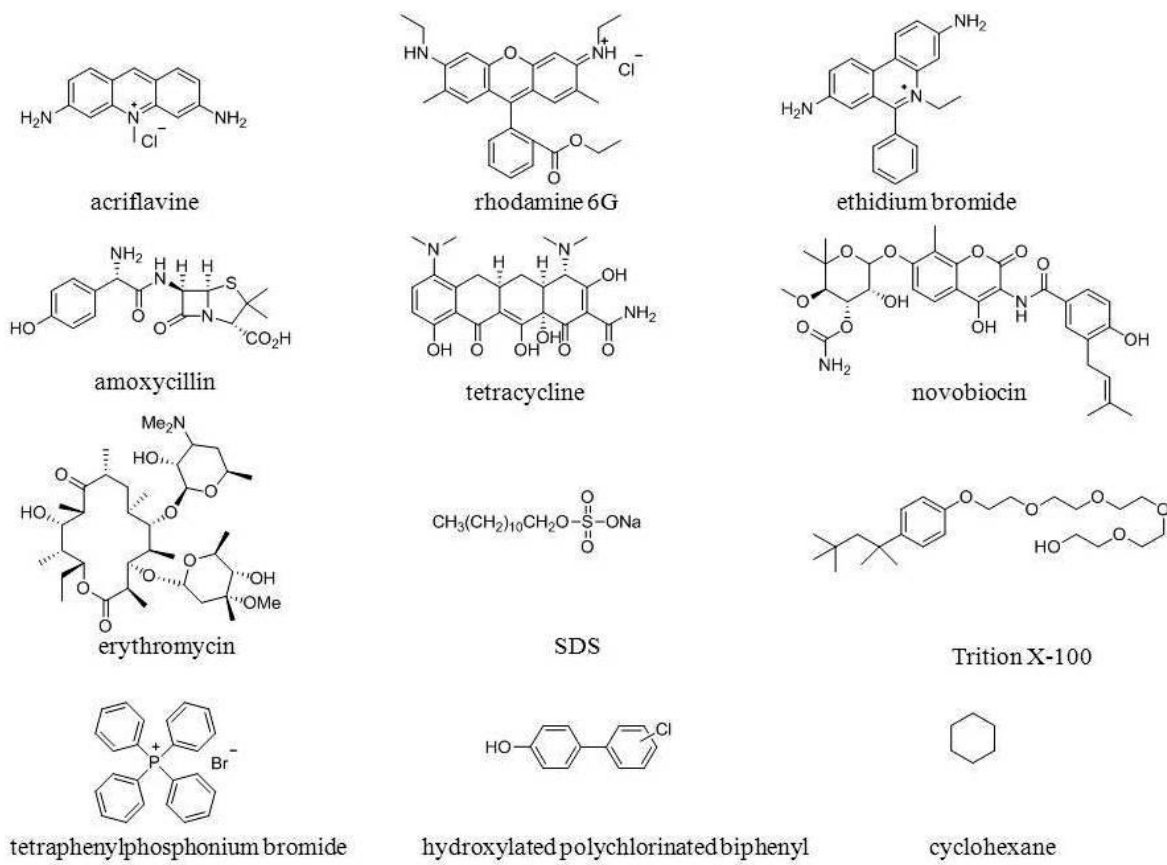


Figure 1.15 Selected substrates of the AcrAB-TolC efflux system.

1.6.1 Mechanism of Drug Extrusion

The first AcrB crystal structure is determined by Murakami et al. in 2002.¹⁰⁷ AcrB was crystallized as a symmetric homo-trimer. Each identical subunit has three distinct domains: a TolC docking domain, a pore domain, and a transmembrane domain with 12 transmembrane helices. The pore and TolC docking domain protrudes over 70 Å into the periplasm and suggests a direct interaction between AcrB and TolC, which creates an inter-membrane channel for drug extrusion (Figure 1.16). A central cavity was formed among the interfaces of the three subunits. The cavity has three vestibules accessible to periplasm. Drug extrusion was original proposed to go through the cavity either from cytoplasm or periplasm, and then go out of the cell via TolC. The later crystal structures of AcrB with substrates bound in the cavity determined in 2003 seemed to support the existence of the central cavity pathway.¹⁰⁸

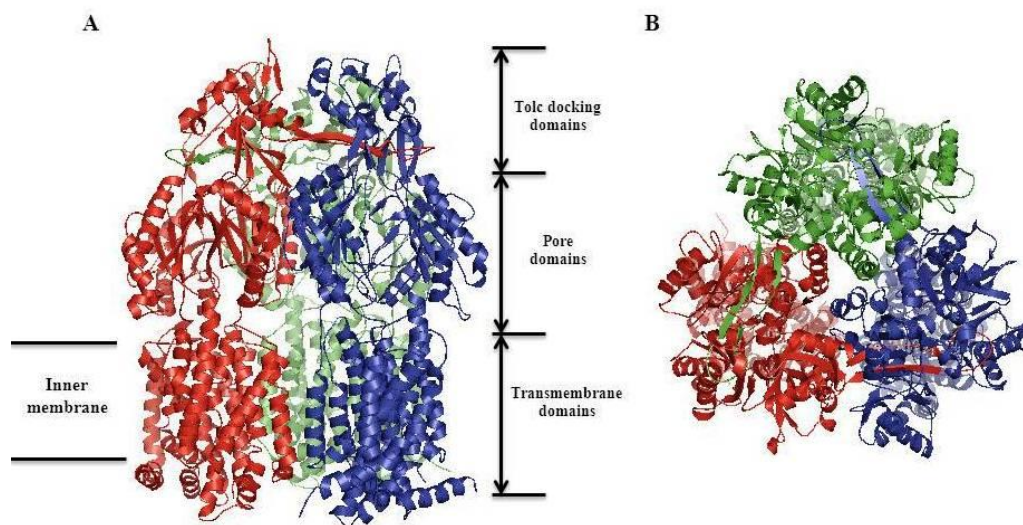


Figure 1.16 Structure of AcrB. A. The side view of ribbon structure of AcrB. (Protein Data Bank ID: 2DHH)⁶¹ B. Top view of ribbon structure of AcrB. The structure was generated with PYMOL.

In 2006 and 2007, three research groups independently reported the asymmetric structures of AcrB, which indicated a conformational cycling model for drug transport (Figure 1.17A).^{61, 109, 110} Murakami et al. co-crystallized AcrB with minocyclin, 9-bromo-minocyclin and doxorubicin, found only one subunit in each trimer bound with a drug molecule. The conformation of each subunit was different and the binding site was located in the periplasmic domain of AcrB. Based on those different conformations, the subunits were designated as access, binding and extrusion state, respectively. By comparison to ATP hydrolysis/synthesis mechanism of the F1-ATPase, a conformational rotation mechanism for drug export was proposed. The substrate binds with the subunit at the loose state, rotates through the tight and then open state before pumped out of the cell.

⁶¹ Seeger et al. also obtained asymmetric AcrB crystal structures. They named those monomers as loose (L), tight (T) and open (O) states corresponding to access, binding and extrusion states in Murakami's paper. They suggested that the asymmetric subunits represent different stages of the pump cycles. From those structures, they proposed a model as "Peristaltic Pump Mechanism" for the functional AcrB, which was close to the conformational rotation model by Murakami.¹⁰⁹ Sennhauser et al. used a Designed Ankirin Repeat Protein (DARPin) to co-crystallize with AcrB and obtained another asymmetric structure at the highest resolution of 2.5 Å. The stoichiometry of AcrB-DARPin complex was 3:2, and the DARPin was shown to stabilize the intermediates conformation in the transport cycles which supported a rotary mechanism for AcrB drug transport.¹¹⁰

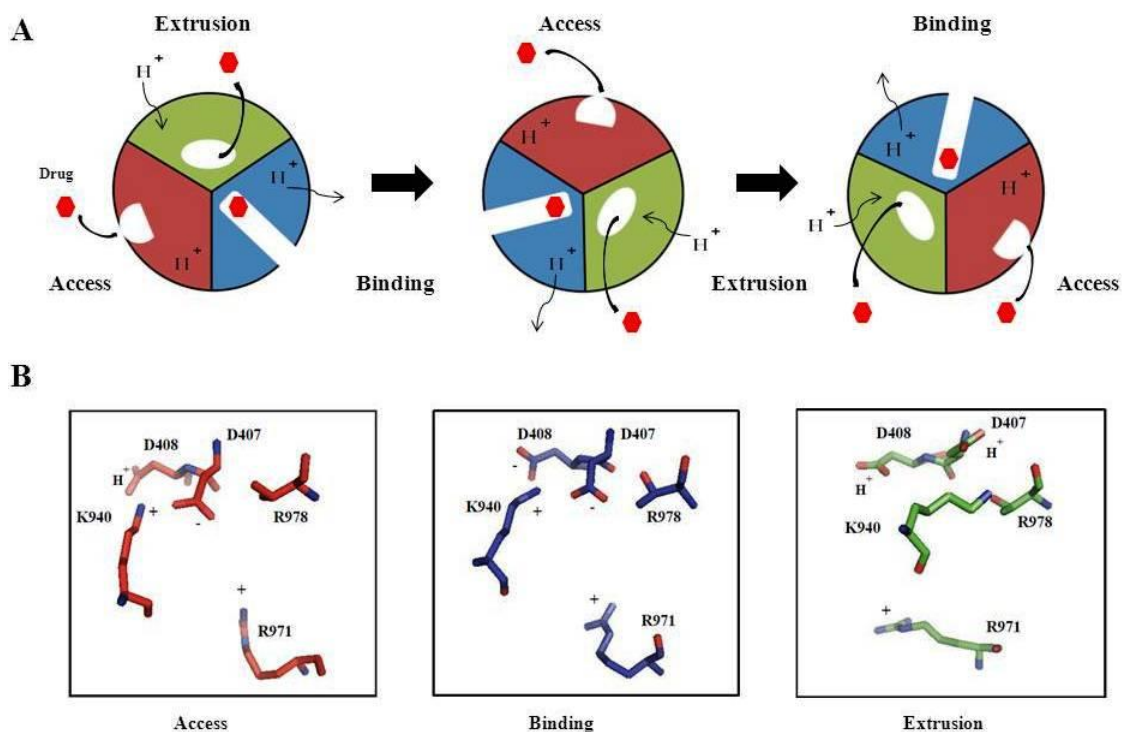


Figure 1.17 Rotation mechanism of AcrB. A. The rotational drug transport mechanism of AcrB. B. The proposed conformation change of proton translocation during the rotational drug transport process

Nikaido's and Pos's research groups used engineered disulfide bond to confirm functional rotation mechanism of multidrug efflux pump AcrB *in vivo*.^{111, 112} Based on the asymmetric crystal structure of AcrB that the large external cleft in the periplasmic domain of AcrB is wide open in the bind state but completely closed in the extrusion state, Nikaido constructed two intra-disulfide pairs in the external cleft and interface in one subunit. And they found that the formation of disulfide bond restricted the conformation change of AcrB and inactivated the pump function. Pos group incorporated several cysteine pairs in the moving domain between the subunits to make inter-disulfide bond.

The cross-link due to the disulfide bond deactivated the pump, and pump activity could be restored after reduction of disulfide cross-link.

In order to learn more about the dynamics of the rotational function model, computer modeling and molecular dynamics simulation were applied to gain more detailed information about the pumping mechanism at the molecular level. Schulz et al. calculated and found that conformation change of subunit helped the drug release from the binding pocket and approach the gate to the central funnel.¹¹³ Yao et al. used a new coarse-grain molecular simulation technique to probe the asymmetric structure AcrB. They found the allosteric coupling between the subunits stabilized the asymmetric structure.¹¹⁴ Wang et al. observed the conformational coupling between the monomers of AcrB, and the trimeric assembly of AcrB was strengthened through the coupling effect between the transmembrane domain and other parts of AcrB.¹¹⁵

The drugs transported from the cell to the outside via AcrAB-TolC system were coupled with proton translocation from the periplasm to cytoplasm. Through the comparison of the amino acid sequence of RND toxic cation efflux pump CzcA and other RND pumps, several conserved charged residues were found in the transmembrane domain. Mutation of those residues abolished the pump functionality.¹¹⁶ The site-directed mutagenesis of MexB, an analogue of AcrB, revealed residues D407, D408 and K940 were essential for the pump function, which suggested a proton-network formation from those residues.¹¹⁷ The first crystal structure of AcrB confirmed that the ion pairs were formed among D407, D408 and K940.¹⁰⁷ T978 and R971, which were the other components for the network in the transmembrane domain, were also identified through site-directed mutagenesis study

of AcrB.¹¹⁸ The asymmetric structures of AcrB showed the different configuration of those residues in the three subunits.^{61, 109} In the access and binding state of subunits, there was a tight association among D407, D408, K940 and T978. In the extrusion state of subunit, the association collapsed and the side chain of K940 was tilted to form a polar contact with T978. The proton is proposed to be bound to D407 or D408 in the extrusion state and the bound proton dissociate when the extrusion state rotated to the access state (1.17B).¹¹⁹ From those findings, it was suggested that the proton traveled from the periplasm to the cytoplasm and changed the configuration of those charged residues. And the configuration change of those charged residues upon protonation and de-protonation affect the drug-binding domain in the periplasm and promote the rotation of the pump. To prove this model *in vivo*, Takatsuka and Nikaido constructed a giant gene in which three monomeric AcrB were covalently linked into a trimer, which could be expressed in a Δ *acrB* strain and showed resistance activity to some toxic compounds.¹²⁰ When D407 was replaced with Ala in one subunit of the fused AcrB, the function of the transporter was completely lost. This result suggested that the function of each subunit was coupled and driven by proton translocation through the transmembrane of AcrB.

One puzzle about AcrB is how the protein recognizes structurally different substrates. So far, drug-bound crystal structures, site-directed mutagenesis studies and computer modeling have begun to draw a picture about the binding pocket and path for substrates transport. The first set of drug-bound AcrB crystal structures showed that the substrates bound in the central cavity of AcrB, which suggested that the drugs were taken up from the vestibules, went through the central cavity and pore of AcrB, and finally escaped from the funnel-like opening at the top of the AcrB trimer to the TolC channel.¹⁰⁸

Murakami et al. conducted cysteine scanning to the residues in the pore area. Two mutants V105C and D112C decreased pump activity, which suggested that the conformation of the pore changed during the transport process.¹²¹ However, site-directed mutagenesis of residues within the central cavity around substrate binding area did not change the AcrB activity. More recent drug-AcrB complex revealed a new periplasmic binding site.¹²² (Figure 1.18)

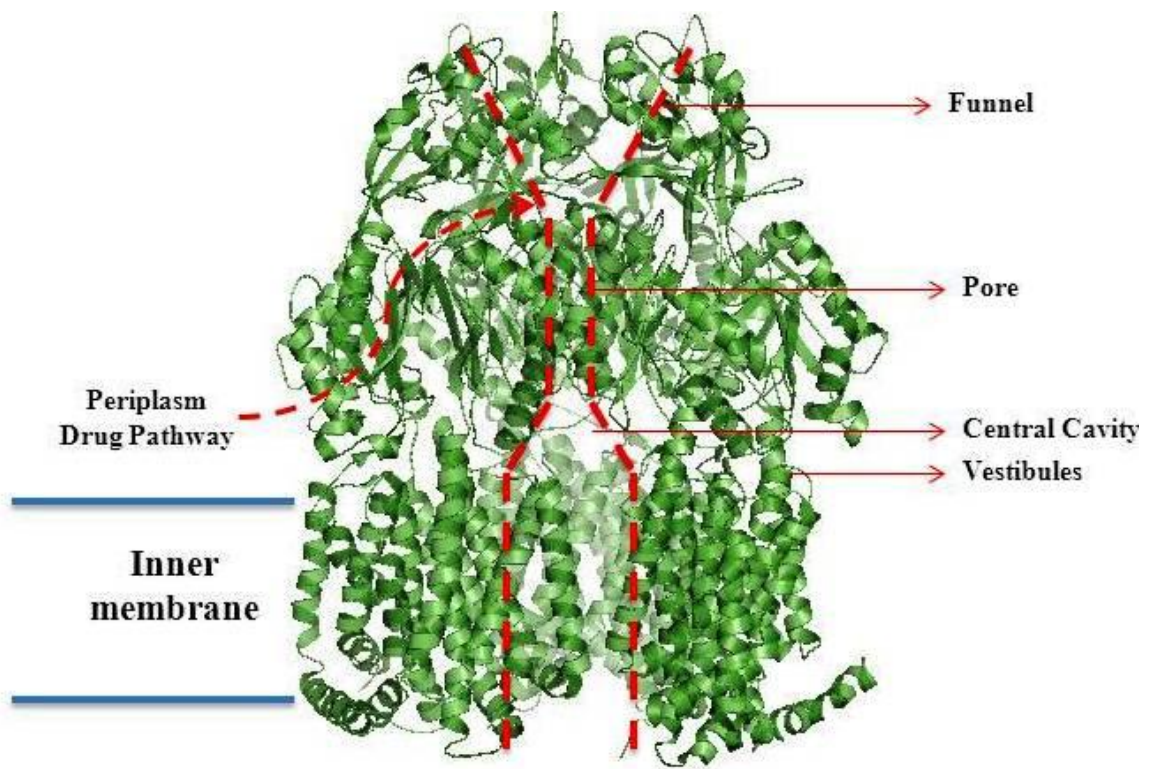


Figure 1.18 The proposed drug pathways. (Protein Data Bank ID: 2DHH)⁶¹ The structure was generated with PYMOL.

The asymmetric AcrB crystal structures reveal a new hydrophobic pocket defined by a cluster of phenylalanines including 136, 178, 610, 615, 617, and 628 (Figure 1.19).^{61, 109,}

¹¹⁰ Site-directed mutation of those phenylalanines to alanines combined with drug

susceptibilities assay revealed an important role of F610 for the substrate extrusion process. The mutant F610A dramatically decreased the pump functionality and increased the drug susceptibilities of bacterial.¹²³ Targeted molecular simulation study suggested that the subtle interaction between the substrate and F610 determine the functionality of the pump.¹²⁴

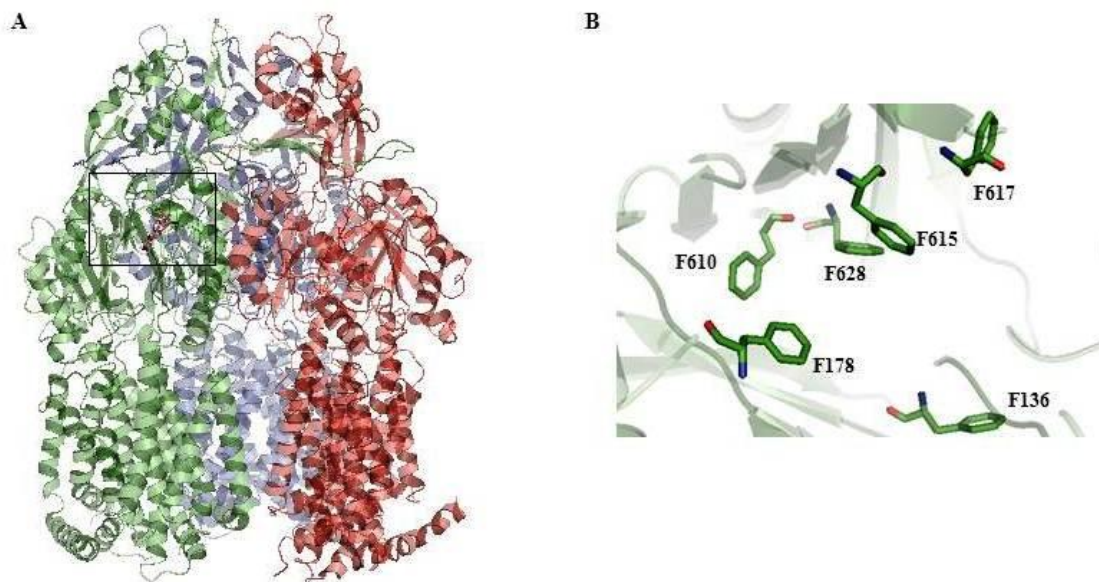


Figure 1.19 Phenylalanines cluster region of binding pocket. A. The side view of ribbon structure of drug bound AcrB. (Protein Data Bank ID: 2DHH)⁶¹ B. Zoom in picture of phenylalanines cluster region for the binding pocket. The structure was generated with PYMOL.

Based on the asymmetric crystal structure of AcrB, Takatuska et al. used computer docking to evaluate the interaction between the binding pocket and the substrates. Depending on the molecule structure of the substrates, they found that some substrates such as doxorubicin, novobiocin and levofloxacin et al. bound to a narrow groove at one end of the substrate binding pocket while substrates like ethidium, SDS, and

chloramphenicol prefer to bind to a wide cave of the binding pocket.¹²⁵ To map out the translocation pathway of substrates through AcrB, Husain and Nikaido devised a fluorescence-based whole cell assay.¹²⁶ They changed residues along the predicted substrate path into cysteines, and labeled these residues with a low concentration of Bodipy FL *N*-(2-aminoethyl) maleimide which is the substrate of AcrB. The labeling reagent traveled through the AcrB channel and covalently reacted with cysteines lining up the translocation pathway. The labeled AcrB were purified, resolved on SDS-PAGE and visualized with Coomassie stain. The intensity of fluorescence due to the labeling could be quantified to determine whether the residues faced the putative drug pathway. Those introduced cysteines at location distant from the drug pathway were not labeled. Several residues were identified to be part of the drug uptake and extrusion pathway. From the labeling results, it was suggested that the substrates were captured in the lower cleft region of AcrB, through the binding pocket, gate and to the funnel of AcrB. With the same method, they found four residues (S836, E842, L868 and Q872) in the vestibules and one residue (G97) in the central cavity could also be labeled with the fluorescent reagent, which indicated that substrate might travel through vestibules to the central cavity.¹²⁷ The investigation of AcrB homologues MexB revealed that the double mutant of conserved residues F4A/F5A, located in the cytoplasm side of the central cavity, affected the efflux of compounds to the cytoplasm target but had no effects on those with targets in the periplasm, cell walls or membranes.¹²⁸ All those results raised an apparent question: does AcrB pick up drugs in the cytoplasm and transport them outside of the cell? It is likely that there is an alternative pathway through which drugs could

enter from through the cytoplasm. The AcrB homologous protein AcrD has been demonstrated to transport aminoglycosides antibiotics from the cytoplasm.¹²⁹

Recently, crystal structures of AcrB bound with high-molecular-mass drugs rifampicin and erythromycin were reported by Nakashima et al.¹³⁰ Those crystal structures revealed a new multi-site binding pocket called proximal pocket in the access state. They proposed that the high-molecular-mass drugs first bind to the proximal pocket and then forced into the distal pocket by a peristaltic mechanism while the low-molecular-mass drugs traveled through the proximal pocket without specific binding and bound to the distal pocket. The other high resolution crystal structures of AcrB/designed ankyrin repeat protein (DARPin) complex bound to the drugs were reported by Eicher et al.¹³¹ They found that the conformation flexibility of loop containing F615 and F617 were important for large substrates transport through the AcrB. All those findings further advanced our understanding of the broad substrates transport specificity of AcrB. The binding affinity between AcrB and its ligands were measured with the fluorescence polarization method *in vitro*.¹³² Fluorescent substrates were titrated with purified AcrB and dissociation constants ranged from 5.5 μM for rhodamine 6G to 74 μM for ciprofloxacin. The kinetic constants of AcrAB-TolC pump was modeling and calculated by Nikaido group.^{133, 134} They used AcrB substrate β -lactams antibiotics and built an influx rate model for intact cell assay. From the known K_m and V_{max} of the periplasmic β -lactamase, they calculated the periplasmic concentration of β -lactam antibiotics. The rate of drug diffusion into the cell (influx rate) could be calculated from periplasmic concentration of β -lactams antibiotics. The rate of drug efflux from the cell through AcrAB-TolC pump was the difference between the influx rate and the rate of drug hydrolysis by periplasmic β -

lactamase. From the efflux rate and Michaelis-Menten equation, the K_m of the pump were calculated to be around 3-5 μM .

1.6.2 Assembly of AcrAB-TolC system

The crystal structures of AcrB and TolC reveals that they might have a direct interaction via their respective periplasmic domains.^{107, 135} The AcrB periplasmic domain extends 70 Å into the periplasm while the α -helical periplasmic domain of TolC is about 100 Å. The AcrB-TolC complex could be cross-linked *in vivo* with a chemical cross-linking reagent dithiobissuccinimidylpropionate (DSP) in the absence of AcrA, which suggests that AcrB and TolC existed in close proximity. However, a strong interaction between AcrB and TolC could not be detected using isothermal titration calorimetry.¹³⁶ Therefore, the interaction between AcrB and TolC was proposed to be stabilized by AcrA. Tamura et al. engineered cysteines residues on the β -hairpins of TolC docking domain in AcrB and the coiled coils at the tip of TolC. Those cysteines form disulfide bonds *in vivo* and the formation of disulfide bond was not affected by AcrA, or substrates, or a putative proton coupling site mutation of AcrB.¹³⁷ Those results indicated a direct interaction between AcrB and TolC. Recently, Tikhonova et al. immobilized AcrB, and measured its binding to TolC with surface plasmon resonance *in vitro*. The calculated binding affinity was 90 nM.¹³⁸

The interaction between AcrB and AcrA was detected through chemical cross-linking and co-purification.^{136, 139, 140} The association of AcrB and AcrA was measured to be 10^6 M^{-1} with isothermal titration calorimetry. Also, the isothermal titration calorimetry analysis revealed that the C-terminal region of AcrB (amino residues from 172-397) had

a strong interaction with AcrB.¹³⁶ In another studies, the residues from 290-357 of AcrA was replaced with YhiU fragments to form a chimeric construct. The hybrid protein did not support efflux function of the AcrAB-TolC.¹⁴¹ Furthermore, a single mutant G363C, located in the C-terminal region of AcrA, greatly impaired the activity of pump.¹⁴² Taken together, those results emphasized the importance of the C-terminal region of AcrA for the interaction of AcrB. However, the crystal structure of AcrA lacks a large portion of N or C-terminal region, which were key parts for the interaction to AcrB and TolC.¹⁴³ To better understand the intermolecular contacts between AcrA and AcrB, Symmons et al used the crystal structures of MexA, a homologue of AcrA, as a model to construct the structure of AcrA. The missing region in the AcrA crystal structure was predicted to be a β -roll, which was proposed to be involved in the interaction to AcrB. To verify the model, a series of chemical cross-linking using chemical cross-linking reagent with different length were conducted *in vivo* by introducing cysteines in both AcrB and AcrA. Based on the results of cross-linking, an optimized docking model between AcrB and AcrA was proposed.¹⁴⁴ Recently, a co-crystal structure of the CusBA, a RND family of metal efflux complex, showed detailed contacts between inner membrane transporter CusA (homologue to AcrB) and membrane fusion protein CusB (homologue to AcrA).⁸² The stoichiometry of the binding between CusA and CusB was 3 to 6. The periplasmic domain of CusA was involved in the interaction with CusB. The co-crystal structure of CusAB indicated that AcrAB might have the same binding stoichiometry and similar periplasmic binding domains.

The interaction between AcrA and TolC has also been investigated intensively. The AcrA could be chemical cross-linked with TolC in the absence of AcrB and the substrates.¹⁴⁵

The detailed map of periplasmic contacts between AcrA and TolC was achieved with chemical specific cross-linkers. Cysteines were introduced to the N-terminal helix of coiled coil in AcrA and α -helical barrel domain of TolC, respectively. The cross-linking results provided a docking model for the interface contracts between the proteins, which suggested that the α -helices of AcrA has a colied-coil interaction with α -helices of TolC periplasm domain.¹⁴⁶ However, the recent chemical cross-linking experiment and electron microscopy studies suggested that AcrA interacts with TolC in a tip-to-tip manner.^{147, 148}

Overall, the bi-partite AcrB-AcrA, AcrB-TolC and AcrA-TolC interactions have been demonstrated *in vitro*. And *in vivo* cross-linking studies have shown that either bi-partite could be linked in the absence of the third part of the pump. One study shown that the substrate of the pump could stabilize the complex formation.¹⁴⁹ Tikhonova et al. used surface plasmon resonance to study the assembly of AcrAB-TolC *in vitro*.¹³⁸ They immobilized AcrB and AcrA on the surface, respectively. They found that the dissociation constants for AcrA-AcrB and TolC-AcrB were in the similar nanomolar range. But the initial association rate of TolC-AcrB was four fold faster than that of AcrA-AcrB. Those results indicated that AcrB –TolC complex formed first, and AcrA interacted with the bi-partite complex to form the tri-partite system. However, questions still remain about how the three components form a functional complex *in vivo*, what is the order for those three parts to assembly, or what are the roles of each individual component play in pump assembly. Moreover, the trimeric AcrB was always considered as a single unit for the study of AcrAB-TolC assembly. There are fewer studies for the

assembly of obligate trimeric AcrB itself. Therefore, in this thesis, I will mainly focus on the study of oligomerization of AcrB.

Chapter 2 An Invariable Residue P223 Is Critical for AcrB Stability and Function

2.1 Introduction

To study the assembly of AcrB, it is necessary to obtain a monomeric AcrB in the cell membrane. To obtain a monomeric AcrB, the inter-subunit interactions need to be disrupted. After examination of crystal structures of AcrB, our research group identified a protruding loop that is important for trimerization. We deleted 17 residues from the loop and obtained a mutant-AcrB_{Δloop} (Figure 2.1). The protruding loop appeared to be involved in the formation of trimeric AcrB *in vivo*.¹⁵⁰ From the crystal structures, the protruding loop penetrates into a “tunnel” in the neighboring subunit, and has no direct contacts with other domains. We found that AcrB_{Δloop} completely lost its transport activity and failed to assemble into trimer but remained well-folded with a conformation similar to the structure of wild-type AcrB.¹⁵¹ These results indicate that AcrB monomers could fold independently without the assistance from the neighboring subunits, suggesting that oligomerization of AcrB might occur through a three stage pathway: the nascent polypeptide chain co-translationally inserts into the lipid membrane, folds into monomers, and then well-folded monomers assemble into a functional trimer. To further investigate which residues in the loop are critical for inter-subunit interaction during trimerization, I mutated individual residues in the loop and characterized the effect of mutation on AcrB structure and function. Among the loop residues studied, mutation of the invariable residue P223 had the most detrimental effect on function.

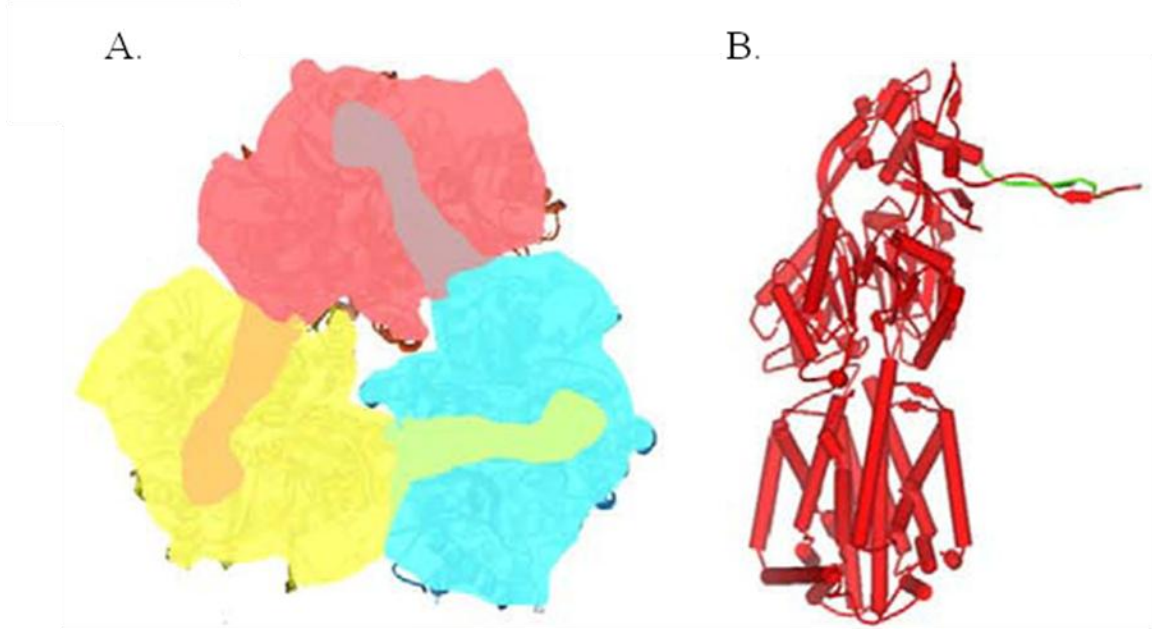


Figure 2.1 Subunit interaction of AcrB. A. The top view of AcrB trimer. The protruding loop was highlighted. B. The monomeric AcrB. The green part was the deleted 17 amino acids in the protruding loop.¹⁵¹

2.2 Materials and Methods

2.2.1 Materials

Protein molecular weight marker (Spectra Multicolor High Range Protein Ladder) for SDS-PAGE was from Thermo (Rockford, IL). The native protein marker was from Invitrogen (name of the product) (Carlsbad, CA). The custom polyclonal rabbit anti-AcrB antibody was obtained from GenScript as described (Piscataway, NJ).¹⁵¹ All enzymes were from New England Biolabs (Ipswich, MA) and all the chemicals from BioWorld (Dublin, OH). The parent wild type (BW25113) and AcrB deficient Δ *acrB* strains were obtained from the Yale *E.coli* genetic stock center. The genotypes of the BW25113 is *rrnB3* Δ *lacZ4784* *hsdR514* Δ (*araBAD*)*567* Δ (*rhaBAD*) *568rph_1*; the Δ *acrB* strain lacks the chromosomal *acrB* gene and is kanamycin resistant.

2.2.2 Site-Directed Mutagenesis of AcrB

Mutations were introduced into the *acrB* gene in plasmid pQE70AcrB followed the Quick Change mutagenesis kit protocol (Agilent Technologies). Mutation was confirmed by sequencing before transformed into the AcrB deficient BW25113 Δ *acrB* strains for expression.

2.2.3 Expression and Purification of AcrB and its mutants

Plasmid pQE70-AcrB was transformed into a Δ *acrB* strain for protein expression. A single colony was picked from a fresh transformed plate and grown with shaking at 37°C in 3 ml Luria Bertani (LB) medium containing 100 µg/ml ampicillin for 12 hours. 1 ml of this cell culture was used to inoculate 300 ml LB medium containing 100 µg/ml

ampicillin and grown overnight. Cells were harvested by centrifugation at 8,000×g for 10 min. The cell pellet was resuspended in buffer A (20 mM Tris-HCl, 100 mM NaCl, 10 % glycerol, 1mM phenylmethanesulfonylfluoride (PMSF), pH 8.0) and sonicated on ice for 5 min with 10 s on/off intervals. After centrifuged at 15, 000×g for 20 min at 4°C, the supernatant was discarded. Pellet was resuspended in buffer B (20 mM Tris-HCl, 100 mM NaCl, 1% Triton X-100, 10 % glycerol, 1mM PMSF, pH 8.0) and incubated with shaking for 1 hour at 4°C, followed by centrifugation at 15,000×g for 20 min at 4°C. The supernatant was incubated with the Ni-NTA resin (Qiagen, Huntsville, AL) with shaking at 4°C for 1 hour, washed with buffer B containing 50 mM imidazole, and finally eluted with buffer B containing 250 mM imidazole

2.2.4 Drug Susceptibility Assays

Drug tolerance of several strains with plasmid-borne AcrB and mutants were examined at 37°C without IPTG induction. The minimum inhibition concentrations (MICs) were determined for known AcrB substrates including erythromycin, novobiocin, rhodamine 6G, tetraphenylphosphonium, SDS and tetracycline. The exponential-phase cultures started from a single colony of freshly transformed cells was diluted to a final OD₆₀₀ of 0.1 unit with LB broth. 10 µl of this dilute culture was used to inoculate each well of 1 ml fresh LB medium in a sterile cultured plate (BD, Franklin Lakes, NJ). The plate was incubated at 37°C with shaking at 200 rpm, for 17-18 hours before the OD₆₀₀ was measured. The turbidity visual detection limit was considered as the MIC. Each assay was repeated at least three times.

2.2.5 Expression Level Analysis with Immunoblotting

BW25113 *ΔacrB* strains with the transformed mutant plasmids were grown in Luria-Bertani medium with ampicillin at 37°C overnight. Cells were harvested, resuspended in sodium phosphate buffer (pH 7.4) buffer, and lysed with a French press. Cell debris was removed through low-speed centrifugation and membrane vesicles were collected by ultracentrifugation at 150,000g for 1hr at 4°C. Membrane vesicles were solubilized in sodium phosphate buffer (pH 7.4) with 2% (wt/vol) SDS at room temperature and separated on an 8% SDS-PAGE gel. Proteins were transferred to a nitrocellulose membrane (Millipore, Bedford, MA) for blotting using a polyclonal anti-AcrB antibody as the primary antibody and an alkaline phosphatase-conjugated anti-rabbit antibody (Abcam, Cambridge, MA) as the secondary antibody. The protein-antibody conjugates were detected after staining using nitroblue tetrazolium chloride and 5-bromo-4-chloro-3'-indoyl phosphate p-toluidine (Sigma-Aldrich, St. Louis, MO).

2.2.6 Circular Dichroism (CD) Measurement

The secondary structure of AcrB and AcrB_{P223G} were characterized with CD spectroscopy conducted on JASCO J-810 spectrometer. The protein samples dialyzed into a low salt buffer (10 Mm sodium-phosphate, 50 Mm NaCl, 10% glycerol, 0.05% DDM, pH 7.5) before the CD measurement. Blank scans were collected using the dialysis buffer. The spectrum wavelength scans from 255nm to 195nm in a 1 cm path-length cuvette. The thermal stability was assayed at wavelength of 222nm with the increasing temperature from 4°C to 98°C, in increments of 1°C at each temperature interval.

2.2.7 Blue Native (BN)-PAGE Analysis

Briefly, blue native loading buffer was added into purified AcrB_{WT} and AcrB_{P223G} at a final concentration of 0.1 M 6-aminocaproic acid, 10 Mm Bis-Tris-HCl, 6% sucrose, 1% Coomassie brilliant blue G-250, pH 7.0. The protein samples were load to a 4-20% gradient polyacrylamide gel. The electrophoresis was performed using the running buffer (25 Mm Tris-HCl, 192 Mm glycine, 0.01% Coomassie brilliant blue G-250, pH 8.3) at 60 V, in the 4°C refrigerator for 14 hours. The protein bands were visualized after Coomassie Blue staining.

2.2.8 Limited Trypsin Digestion

The dynamic property of AcrB and its mutant were compared under the limited proteolysis condition. Trypsin (Sigma-Aldrich, St. Louis, MO) was mixed with AcrB_{WT} or AcrB_{P223G} at the weight ratio of 1:200 in buffer (10 mM sodium-phosphate, 50 mM NaCl, 10% glycerol, 0.05% DDM, pH 7.5) at room temperature. At the indicated time interval, digestion was quenched with the addition of SDS protein loading buffer and PMSF. The samples were resolved on SDS-PAGE.

2.2.9 Disulfide Trapping

Disulfide trapping was performed as described.¹⁵² Briefly, cell pellet from 100 mL overnight culture was suspended in a lysis buffer (30 mM iodoacetamide (IAM), 0.5 mM phenylmethanesulfonylfluoride (PMSF), 30 mM Tris, 0.5 M NaCl, pH 7.9) and sonicated for 15 minutes on ice. The cell lysate was centrifuged. The pellet was then suspended again in a buffer containing 1.5% TritonX-100, 10 mM IAM, 0.5 mM PMSF, 30 mM

Tris, 0.5 M NaCl (pH 7.9) and sonicated gently at low amplitude for 10 minutes on ice. The mixture was then incubated on ice with shaking for 2 hours, followed by centrifugation. The supernatant, containing the detergent solubilized AcrB, was collected. Imidazole was added into the supernatant to a final concentration of 10 mM to reduce non-specific binding during purification. The supernatant was mixed with Ni-NTA sepharose resin (Qiagen Inc., Valencia, CA) and rotated for 40 minutes. The suspension was packed into an empty column and subsequently washed with wash buffer (1.0% Triton X-100, 20 mM Tris, 100 mM NaCl, 50 mM Imidazole pH 7.9). The target protein was eluted using an elution buffer (1.0% Triton X-100, 20 mM Tris, 100 mM NaCl, 250 mM Imidazole pH 7.9). After elution, maleimide (MAL) and SDS were immediately added to protein samples to final concentrations of 50 mM and 4% (w/v), respectively. The high percentage of SDS denatured the protein and MAL was included as a precaution to further block any residual free cysteines. After 30 minutes incubation at room temperature, proteins were precipitated using 15% trichloroacetic acid (TCA). After centrifugation, the precipitate was washed with cold acetone and then re-solubilized in a buffer containing 4% SDS and 50 mM Tris (pH 8.0). The precipitation and washing step was used to remove IAM and MAL from the sample. The protein concentrations of different AcrB mutant samples were adjusted to the same level by measuring the absorbance at 280 nm. Labeling was performed following three steps. First, β -mercaptoethanol (BME) was added to the samples at a final concentration of 50 mM. The samples were then incubated at 37 °C for 1 hour. Second, proteins in the samples were precipitated using 15% TCA. After centrifugation, the protein pellet was washed using ice cold acetone. Finally, a buffer containing 4% SDS, 50 mM Tris, pH 8.0, and 5 mM

N-(5-fluoresceinyl) maleimide (F-MAL) was added immediately to the protein pellet to label the newly reduced free thiol groups. The pellet was resuspended using a pipette tip and incubated at room temperature for 30 minutes. After the incubation, 10 mM BME was added to quench the labeling reaction. The labeled samples were analyzed using SDS-polyacrylamide gel electrophoresis (SDS-PAGE) on 8% gels. After the extra fluorescence dye migrated out of the gel, the gel was removed and the fluorescence image was taken using the Mini-Visionary gel documentation system (FOTODYNE Inc., Hartland, WI) under UV light. The same gel was then stained using Coomassie blue stain and the image of the gel was taken again under normal white light.

2.3 Results

2.3.1 Construction of P223 Mutants

The protruding loop of AcrB was composed of 30 amino acid residues (Figure 2.1). Through primary sequence alignment with other AcrB homologues and analysis of the crystal structure, P223 in the loop attracted our interests for investigation. It was an invariable amino acid according to sequence alignments (Figure 2.2). The crystal structure of AcrB showed that P223 caused a sharp turn at the tip of the loop (Figure 2.3). Proline is a unique amino acid among the twenty common amino acids. The rigidity of Pro backbone conformation originates from its cyclic structure. The structure feature of the proline played an important role in the functions of many proteins.^{153, 154} Based on this analysis, I hypothesize that the rigidity of P223 contributes to the stability of AcrB. The P223 was mutated to glycine, alanine, valine, tyrosine and asparagines for side chains of various flexibility, length and polarity to exam the importance of P223 on AcrB trimer stability.

```
EC          211NAQVAAGQLGGTPVPKGGQ-QLNASIIAQTRL240
NM          NVQISAGSIGSLPAVRGQ-TVTATVTAQGQL
PA          NVQISSGQLGGLPAVKGGQ-QLNATIIIGKTRL
HC          NSQFAAGFFGQEPVRKDL-DF'TYTVTTQGRF
SE          NAQVAAGQLGGTPVPKGGQ-QLNASIIAQTRL
LL          NQEISSGQIGAPPSAGTP-AYQFTVNVPGQL
SM          NAQVAIGQLGGAPPSVKGGQ-QLNATINAQSRL
MC          NVQVSAGQLGTLPTNTDRVVINATISVQSYL
          *  :  :  *  :  *  *          :  :          :
```

Figure 2.2 Sequence alignments of loop region of AcrB homologues. AcrB, AcrD and YhiV are from *E.coli*, MexB and MexD from *Pseudomonas aeruginosa*, Ame from *Agrobacterium tumefaciens*, AdeB from *Acinetobacter baumannii*, CeoB from

Burkholderia cenocepacia, and MtrD from *Neisseria gonorrhoeae*. Asterisks, colons and periods indicate identical, conserved and semi-conserved residues, respectively. P223 was an identical residue in the alignment. The alignment is performed with online T-Coffee Alignment Tools (<http://www.tcoffee.org/Projects/tcoffee/>).

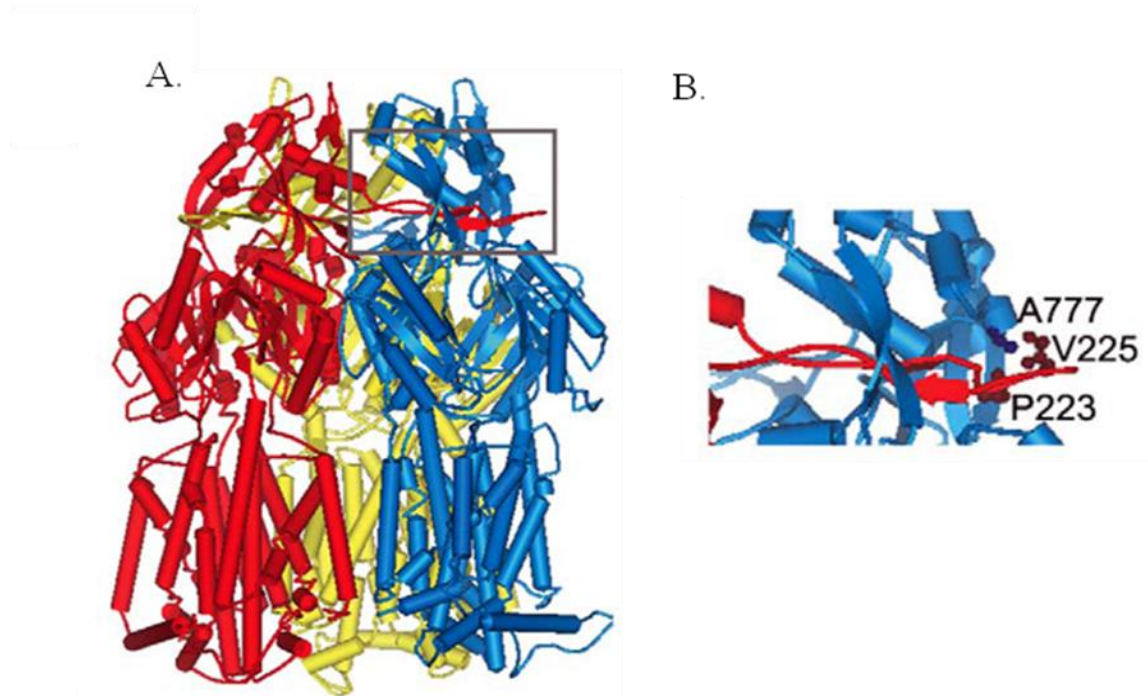


Figure 2.3 Crystal structure of AcrB (Protein Data Bank ID 2HRT).¹⁰⁹ A. AcrB trimer with each subunit color coded. B. Zoom in view of the loop region (grey box in A). Residues P223 and V225 from the red subunit, and A777 from the blue subunits are highlighted using ball-and-stick models.

2.3.2 Efflux Activity of Mutants

Six representative drugs known as substrates of AcrB including antibiotics, dye and detergent, with diverse chemical structures, were used for the drug susceptibilities assay.¹²⁵ The drug resistance of *E. coli* BW25113 Δ *acrB* transformed with plasmid

encoding AcrB mutated plasmids were measured as shown in Table 2.1. Compared with the strain expressing wild type AcrB, the strain containing mutations of P223 reduced the drug susceptibilities by a factor of 4 to 32. Among these mutations P223G had the lowest minimum inhibitory concentration (MICs) to all drugs; P223V and P223Y had similar MICs; P223A and P223N had the highest MICs. The order of mutations activity implied that not the length or the polarity of side chains, but the inflexibility of P223 was the key to the functionality of AcrB. I have also mutated the neighboring amino acid P224, which was not conserved in the alignment, to glycine. Mutant P224G remained fully functional and did not change the drug susceptibilities of the cells (Table 2.1). P223 appeared to be a critical amino acid for the function of AcrB. Therefore, P223G was chosen for further structural analysis. To examine if replacement of P223 by Gly affected the expression level of AcrB, the relative expression level of AcrB_{P223G} and wild type AcrB were determined using both membrane vesicles extracted from the cells and subjected to western blot analysis. The same samples were diluted 5- and 25-fold to reveal the expression levels of the two proteins in the cell. As shown in Figure 2.4, the expression level of the two proteins were comparable, indicating that the decrease of drug resistance was not due to expression level variation (Figure 2.4).

Table 2.1 MIC of BW25113 Δ *acrB* containing plasmid encoding the indicated AcrB constructs.

Plasmids or Mutations	MIC (μ g/ml)					
	Ery	Nov	R6G	TPP	SDS	Tet
pQE70 AcrB	80	160-320	320-640	640	>0.8%	1.28
pQE70	2.5	5	5	5	0.00625%	0.32
P224G	80	160	320	320	>0.8%	1.28
P223G	5	10	20	20	0.2%	0.32
P223A	10	40	80	40	>0.8%	0.64
P223V	5	20	40-80	40	>0.8%	0.64
P223Y	5	20	40-80	20	>0.8%	0.64
P223N	5	40	80	40	>0.8%	0.64
P223G V225C	2.5	5	5	5	0.00625%	0.32
P223G V225C A777C	40	40	160	80	>0.8%	0.64
V225C A777C	80	160	320	640	>0.8%	1.28

*Drugs tested were Erythromycin (Ery), Novobiocin (Nov), Rhodamine 6G (R6G), Tetraphenylphosphonium (TPP), Sodium dodecyl sulfate (SDS), and Tetracycline (Tet).
The unit of MIC for SDS wt/vol.

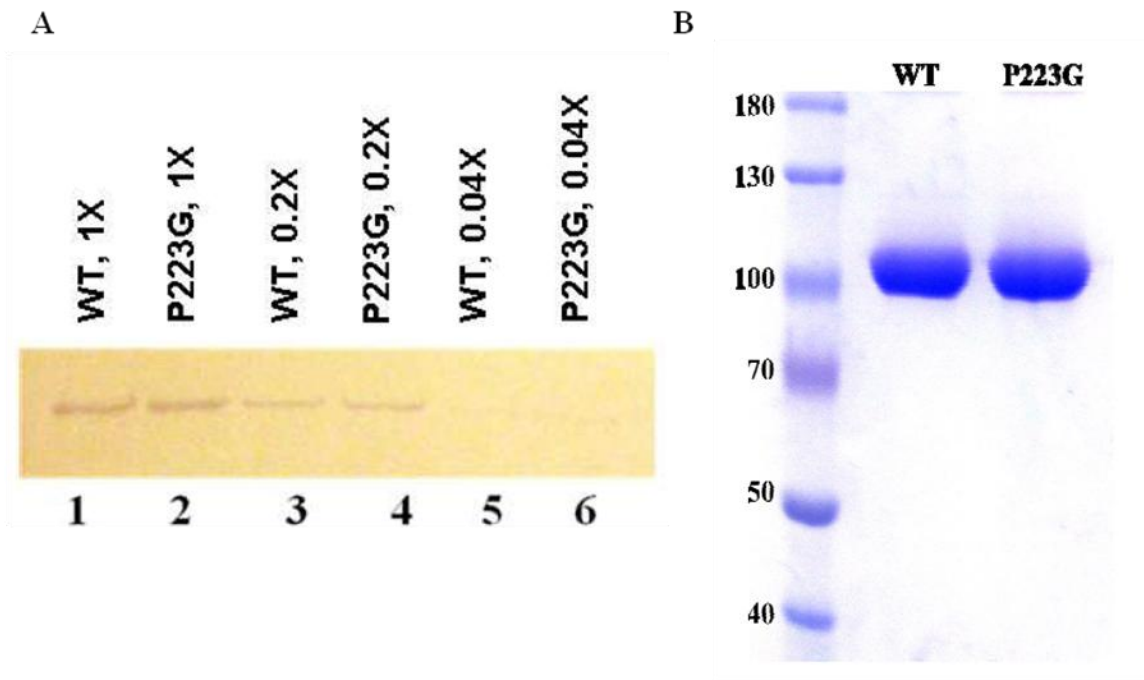


Figure 2.4 Comparison of the expression levels of wild type AcrB and AcrB_{P223G}. A. Western blot analysis of membrane vesicles extracted from BW25113 Δ *acrB* expressing wild type AcrB (WT) or AcrB_{P223G} (P223G). Same amount of bacterial cells for expression of different proteins are used for analysis. Each sample was diluted 1, 5, and 25 fold. B. SDS-PAGE analysis of purified wild-type AcrB and AcrB_{P223G}. The expression level of the WT and P223G are similar in the BW25113 Δ *acrB* strains. B. SDS-PAGE analysis of purified AcrB (WT) and AcrB_{P223G}.

2.3.3 Structure Analysis of AcrB_{WT} and AcrB_{P223G}

AcrB_{WT} and AcrB_{P223G} could be expressed and purified with a decent amount and purity as shown in Figure 2.4. Purified proteins were first analyzed using circular dichroism (CD) spectroscopy to characterize their secondary structure compositions. AcrB_{WT} and AcrB_{P223G} had similar CD spectra and had high content of α -helices as revealed by the negative peaks in the far-UV region (Figure 2.5A). Mutant AcrB_{P223G} had a close secondary structure as AcrB_{WT} and the structure of purified proteins were similar to the reported crystal structure of AcrB-a helix-bundle protein.

Thermal denaturation analysis is a useful tool to investigate the thermal and chemical stability of the membrane proteins *in vitro*.^{155, 156} The purified proteins gradually lose their secondary structures with the increase of temperature, which can be monitored with the change of ellipticity at 222nm. Overall, about 40% loss of α -helical content was observed when temperature increased to 98°C for both AcrB_{WT} and AcrB_{P223G} (Figure 2.5B). The ellipticity at 222 nm of the proteins could not recovery when temperature lowed back to 4 °C, which indicated that unfolding transitions were irreversible. The similar melting curves of AcrB_{WT} and AcrB_{P223G} resembled their structure similarity.

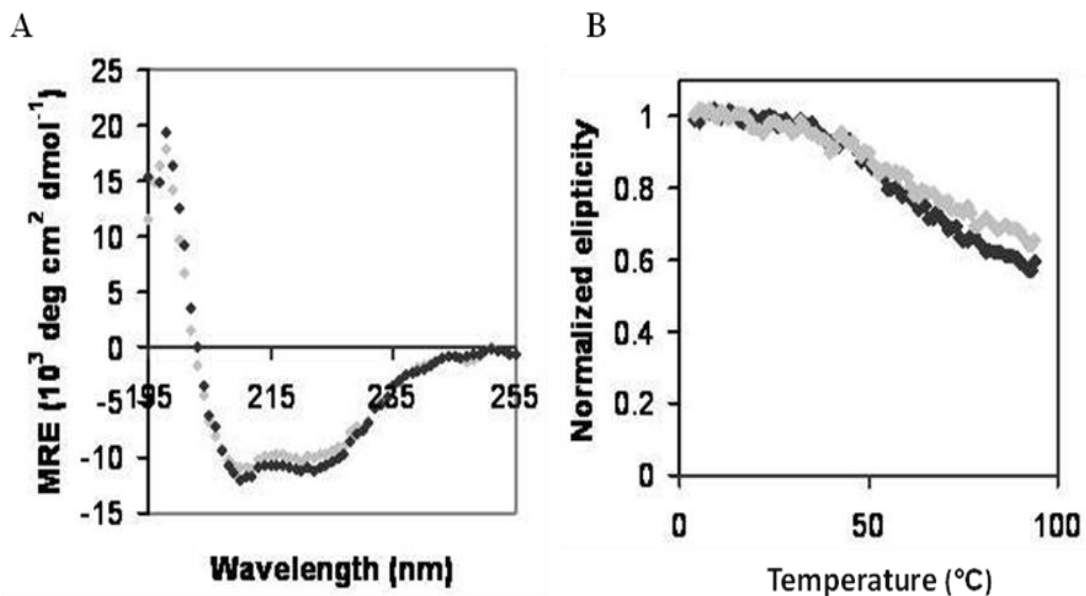


Figure 2.5 Circular Dichroism (CD) characterization of wild type and the mutant. A. Far UV CD spectra of wild type AcrB (black) and AcrB_{P223G} (grey) superimposed well onto each other, indicating the two proteins had similar secondary structure contents. B. Temperature denaturation curves of wild-type AcrB (open diamonds) and AcrB_{Δloop} (filled squares). The ellipticity values monitored at 222 nm were normalized to the reading at 4 °C. The thermal stabilities of the two proteins were very similar.

Limited proteolysis has been widely used to reveal the functional domains, assess the flexible elements and examine the topology of proteins.¹⁵⁷⁻¹⁵⁹ In this study, limited proteolysis was used as an additional method to compare the conformation difference between AcrB_{WT} and AcrB_{P223G}. Clearly, AcrB_{WT} was more resistant to the trypsin digestion than AcrB_{P223G} (Figure 2.6). At room temperature, AcrB_{P223G} were completely digested to smaller fragments in 40 minutes, while detectable AcrB_{WT} full length protein remained after the same digestion period. Based on the proteolysis results, the simple mutation P223G greatly increased the flexibility of the protein and made it more dynamic. The dynamic behavior of the mutated protein might be the reasons that P223G changed the tertiary structure of the protein, especially for the protruding loop part; or it loosen the assembly of the protein and exposed the active sites for digestion.¹⁶⁰

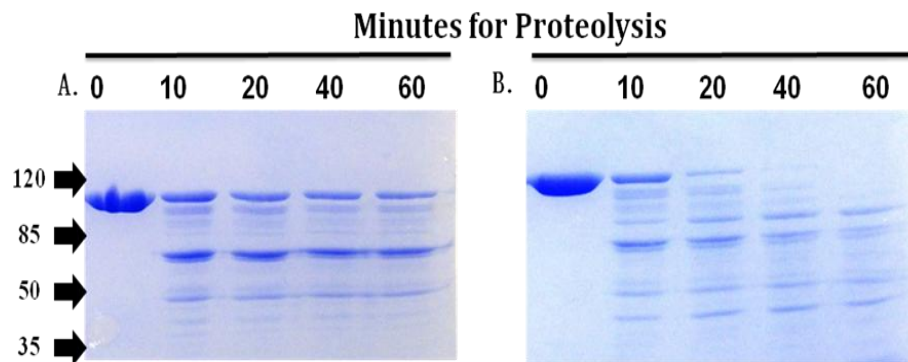


Figure 2.6 Limited trypsin digestion of purified wild type AcrB (A) and AcrB_{P223G} (B). Under the current experimental condition (at room temperature, the weight ratio between trypsin and the protein was 1:200), wild type AcrB was digested much slower than AcrB_{P223G}. Molecular weights (kDa) of bands in the molecular weight marker were marked on the left of the gel.

The CD spectroscopy result showed that AcrB_{WT} and AcrB_{P223G} shared similar secondary structure but cannot explain the increased flexibility due to the mutation. To demonstrate whether P223G changed the tertiary structure of the protein in the molecular level, a disulfide-trapping method was used to probe the conformational change of the mutant. Our group further applied this method for membrane protein study and established a reporter platform for the detection of tertiary change of AcrB under native condition.¹⁶¹ In general, two amino acid residues within a close distance were mutated to cysteines. The introduced cysteines pair formed a disulfide bond under the oxidative environment of the periplasm, detected and visualized after (Figure 2.7A). If the structure of the protein changed, then the distance between the reporter Cys pair would change as well, this would lead to variations in the disulfide bond formation. Five cysteine pairs were introduced into the periplasmic domain of AcrB (Figure 2.7 B). It has been proved that the engineered cysteine pairs did not reduce the activity of the proteins.¹⁶¹ Experimental details could be found in Materials and Methods. As shown in Figure 2.7C, each set of data contains two SDS-PAGE gel pictures, one was stained with Coomassie blue dye and the other visualized with fluorescence imaging. Coomassie blue staining was used to measure the amount of the protein and fluorescence image was to reflect formation of the disulfide bond. In lane 1, the addition DTT released all free cysteines and activated the thiols group to react with fluorescein-5-maleimide (Flu-MAL) as a positive control. In lane 2, the iodoacetamide (IAM) blocked the free cysteines and deactivated the labeling reaction as a negative control. In lane 3, IAM blocked the free cysteines and DTT broke the existed disulfide bond formation and activated the labeling reaction. For each reporter, the mutant P223G had a strong fluorescence intensity band as the respectively positive

control and wild-type, which indicated that the disulfide bond still formed in the mutant. Especially for cysteine pair 216-234, located in the protruding loop and close to P223, the disulfide bond level was the same as wild-type, which conveyed the important information that tertiary structure of the loop might be similar as the wild type. Based on the results, I concluded that the P223G mutation did not detectably change the tertiary structure of the proteins.

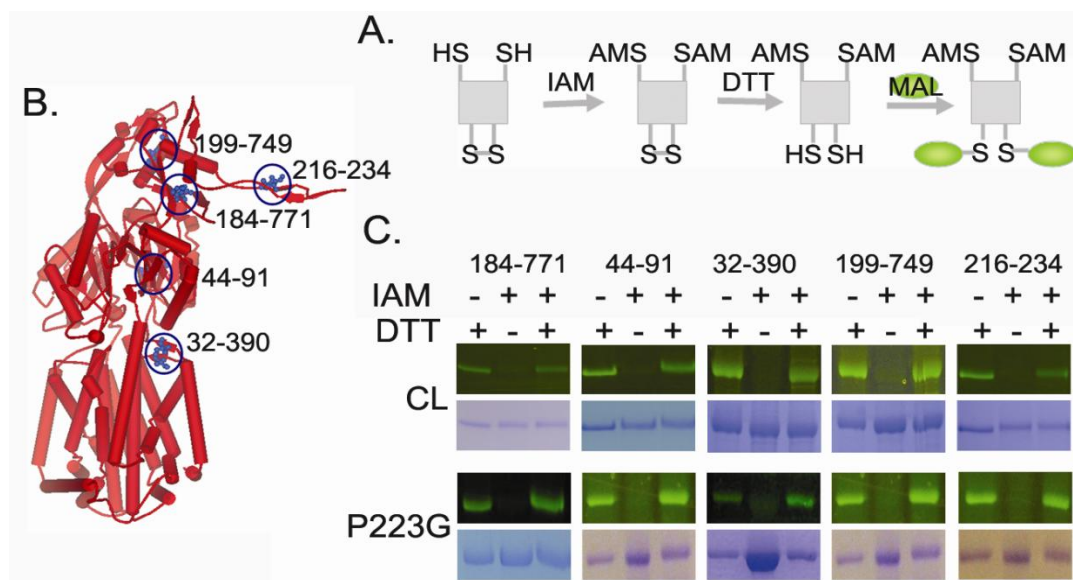


Figure 2.7 The disulfide trapping method. A. Schematic illustration of the blocking-reducing-labeling procedure. B. The location of cysteine mutations for cross-linking pairs in overall structure of AcrB. The reporter pairs were emphasized with stick-ball models. C. Tertiary structure as revealed by the disulfide trapping method. CL is the wild type AcrB with two intrinsic cysteines mutated to alanine. The extents of disulfide bond formation for each reporter were very similar in AcrB_{P223G} as compared to wild type AcrB. Therefore, the overall conformation, or tertiary structure, of AcrB_{P223G} was very similar to that of wild type AcrB.

2.3.4 AcrB_{P223G} Forms Monomer *in vitro* and Trimer *in vivo*

In order to clarify the results of limited proteolysis, Blue native (BN) PAGE is used to characterize the oligomer state of purified AcrB_{P223G}. BN-PAGE is a powerful, convenient and inexpensive technique to determine the oligomeric state of membrane proteins and identify physiological protein-protein interaction.^{162, 163} It has been used to confirm the oligomer state of wild-type AcrB was a trimer.¹²⁰ In figure 2.8A, AcrB_{WT} migrated as a trimer as reported and AcrB_{P223G} migrated as a monomer on the gel. The BN-PAGE result suggested an interpretation for the difference in the limited proteolysis data. The monomeric AcrB_{P223G} exposed additional active digestion site for trypsin. However, the drug resistance results showed that the AcrB_{P223G} still maintained a low level of activity, which implied that the oligomerstate of AcrB still could be a trimer *in vivo*. To further examine the oligomer state of AcrB_{P223G} *in vivo*, an intermolecular disulfide bond (V225C_A777C) was introduced into the mutant AcrB_{P223G} (Fig 2.3B). Western blot analysis of membrane vesicles showed that AcrB_{P223G/V225C/A777C} migrated as trimer in the absence of DTT and was fully reduced in the presence of DTT, confirming the formation of inter-subunit disulfide bond in AcrB_{P223G/V225C/A777C}. The results not only suggested that AcrB_{P223G} existed as trimers *in vivo*, but also further confirmed that the P223G maintained the tertiary structure of the protein, consistent with our previous observation during the intra-molecular disulfide trapping experiments. Through the oligomer state characterization of AcrB_{P223G} *in vitro* and *in vivo*, the functional role of P223 could be derived. It was a key residue to stabilize the functional oligomer state of AcrB. The mutant P223G drastically loosens the association of trimeric AcrB *in vivo* and

affected its function. And the weakly associated trimeric mutant AcrB_{P223G} was easy to dissociate when purified.

Interestingly, the inter-molecular disulfide cross-link (V225C_A777C) also partially restored the pump activity of the mutant AcrB_{P223G} (Table 2.1). Mutant AcrB_{P223G/V225C} was completely functionless; indicating that the restored activity of AcrB_{P223G/V225C/A777C} was not due to the possibility that introduction of V225C changed the overall tertiary structure of the protruding loop. As V225 was very close to P223 according to the crystal structure, the engineered intermolecular cross-link formed strong covalent bond, stabilize the interaction of trimeric AcrB_{P223G} and offset the effect of the glycine. Also, the oligomer state of purified AcrB_{P223G/V225C/A777C} was characterized with BN-PAGE (Fig 2.8A). The AcrB_{P223G/V225C/A777C} maintained trimeric state like AcrB_{WT} under non-reducing condition and reduced to a monomer as AcrB_{P223G} under reducing condition. Moreover, MIC tests have been performed in the presence of 4 mM DTT. Our data showed that the addition of 4 mM DTT had no effect on the drug resistance of AcrB_{WT}, AcrB_{P223G} or the bacterial with the empty plasmid pQE70, but reduced the MIC of AcrB_{P223G/V225C/A777C} (Table 2.2). Western blot analysis of membrane vesicles showed that most AcrB_{P223G/V225C/A777C} was reduced to monomeric state with 4 mM DTT addition to culture condition (Figure 2.8B). All these results supported the fact that V225C_A777C cross-linking favored the assembly of the AcrB_{P223G} trimer.

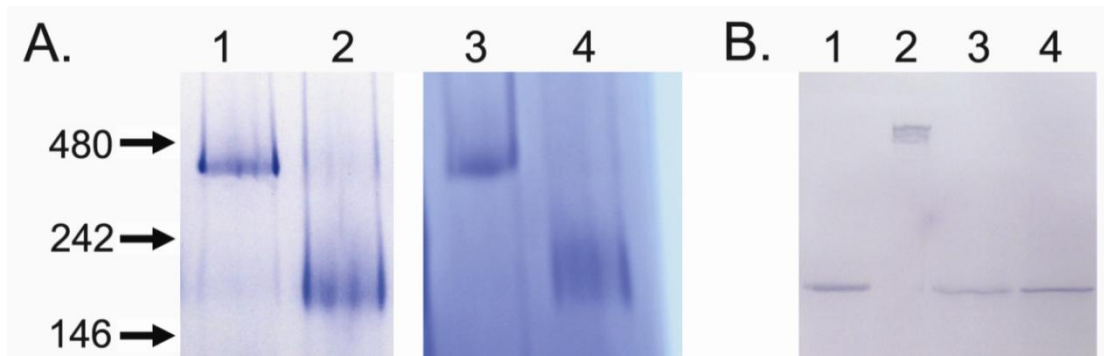


Figure 2.8 BN-PAGE and western-blot analysis of AcrB_{P223G/A225C/N777C}. A. After detergent purification, freshly prepared wild type AcrB samples migrated as a trimer (lane 1) in BN-PAGE. Under the same condition, purified AcrB_{P223G} most migrated as a monomer (lane 2). AcrB_{P223G/A225C/N777C} migrated as a trimer in the non-reducing condition (lane 3), while as a monomer when reduced (lane 4). A 4-20% gradient gel was used in this experiment. B. Western blot analysis of membrane vesicles extracted from BW25113*DacrB* expressing wild type AcrB (lane 1 and 3) or AcrB_{P223G/A225C/N777C} (lane 2 and 4) in the absence (lane 1 and 2) or presence (lane 3 and 4) of 4 mM DTT. Dr Wei Lu performed BN-PAGE analysis for AcrB_{P223G/V225C/A777C}.

Table 2.2 MIC of BW25113 Δ *acrB* containing plasmid encoded AcrB measured in the presence or absence of DTT.

Plasmids or Mutations	MIC (μ g/ml)			
	No DTT	4 mM DTT	No DTT	4 mM DTT
	(Ery)	(Ery)	(TPP)	(TPP)
pQE70 AcrB	80	80	640	640
pQE70	2.5	2.5	5	5
P223G	5	5	20	20
P223G V225C_A777C	40	20	80	20-40

*Drugs tested were Erythromycin (Ery) and Tetraphenylphosphonium (TPP).

2.4 Discussion and Conclusion

In a previous study, our group had created an AcrB mutant with truncated loop and found that the mutant folded into a monomer, consistent with a three-stage pathway for the assembly of AcrB: the first well-folded AcrB monomer and then packed into a functional trimer.

In this work, I studied the amino acid residue P223 in the loop and identified its functional role. Based on previous research, it appeared that P223 was not involved in the substrate binding site, proton translocation network and drug extrusion pathway.^{61, 109, 121-123, 125, 164-166} I assumed that the rigidity of P223 helped to stabilize the oligomer of AcrB. To test the hypothesis, I first used site-mutagenesis to replace P223 with several other amino acids and evaluated their transport activity with different substrates of AcrB. All mutations of P223 greatly reduced its activity. Especially, the mutant P223G had the lowest activity, which indicated the importance of side chain rigidity. The expression level analysis showed that the loss of the pump activity was not caused by a decrease of level of the mutant proteins. AcrB_{P223G} was chosen for further structure characterization. The secondary and tertiary structure of AcrB_{P223G} and AcrB_{WT} were compared via CD spectroscopy and intramolecular disulfide trapping method. AcrB_{P223G} was found to fold into a structure similar to individual subunits in AcrB_{WT}. However, limited proteolysis revealed that AcrB_{P223G} contained more accessible digestion sites. BN-PAGE determined that most purified AcrB_{P223G} exists as monomer. The disulfide cross-linking experiment revealed the AcrB_{P223G} formed trimer *in vivo*. The different oligomer states of AcrB_{P223G} *in vitro* and *in vivo*, correlated with its loss of activity, indicated a pivotal role of P223 in

stabilizing the entire trimeric structure. The inactivation of AcrB_{P223G} could be partially rescued by the V225C_A777C intermolecular cross-linking.

From the protein characterization data and crystal structure, the unique backbone structure of P223 lead to the formation of a kink (Figure 2.3). It may acts as a wedge to lock the loop in the tunnel in the neighboring subunit and stabilize the trimeric structure. This study revealed the importance of the loop to tunnel interaction for AcrB trimer stability. There are three possibilities for the loop-tunnel interaction process: loop first, the loop forms a stable tertiary structure and the tunnel maintains a certain degree of flexibility; tunnel first, the tunnel forms a stable tertiary structure and the loop still maintains a certain degree of flexibility; or both the loop and tunnel keep some degree of flexibility during the association. To test the flexibility of the loop during trimerization, a reporter Cys-pair C216-C234 was introduced to the loop (Figure 2.7B). This pair of intramolecular cysteines formed a disulfide bond both in AcrB_{WT} and AcrB_{P223G} as indicated in Figure 2.7C, which indicated the mutant P223G did not change the conformation of loop. C216-C234 disulfide bond formation also restricted the conformation of the loop, but had no effect on the transport activity of AcrB_{WT} or AcrB_{P223G}. These results would suggest that the loop formed a stable tertiary structure during the association. In addition, the mutant P223Y is still partially active, which indicated that the AcrB_{P223Y} remains a trimeric structure *in vivo*. If the tunnel forms a fixed structure, it is difficult for the loop of AcrB_{P223Y} to penetrate due to the bulky side chain. Taken together, the “loop first” mechanism for the assembly is supported by our results.

A similar observation was also made in the AcrB homologous-MexB in *Pseudomonas aeruginosa*¹⁶⁷. Point mutations in the loop affected MexB activity and it was speculated that the amino acid residues were involved in its trimerization. Our observations of the importance of P223 in AcrB also supported their assumptions. Combined with our previous study¹⁶⁰, the role of P223 helped us to further understand the oligomerization process of AcrB--the well folded AcrB monomer recognized its neighbor subunit with the protruding loop, packed into a stable and fully functional trimer with the P223 residues.

The oligomer structure is the essential architecture for the function of many membrane proteins. The stability of the oligomer complex modulates the functionality of the membrane proteins.^{168, 169} Here I used a homo-trimeric membrane protein, AcrB, as a model system and investigated the correlation between the oligomer stability and protein activity. We found the mutation of a residue P223 “loosened” the AcrB trimer and thus drastically decreased the transport activity of the efflux pump. The engineered inter-subunit disulfide bond partially the activity of the mutant. My result implied that the long protruding loop remained a rigid tertiary structure and the tunnel in the neighboring subunit kept a certain degree of flexibility during the association.

Chapter 3 Alanine-Scanning Study of the Protruding Loop of AcrB

3.1 Introduction

In chapter 2, a conserved residue P223 in the protruding loop was found critical for trimerization of AcrB. Replacement of P223 with glycine or alanine “loosened” the stability of trimer and dramatically reduced the protein activity. In this chapter, I further investigated the role of each residue in the loop. The question I want to answer in this chapter is: whether the backbone structure of the loop or the side chain of each residue is more important for the assembly of AcrB and its efflux activity. I used the alanine-scanning method to substitute each residue with alanine and test the activity of each mutant using a drug susceptibility assay. The alanine-scanning method has been used to determine the contribution of a specific residue for the stability or function of a protein.¹⁷⁰ The residues on the interface of protein are usually replaced with alanine for study the protein-protein interaction.¹⁷¹ Important residues involved in the protein-protein interaction could be identified through the method. In addition, to investigate the importance of backbone structure, a chimeric AcrB construct-AMA has been designed and constructed. The protruding loop (residues from 211-240) of AcrB was replaced with a loop from its homologue—MexB. AcrB and MexB are the only two proteins from the multidrug resistant proteins of RND family with their crystal structures determined.^{107, 172} The overall structures of those two proteins are similar, including the loop part. The backbone structure of the loops overlapped very well (Figure 3.1A). The structure analysis and activity test of chimeric AcrB-AMA would reveal the importance of backbone structure as compared to the side chain composition to the oligomerization stability and function of AcrB.

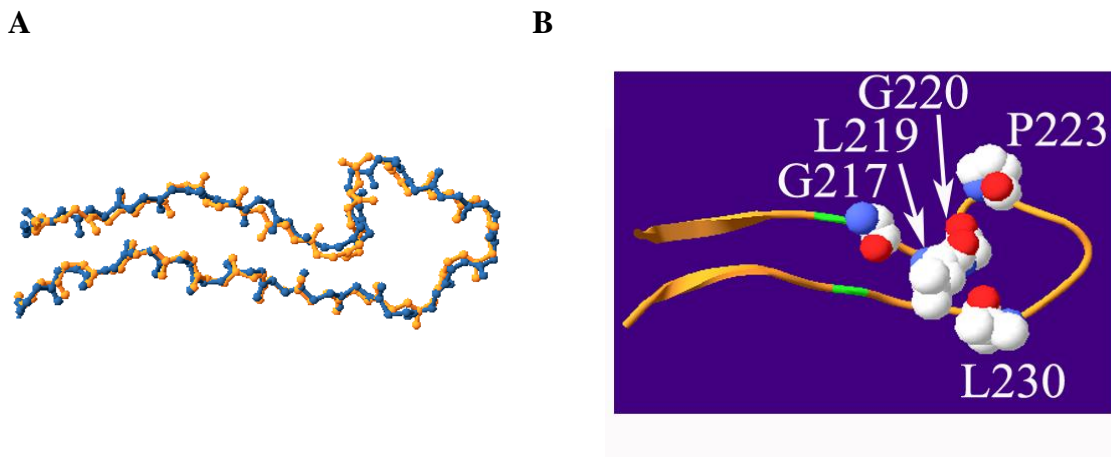


Figure 3.1 The structure and amino acid composition of loop. A. Superposition of the backbone traces of loops from AcrB (blue) and MexB (orange). B. The residues in the loop affected the activity of AcrB. The residues are highlighted with ball model. The position A214 and I234 were green. The pictures were adopted from reference

3.2 Materials and Methods

3.2.1 Site-Directed Mutagenesis, Expression, Purification and Activity Assay

Single point mutations were introduced with the Quick-Change site directed mutagenesis kit (Stratagene, La Jolla, CA). AcrB and its mutants were expressed and purified as described in section 2.2.3. AcrB drug efflux activity was measured by recording the minimum inhibitory concentration (MIC) of an *acrB* gene knockout strain (BW25113 Δ *acrB*) transformed with plasmid encoded AcrB or its mutant using agar plates as described in section 2.2.4.

3.2.2 Construction of AMA

Construct AMA, which is basically AcrB sequence containing the loop from MexB, was created by Dr. Jun Fang. The experimental process is included here for the completeness of the discussion. The AMA gene was constructed using overlapping PCR, as shown in Figure 3.2. Primers AMA-loop1F, AMAloop1R, AMA-loop2F, and AMA-loop2R are chimeric primers that contain a fragment of AcrB sequence and a fragment of MexB sequence (underlined). The MexB loop was amplified using primers AMA-loop1F (5'-GGTTGATGTCATTACCGCCATCAAAGCGCCAGAACGTGCAGATTTCTCCG-3') and AMA-loop2R (5'-CAGGATTTTGCCGAACTCT TCAGTGGTCTGCAGGCGGGTCTTGCCGATGATG-3'). The fragment of the 5'-end portion of AcrB was amplified using primers pET22-AcrB-F (5'-GTACCATATGCCTAATTTCTTTATCGATCGCCC-3') and AMA-loop1R: (5'-CCGAGCTGGCCGGAGGAAATCTGCACGTTCTGCGCTTTGATGGCCGGTAAT-3'). The above two PCR products were gel purified and mixed at a 1:1M ratio to serve as the template for the second round of PCR, using primers pET22-

AcrB-F and AMA-loop1R. The resultant product encodes the N-terminal 210 residues of AcrB and residues 211 to 240 from MexB (the loop), and then residues 241 to 249 of AcrB (fragment AM). The fragment of the 3'-end portion of AcrB was amplified using primers AMA-loop2F (5'-CATCATCGGCAAGACCCGCCTGCAGACCACTGAAGAGTTCGGCAAATCCTG-3') and pET22-AcrB-R (5'-GTACCTCGAGATGATGATCGA CAGTATGGCTGTGCT-3'). Finally, full-length AMA gene was constructed similarly through PCR using a mixture of AM and the 3'-end portion of AcrB as template and pET22-AcrB-F and pET22-AcrB-R as primers. The PCR product corresponding to the chimeric gene of AMA was purified after agarose gel electrophoresis and digested using *NdeI* and *XhoI*. The digested PCR was subsequently ligated into pET 22b digested with *NdeI* and *XhoI*. The construct gene was confirmed by DNA sequencing.

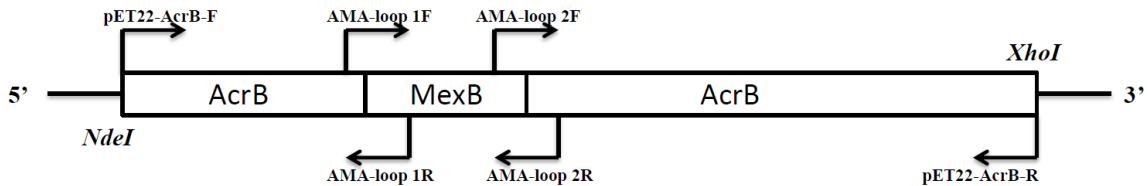


Figure 3.2 The strategy to construct chimeric AMA gene using overlapping PCR. Primers AMA-loop1F, AMA-loop1R, AMA-loop2F, and AMA-loop2R are chimeric primers that contain a fragment of AcrB sequence and a fragment of MexB sequence.

3.2.2 Expression Level Analysis Using Western Blot

BW25113 Δ *acrB* cells transformed with plasmids encoding AcrB or its mutants were cultured at 37 °C overnight. The cells were harvested, resuspended in sodium phosphate buffer (pH 7.4), and lysed using a French press. Cell debris was removed through a low-

speed centrifugation and membrane vesicles were collected by ultracentrifugation at 150,000 g for 1 h at 4 °C. Membrane vesicles were solubilized in sodium phosphate buffer (pH 7.4) containing 2% (wt/vol) SDS at room temperature and separated on a 8% SDS-PAGE gel. The proteins were transferred to a nitrocellulose membrane (Millipore, Bedford, MA) and detected as described in 2.2.5.

3.2.3 CD Spectroscopy, and BN-PAGE Analysis

CD spectra and temperature denaturation scans were collected on a JASCO J-810 spectrometer as described in section 2.2.6. BN-PAGE was performed as described in section 2.2.7.

3.3 Results

3.3.1 Ala-Scanning of Loop

Before I started the Ala-scanning experiment of the loop and test each mutant, the primary sequence alignment for the loop from different homologues of AcrB provided a guideline to identify critical residues (Figure 2.2). Among the 30 residues in the loop, 4 were identical (N211, G217, G220, and P223), and 7 conserved (Q213, V214, A215, L219, S233, I234 and L240). Each non-Ala residue in the loop was replaced with alanine systematically and the activity of the mutants was examined with drug susceptibilities assay (Table 3.1). As shown in Table 3.1, most Ala substitutions did not affect the MIC level of the bacteria, which indicated that the mutated AcrB was still well functional. Only five mutations (G217A, L219A, G220A, P223A, and L230A) drastically reduced the MIC (bold fonts in Table 3.1). P223 has been characterized and discussed in detail in the previous chapter. Compare with the sequence alignment, I found that not all conserved residues were important for AcrB function and not all critical residues were conserved. Residues N211A, Q213A, V214A, S233A, I234A, and L240A had no observable effect on the efflux activity of the protein. Among the five residues that were sensitive to Ala replacement, L230 not conserved, L219 are conserved, while G217, G220, and P223 are identical among all sequences aligned. Positions of these residues along the loop are highlighted in Figure 3.1B. I found that all five residues clustered close to the tip of the loop.

The expression level of each mutant was measured with Western blot to test whether the decreased activity of protein was due to reduced expression (Figure 3.3A). The

expression level of all the mutants was similar. These results ruled out the possibility that the five mutants expressed low level of AcrB and reduced its activity.

The substrate binding site in AcrB locates in the center of the periplasmic domain, distant from the loop.^{110, 122, 130, 131} Mutations in the extended loop are not likely to directly affect substrate binding. However, it is possible that substrate binding might be affected as a result of changes of inter-subunit interaction caused by mutations in the loop. To examine if mutations in the loop impaired the inter-subunit interaction and decreased the trimer stability, AcrB_{L230A} was chosen for further investigation of its oligomeric state using BN-PAGE (Figure 3.3B). BN-PAGE has been used to confirm that wild type AcrB is a trimer in the chapter 2 and other publications.^{120, 173} The results of BN-PAGE showed that after purification, AcrB_{L230A} existed as a mixture of monomer and trimer. It was confirmed that under the same experimental conditions, wild type AcrB migrated as a trimer.

Table 3.1 Drug resistance of BW25113*ΔacrB* expressing plasmids and mutations.

Plasmids	Ery	R6G	Nov	Aci	TPP	SDS(%)
pQE70-AcrB	80	320	320	80	640	>0.8
pQE70	2.5	5	10	10	10	0.01
pQE70-AcrB _{N211A}	80	320	320	80	640	>0.8
pQE70-AcrB _{Q213A}	80	320	320	80	640	>0.8
pQE70-AcrB _{V214A}	80	320	320	80	640	>0.8
pQE70-AcrB _{G217A}	10	80	40	20-40	80	0.2
pQE70-AcrB _{Q218A}	80	320	320	80	640	>0.8
pQE70-AcrB _{L219A}	20-40	20-40	20	20-40	10	0.05-0.1
pQE70-AcrB _{G220A}	5	80	40	40	20	0.80
pQE70-AcrB _{G221A}	80	320	320	80	640	>0.8
pQE70-AcrB _{T222A}	80	320	320	80	640	>0.8
pQE70-AcrB _{P223A}	10	80	40	40	40	>0.8
pQE70-AcrB _{P224A}	80	320	320	80	640	>0.8
pQE70-AcrB _{V225A}	80	320	320	80	640	>0.8
pQE70-AcrB _{K226A}	80	320	320	80	640	>0.8

Plasmids	Ery	R6G	Nov	Aci	TPP	SDS(%)
pQE70-AcrB _{G227A}	80	320	320	80	640	>0.8
pQE70-AcrB _{Q228A}	80	320	320	80	640	>0.8
pQE70-AcrB _{Q229A}	80	320	320	80	640	>0.8
pQE70-AcrB _{N211A}	80	320	320	80	640	>0.8
pQE70-AcrB _{L230A}	5	20	20	20	10	0.10
pQE70-AcrB _{N231A}	80	320	320	80	640	>0.8
pQE70-AcrB _{S233A}	80	320	320	80	640	>0.8
pQE70-AcrB _{D234A}	80	320	320	80	640	>0.8
pQE70-AcrB _{D235A}	80	320	320	80	640	>0.8
pQE70-AcrB _{Q237A}	80	320	320	80	640	>0.8
pQE70-AcrB _{T238A}	80	320	320	80	640	>0.8
pQE70-AcrB _{T239A}	80	320	320	80	640	>0.8
pQE70-AcrB _{L240A}	80	320	320	80	640	>0.8

Notes: Drugs tested were erythromycin (Ery), novobiocin (Nov), rhodamine 6G (R6G), tetraphenylphosphonium bromide (TPP), acriflavine (Aci) and sodium dodecyl sulfate (SDS)

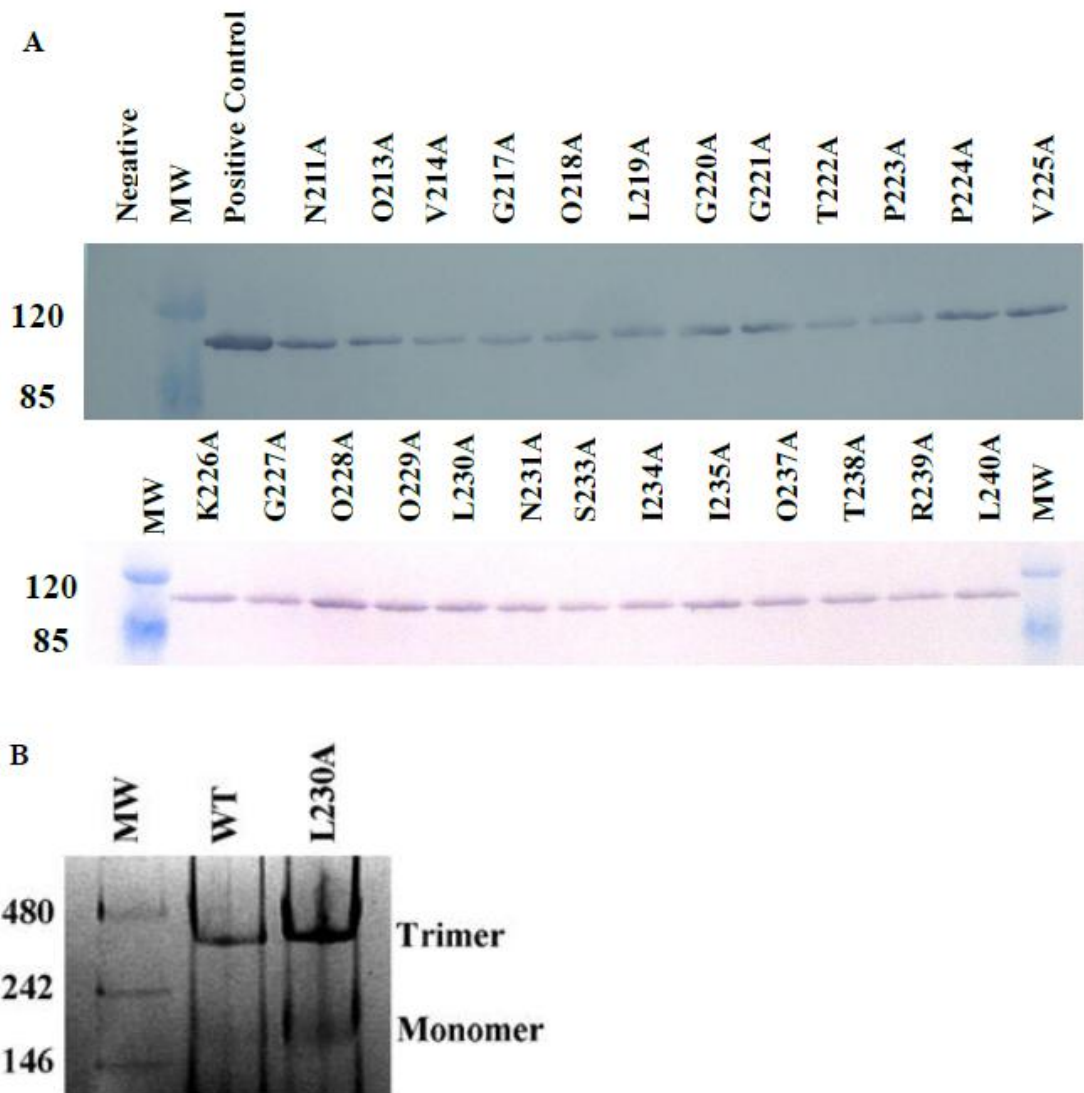


Figure 3.3 Expression levels of loop mutants and BN-PAGE analysis of AcrB_{L230A}. A. Western blot analysis of membrane vesicles extracted from BW25113Δ*acrB* containing different plasmid encoded wild type AcrB or AcrB mutants. The strain containing no plasmid was used as the negative control, and purified AcrB was used as the positive control. The five mutants that affected the MIC are underlined. B. BN-PAGE analysis of AcrB L230A. WT AcrB was also loaded as a control. MW is the molecular weight

marker and the molecular weights of each band are labeled on the left (kDa). Dr. Jun Fang performed the BN-PAGE experiment.

3.3.2 Activity of Chimeric AcrB

To probe the tolerance of the protein to multiple loop mutations, a chimeric AcrB construct was created, in which the loop sequence was replaced with the loop from protein MexB. The overall structures of the two proteins are very similar, including the loops. Their backbone traces superimposed onto each other very well (Figure 3.1A). Apparently both sequences are compatible with the same backbone conformation, although the exact amino acid compositions of the two loops are not identical. Of the 30 residues in the loop, 9 are different (Figure 2.2). Through genetic modification, we have replaced the loop of AcrB (residues number 211 to 240) with the loop of MexB, and then examined the function of the mutant protein. If the backbone conformation rather than the composition of the side chains plays a dominant role, then the MexB loop should perform well and facilitate the assembly of the AcrB trimer. On the contrary, if AcrB mutant containing the MexB loop cannot assemble into a functional trimer, then more specific interactions between side chains of interface residues are necessary. In this case, the 9 different residues were replaced simultaneously with the corresponding residues from AcrB. It was found that the resultant chimeric protein, AMA, remains partially active. Although 9 residues have been changed, the activity level of the chimeric protein is similar to or even better than several mutants containing Ala mutation at a single invariable or conserved site (Table 3.1).

3.3.4 Structural Characterization of AMA

The expression level of AMA was comparable to wild type AcrB (Figure 3.4A). AMA was purified for further structural characterizations. The secondary structure of the mutant was compared with that of wild type protein (Figure 3.4 C/D). The far UV CD spectra of the two proteins superimposed well, indicating that AMA has similar secondary structure as WT. To examine the effect of mutation on the stability of the protein structure, reduction of the ellipticity at 222 nm was monitored with increase of temperature. As shown in Figure 3.4 D, the melting curve of wild type AcrB (black) was slightly steeper than the curve of AMA, while the midpoint transition temperatures of the two proteins were very similar. This result suggests that the overall stabilities of the two proteins are similar, while the unfolding of wild type AcrB might be slightly more cooperative. The oligomeric state of purified AMA was characterized with BN-PAGE (Figure 3.4 B). The purified AMA existed as a mixture of monomer and trimer on BN-PAGE. Under the same condition, wild type AcrB migrated predominantly as a trimer. AMA trimer is less stable than AcrB trimer. However, it is difficult to speculate exactly to what extent AMA formed trimer in the cell. Since AMA was partially active, at least a portion of AMA existed as trimer in the cell.

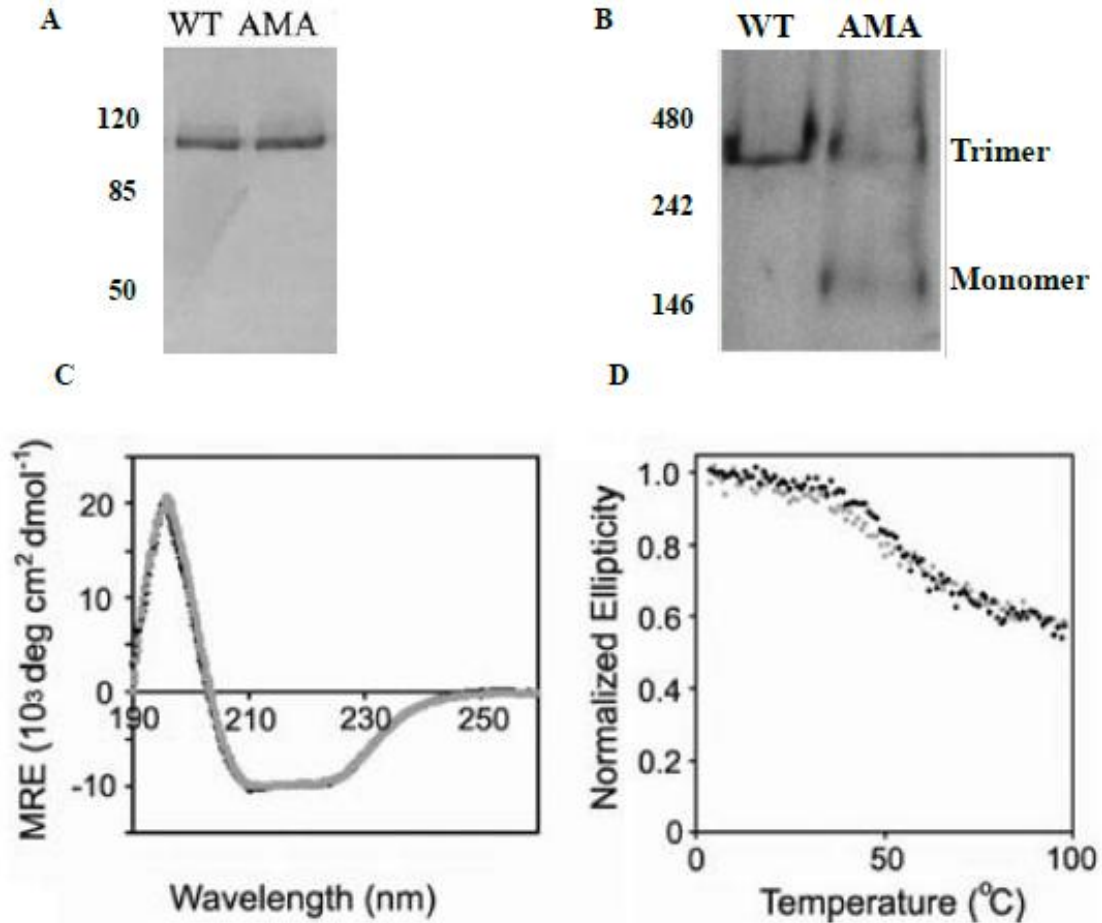


Figure 3.4 Structural characterization of AMA. A. Expression level comparison between wild type AcrB and AMA. B. BN-PAGE analysis of wild type AcrB and AMA. C. CD spectra of purified WT AcrB and AMA. Wavelength scans at the far UV region of WT AcrB (black) and AMA (gray) superimposed well each other. D. Temperature denaturation curves of WT AcrB and AMA. The ellipticity values monitored at 222nm from 4 °C to 98 °C. Dr. Jun Fang performed those experiments.

3.4 Discussions

AcrB is an obligate trimer. No monomeric or dimeric wild type AcrB have been observed in the cell membrane. Freshly purified AcrB samples migrate exclusively as a trimer band in native gel electrophoresis. It was demonstrated that individual subunits of AcrB were capable of folding into independent structurally stable monomers.¹⁵¹ In other words, assistance from neighboring subunit was not necessary for an AcrB subunit to achieve its tertiary structure. If AcrB monomers are capable of folding into stable structures, then why are AcrB monomers so scarce in the cell membrane? The lack of monomeric AcrB indicates that its oligomerization in cell membrane must be very efficient—the inter-subunit association must be kinetically fast, dissociation must be slow, and the resultant oligomer must be thermodynamically very stable. Fascinated by the efficiency of AcrB trimerization in cell membrane, the inter-subunit interaction was investigated in AcrB, which leads to oligomerization.

AcrB contains both a transmembrane domain and a periplasmic domain, with the major inter-subunit interaction contributed by the periplasmic domain. When AcrB trimerizes, the loop-and-tunnel interaction between neighboring subunits contributes approximately 1,500 Å² of buried surface area (BSA), which corresponds to 45% of the overall inter-subunit interface.¹⁷⁴ Studies have shown that protein-protein interactions with interfaces larger than ~1000 Å² are likely to undergo conformational changes upon binding.^{175, 176} In chapter 2, I introduced a Cys-pair in the loop, A216C-I234C.¹⁷³ This pair of Cys did form a disulfide bond in AcrB, which greatly restricted the flexibility of the loop but had no effect on the drug efflux activity. These results suggested that the loop remained rigid during trimerization. Consistent with previous observation, here I found that the

compatibility of the loop sequence with a pre-determined loop conformation is more important than the actual identity of residues making up the loop. The replacement of 9 residues simultaneously in the loop only led to a partial loss of trimer stability and efflux activity, indicating that AcrB trimers tolerated non-ideal interactions among residues, providing the backbone conformation of the loop was satisfied. Similarly, when ranked according to their contributions to the BSA (Table 3.2), the top 8 contributors in the loop are I235, P223, L219, T222, Q213, A215, I234 and N231 with respective 121.94, 94.41, 93.66, 89.58, 76.42, 75.52, 75.43, and 69.52 Å². And yet, Ala substitutions of these residues, except for P223 and L219, had little effect on the structure and function of AcrB. Residues that are sensitive to Ala replacement clustered close together, forming a collar or belt, close to the tip of the loop (Figure 3.1B). In addition, two out of the five residues are glycine. These residues are more likely to be geometrically important to the backbone conformation of the loop. However, the potential contribution from side chains that engages in specific interactions with other residues in the neighboring subunit could not be completely ruled out. The belt of functionally sensitive residues may be the site of inter-subunit recognition during trimerization, serving as a fishing pole, or a locking zone to stabilize the inter-subunit interaction after two subunits bind together.

Table 3.2 The surface area of residues in the loop, the calculated area is based on the server (PDBePISA)¹⁷⁴

Residues in the loop	ASA	BSA
N211	0.07	0.00
A212	26.27	0.00
Q213	90.96	76.42
V214	69.78	46.22
A215	91.59	75.52
A216	42.55	41.81
G217	53.30	51.05
Q218	98.19	51.13
L219	93.66	93.66
G220	12.40	12.11
G221	26.88	25.04
T222	137.02	89.58
P223	113.15	94.41
P224	96.54	55.62
V225	100.32	60.42
K226	209.70	10.18
G227	61.49	23.42
Q228	86.00	67.23
Q229	164.93	33.13
L230	116.68	54.99
N231	97.56	69.52
A232	32.50	25.03
S233	72.25	60.06
I234	75.79	75.43
I235	141.36	121.94
A236	44.64	41.38
Q237	88.22	64.57
T238	75.59	5.97
R239	65.25	20.90
L240	27.45	0.00

Note: ASA, accessible surface area Å²; BSA, Buried Surface Area, Å²

Chapter 4 Role of R780 for the Stability and Functionality of AcrB

4.1. Introduction

In chapter 2 and 3, the protruding loop of AcrB related to its functionality has been investigated in detail. A conserved residue P223 was identified to be critical for the function of AcrB. The site-mutagenesis studies of the residue showed that a single mutant P223G severely reduced the protein activity. Then a systematically alanine-scanning study of the loop and construction of a chimeric AcrB with the loop replaced with its analogue MexB revealed that the conformation of the loop, especially the collar or belt conformation close to the tip of the loop is extremely important for the trimerization of AcrB and its function. P223 is located at the tip of the loop and serves as a “wedge” to stabilize the trimeric AcrB. To further understand the interaction between the loop and tunnel of AcrB, the residues in the tunnel which is involved in the association with P223 is studied in this chapter. From the crystal structure, a semi-open binding pocket for P223 is composed of residues W187, Y275, Q584, A777 and R780 from the neighboring subunit (Figure 4.1). The side chains of W187, Y275, Q584 and A777 anchor the rigid P223 via van der Waals interactions; the side chain of R780 forms a hydrogen bond to the backbone carbonyl oxygen of and potentially plays a critical role in bridging the two subunits. Here I focused on the investigation of the role played by R780 in AcrB structure and function.

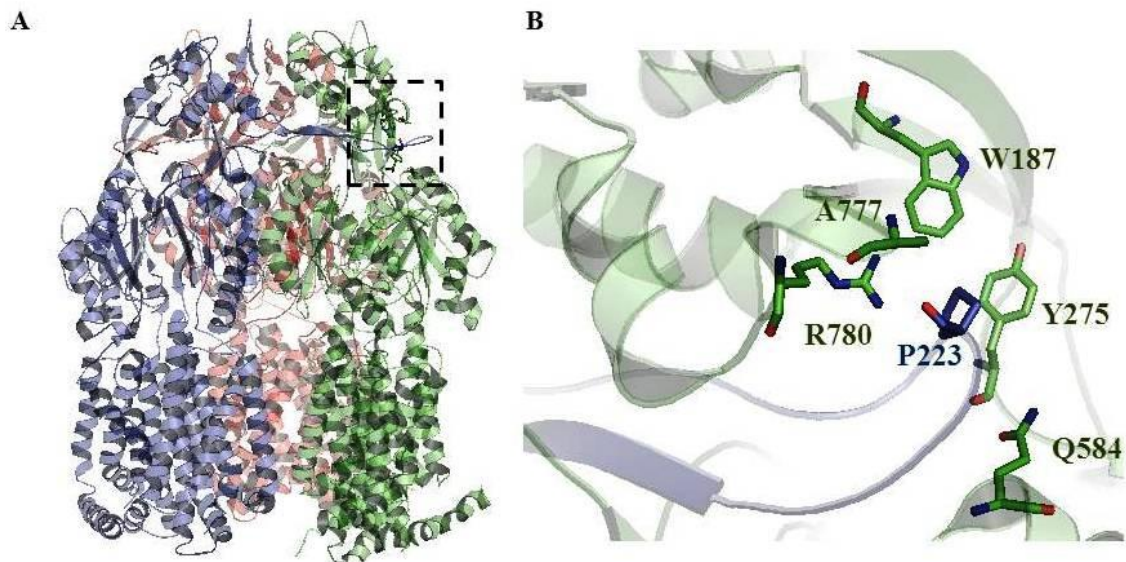


Figure 4.1 Proposed binding pocket of P223. **A.** AcrB trimer with each subunit color coded (Protein Data Bank ID 2DRD)⁶¹ **B.** Proposed binding pocket of P223, residues that form the binding pocket was shown in green.

4.2 Materials and Methods

4.2.1 Materials

Protein molecular weight markers for SDS-PAGE and BN-PAGE were from Fermentas (Glen Burnie, MD) and Invitrogen (Carlsbad, CA), respectively. The custom polyclonal rabbit anti-AcrB, AcrA and TolC were ordered from GenScript (Piscataway, NJ) and Pacific Immunology (Ramona CA), respectively. *Escherichia coli* gene knockout kit was from Gene Bridges (Heidelberg, Germany). Oligonucleotides were from Integrated DNA Technologies, Inc (Coralville, IA). All enzymes were from New England Biolabs (Ipswich, MA). The parent WT (BW35113) and Δ *acrB* knockout strain BW35113 Δ *acrB* strains were obtained from the Yale *E. coli* genetic stock center.

4.2.2 Site-Directed Mutagenesis, Expression, Purification, Activity Assay and Expression Level measurement

AcrB and its mutants were expressed and purified as described in section 2.2.3. AcrB drug efflux activity was measured by recording the minimum inhibitory concentration (MIC) of an *acrB* gene knockout strain (BW25113 Δ *acrB*) transformed with plasmid encoded AcrB or its mutant using agar plates as described in section 2.2.4.

4.2.3 CD Spectroscopy and Disulfide Trapping Method

CD spectra and temperature denaturation scans were collected on a JASCO J-810 spectrometer as described. Disulfide trapping was performed as described in section 2.2.6

4.2.4 Blue Native (BN)-PAGE Analysis

BN-PAGE was performed with modified procedure.¹⁶² Briefly, blue native loading buffer was added into purified AcrB_{WT}, AcrB_{P223G}, and AcrB_{R780A} at a final concentration of 0.1 M 6-aminoocaproic acid, 10 mM Bis-Tris-HCl, 6% sucrose, 1% Coomassie brilliant blue G-250, pH 7.0. Protein samples were load to a 4-20% gradient polyacrylamide gel (Bio-Rad, Hercules, CA). The electrophoresis was performed using a cathode running buffer containing 50 mM tricine, 7.5 mM imidazole, 0.02% coomassie blue G-250, pH 7.0 and anode buffer with 25 mM imidazole, pH 7.0 in the 4 °C refrigerator at 15 mA for 2 hours. The protein bands were visualized with Coomassie Blue stain and analyzed with ImageJ (NIH).

4.2.5 Ethidium Bromide Accumulation Assay

The ethidium bromide accumulation assay was performed followed the reference.¹⁷⁷ Briefly, the bacterial cells with the mutant AcrB were cultured to OD₆₀₀ of 1. The cells were harvested and resuspended in buffer containing 10 mM sodium phosphate, 100 mM sodium chloride, 0.1% glycerol, pH 7.4. The cells were diluted to OD₆₀₀ of 0.2 in the same buffer above. 5 μM ethidium bromide was added to the diluted cells to monitor the fluorescence change at the room temperate using a Perkin Elmer LS-55 fluorescence spectrometer (Perkin Elmer, Waltham, MA). The excitation and emission wavelength were set 520 and 590 nm respectively.

4.2.6 Fluorescent Dye Labeling Assay

The fluorescent substrate labeling assay was performed following a published protocol.¹⁷⁸ 10 ml cells were grown overnight at 37 °C, and were washed twice and resuspended with 10 ml phosphate buffer (50 mM potassium phosphate, 0.5 mM MgCl₂, pH 7.0). The cell density was adjusted to OD₆₀₀ about 2.5. Glucose and Bodipy-FL-maleimide (Sigma-Aldrich, St. Louis, MO) were added to the 10 ml cells to the concentration of 0.4% (w/w) and 6 mM, respectively. The cells were cultured for 1 hour at 30 °C and then washed twice with 5 ml phosphate buffer with 0.4% glucose and again with 5 ml phosphate buffer. The cells were lysed by sonication on ice for 3 min with 10 s on/off intervals. After centrifuged at 15,000×g for 20 min at 4°C, the supernatant was discarded. Pellet was resuspended in extraction buffer A (20 mM Tris-HCl, 100 mM NaCl, 1% Triton X-100, 1mM PMSF, pH 8.0) and incubated with shaking for 3 hours at 4°C, followed by centrifugation at 15,000×g for 20 min at 4°C. The supernatant was incubated with 10 µl Ni-NTA resin (Qiagen, Huntsville, AL) with shaking at 4°C for 2 hours, washed with buffer A containing 50 mM imidazole, and finally eluted with buffer A containing 250 mM imidazole. The labeled samples were analyzed using SDS-polyacrylamide gel electrophoresis (SDS-PAGE) on 10% gels. After the extra fluorescence dye migrated out of the gel, the gel was removed and the fluorescence image was taken using the Typhoon 9410 phosphorimage/fluorescence imager (GE life science, Pittsburgh, PA) with an excitation 488nm. The same gel was then stained using Coomassie blue stain and the image of the gel was taken again under normal white light. The protein intensity was analyzed with ImageJ (NIH).

4.2.6 Knockout Strain (MG 1655 Δ acrAB tolC) Construction

Construction of bacterial gene knockout strains was performed following the kit instruction manual. The designed functional DNA cassette (to knockout TolC) flanked by homology arms was generated by PCR reaction. The designed primers were as follow and the amplification of the cassette are underlined.

Primer 1,

CGCAGTCCATTACTGCCACGCTAGGTTTAGGTGCAGATTACACCTATAGAAATT
AACCCTCACTAAAGGGCG

Primer 2,

ACGCACTGGTCGCGTTAGAGTTGATGCCGTTTCGCGTCGCGGTACGCCGTTGTA
ATACGACTCACTATAGGGCTC

The PCR reaction is set for 50 μ l. 39.5 μ l deionized water, 5 μ l 10x vent polymerase reaction buffer, 2 μ l 5 mM deoxyribonucleotide solutions, 1 μ l 50 mM primer 1 and primer 2, 1 μ l *Escherichia coli* genome, 0.5 μ l vent polymerase. The PCR reaction condition is, initial denaturation at 94°C for 30 seconds, thirty cycles (94°C for 30 seconds, 55°C for 45 seconds, 72°C for 90 seconds), and final elongation step 72°C for 10 minutes. The PCR product was separated on the 1% agarose gel and collected with gel extraction kit (Qiagen, Huntsville, AL).

The MG 1655 strain was transformed with pRed/ET plasmid and incubated at 30 °C overnight with 5 μ g/ml tetracycline as selection marker. A single colony was picked up

and cultured overnight at 30 °C. 2 ml overnight culture was transferred to 200 ml LB medium and cultured at 30 °C in LB with 10 µg/ml tetracycline until the density reaching OD600 of 0.3. L-arabinose was added to the culture to a final concentration of 0.3% and temperature was increased to 37 °C for continuing culturing until OD600 reached 0.5. The culture was centrifuged and cells were collected. 10% glycerol was used to wash the cell pellet for 4 times. The cells were resuspended in 10% glycerol to OD600 about 30. 400 ng DNA cassette was added to the resuspended cell and electroporated at 2500 V with 2 mm width slit of electroporation curvette. The electroporated cells was resuspended in 1 ml LB medium without antibiotics and incubated at 30 °C for 2 hours. 200 µl cells was spread onto a LB agar plates containing kanamycin (100 µg/ml) and incubated at 37 °C overnight. Single colonies were picked and verified with colony PCR.

The single *Δtolc* MG 1655 strain colony was picked up and prepared for electroporation competent cell as previous procedure. The 707-FLP plasmid was transformed into *Δtolc* MG 1655 strain with electroporation. The electroporated cells was resuspended in 1 ml LB medium without antibiotics and incubated at 30 °C for 1 hour. 200 µl cells were spread onto a LB agar plates containing kanamycin (100 µg/ml) and 5 µg/ml tetracycline, incubated at 37 °C overnight. A single colony was picked and grew in 1 ml LB medium without antibiotics at 30 °C for 2 hours. The temperature increased to 37 °C and the cells were cultured continuously for 7 hours. 200 µl cells were spread onto a LB agar plates containing no antibiotics. The colonies were stroke on two different LB agar plates in parallel, one with kanamycin (100 µg/ml) and the other without antibiotics. Those colonies which grew only on LB agar plates without kanamycin but no longer on the plates with kanamycin were removed of the selection marker. The single *Δtolc* MG 1655

strain colony without kanamycin marker was used to construct addition knockout in which *acrAB* gene was removed following the same procedure. The designed primers were as follow and the amplification cassette are underlined.

Primer 3:

CGATCGCGTAGTAATAAGTGGGCTGCAGAAAGTGCGTCCTGGTGTCCAGGAA
TTAACCCCTCACTAAAGGGCG

Primer 4:

CATCAGCGCCGGGGTAGGAGGCGGAGATCGTTACTGCCGGCGGTGCAATCTA
ATACGACTCACTATAGGGCTC

4.2.7 *In Vivo* Chemical Cross-Linking

In vivo chemical cross-Linking was performed in BW25113 Δ *acrB* strain. The plasmid pQE70-AcrB (WT or mutants) was transformed into the Δ *acrB* strain for expression. A single colony was picked from a freshly transformed plate and grown with shaking at 37 °C in 3 ml LB medium containing 100 µg/ml ampicillin for 12 hours. 2 ml of this cell culture was used to inoculate 200 ml LB medium containing 100 µg/ml ampicillin. Cells were grown to OD600 of 0.7. Cells were harvested by centrifugation at 5,000×g for 10 min. The cell pellet was resuspended in 10 ml cross-linking buffer (20 mM sodium phosphate, 100 mM NaCl, pH 7.2) and incubated with 0.4 mM dithiobis succinimidyl propionate (DSP) (Thermo, Rockford, IL) cross-linker at 37 °C for 30 min. After quenched with 20 mM Tris, cells were centrifuged, harvested and resuspended in lysis buffer (20 mM Tris-HCl, 100 mM NaCl, pH 8.0). Cells were lysed by sonication on ice

for 3 min with 5 s on/off intervals. After centrifuged at 15,000×g for 20 min at 4 °C, the supernatant was discarded. Pellet was resuspended in extraction buffer (20 mM Tris-HCl, 100 mM NaCl, 5% Triton X-100, pH 8.0) and incubated with shaking for 5 hours at 4 °C, followed by centrifugation at 15,000×g for 30 min at 4 °C. The supernatant was incubated with 80 µl Ni-NTA resin (Qiagen, Huntsville, AL) with shaking at 4 °C for 5 hours, washed with washing buffer (20 mM Tris-HCl, 100 mM NaCl, 0.4% DDM, pH 8.0 50 mM imidazole), and eluted with elution buffer (20 mM Tris-HCl, 100 mM NaCl, 0.4% DDM, pH 8.0 500 mM imidazole). The eluted fractions were reduced with 16 mM dithiothreitol (DTT) for 30 min at 37 °C, resolved by 10% SDS-PAGE and immunoblotted with a polyclonal anti-AcrA, AcrB and TolC antibodies as the primary antibodies, and an alkaline phosphatase-conjugated anti-rabbit antibody (Abcam, Cambridge, MA) as the secondary antibody. The protein-antibody conjugates were detected after staining using nitroblue tetrazolium chloride and 5-bromo-4-chloro-3'-indoyl phosphate p-toluidine (Sigma-Aldrich, St. Louis, MO).

4.2.9 *In Vivo* AcrB-TolC Disulfide Cross-Linking Assay

ΔacrAB tolC Escherichia coli MG1655 strain was transformed with a pair of plasmids (pBAD-AcrB and pAC5-TolC). The two proteins AcrB and TolC were co-expressed in 150 ml LB medium at 30°C. Protein was induced to express at OD₆₀₀ around 0.8 with 0.1 mM IPTG for 1 hour. Cultures were centrifuged and resuspended in a lysis buffer (30 mM iodoacetamide (IAM), 0.5 mM PMSF, 20 mM Tris-HCl, 100 mM NaCl, pH 8.0) and sonicated for 5 minutes on ice with 5s on/off intervals. After centrifuged at 15,000×g for 30 min at 4 °C, the supernatant was discarded. Pellet was resuspended in extraction buffer

(20 mM Tris-HCl, 100 mM NaCl, 5% Triton X-100, pH 8.0) and incubated with shaking for 5 hours at 4 °C, followed by centrifugation at 15,000×g for 30 min at 4 °C. The supernatant was incubated with 80 µl Ni-NTA resin (Qiagen, Huntsville, AL) with shaking at 4 °C for 5 hours, washed with washing buffer (20 mM Tris-HCl, 100 mM NaCl, 0.4% DDM, 50 mM imidazole, pH 8.0), and eluted with elution buffer (20 mM Tris-HCl, 100 mM NaCl, 0.4% DDM, 500 mM imidazole, pH 8.0). The eluted fractions were resolved on 10% SDS-PAGE and immunoblotted with polyclonal anti-AcrB or anti-TolC antibodies as the primary antibodies, and an alkaline phosphatase-conjugated anti-rabbit antibody (Abcam, Cambridge, MA) as the secondary antibody. The protein-antibody conjugates were detected after staining using nitroblue tetrazolium chloride and 5-bromo-4-chloro-3'-indoyl phosphate p-toluidine (Sigma-Aldrich, St. Louis, MO).

4.3 Results

4.3.1 Alanine Scanning Studies of Proposed P223 Binding Pocket

I previously found that P223 changed the backbone conformation of the loop and formed a kink, which may have served as a “wedge” to stabilize binding between neighboring subunits in an AcrB trimer. To investigate the receiving site of the interaction, I conducted Ala scanning of residues forming the binding pocket in the neighboring subunit. Each residue that contacted P223 in the neighboring subunit was replaced with Ala one at a time and the transport activity of the resultant mutant was examined using a drug susceptibility assay. The result is shown in Table 4.1. Y275A and Q584A did not have observable effects on protein activity while W187A slightly decreased the activity. Strikingly, R780A was completely nonfunctional.

The side chain of arginine has the highest pKa value among the twenty common amino acids. Thus, it usually forms salt bridges with other negatively charged amino acid. The positive charged guanidinium group of arginine could also form hydrogen bonds to backbone carbonyl oxygen atoms.¹⁷⁹ This kind of hydrogen bond formation plays combined structural and functional roles at the active site of enzymes.^{180, 181} The crystal structure reveals that the side chain of R780 forms a hydrogen bond with the backbone oxygen of P223. To further examine the role of R780, I also replaced it with other residues of various charge, polarity, and length to create R780M, R780Q, and R780K. R780M and R780Q also abolished the functionality of the protein similar as R780A, while R780K partially decreased its activity, indicating that a positive charge at this position is critical for function.

To confirm that the difference in activity was not a result of variation in protein expression due to the mutation, I measured the expression level of each mutant. Plasmid encoding each mutant was transformed into strain BW25113 Δ *acrB* for expression under the basal condition. Protein levels in the extracted membrane vesicles were then evaluated using Western blot analysis with an anti-AcrB antibody (Figure 4.2). There was no significant difference among expression levels of AcrB_{WT} and the other mutants, which indicated that the observed loss of activity was not a result of decreased protein expression.

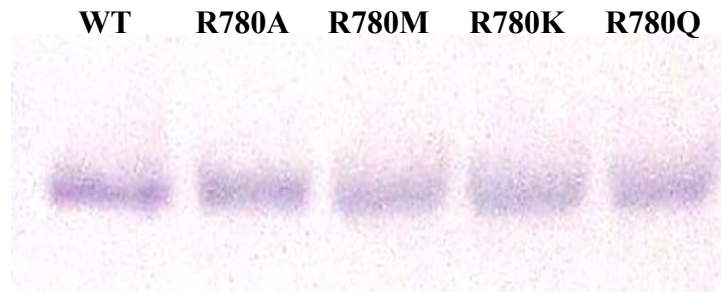


Figure 4.2 Comparison of the expression levels of wild type AcrB and the other mutants. Western blot analysis of membrane vesicles extracted from BW25113 Δ *acrB* expressing wild type AcrB (WT), AcrB (R780A), AcrB (R780M), AcrB (R780K) and AcrB (R780Q). Same amount of bacterial cells for expression of different proteins are used for analysis.

Table 4.1 Drug resistance of BW25113 Δ *acrB* expressing plasmids and mutations.

Plasmids or Mutations	MIC (μ g/ml)				
	Aci	Ery	Nov	R6G	TPP
pQE70-AcrB	160	80	160-320	320-640	640
pQE70	10	2.5	5	5	5
pQE70-AcrB _{W187A}	80	40	160	320	160
pQE70-AcrB _{Y275A}	160	80	160-320	320-640	640
pQE70-AcrB _{Q584A}	160	80	160	320	640
pQE70-AcrB _{R780A}	10	2.5	5	5	5
pQE70-AcrB _{R780K}	20	20	40	40	20
pQE70-AcrB _{R780M}	10	2.5	5	5	5
pQE70-AcrB _{R780Q}	10	2.5	5	5	5
pQE70-AcrB _{R780A/V225C/A777C}	10	2.5	5	5	5
pQE70- <i>CL</i> AcrB _{V225C/A777C}	160	80	160-320	320-640	640

Drugs tested were Acriflavine (Aci), Erythromycin (Ery), Novobiocin (Nov), Rhodamine 6G (R6G), and Tetraphenylphosphonium (TPP).

4.3.2 Efflux Ability Assay

To further confirm the bacterial susceptibilities data, ethidium bromide accumulation assay was performed using intact BW25113 or BW25113 Δ *acrB* cells transformed with plasmid encoded AcrB constructs. Ethidium bromide is weakly fluorescent in buffer. Once inside *E. coli*, it binds to DNA and fluoresces intensely. Therefore, the entrance of ethidium bromide can be monitored through an increase of fluorescence emission, which gradually reaches a plateau at saturation. Ethidium bromide is a substrate of AcrB. Without the active efflux by AcrAB-TolC, it would enter the cell at a much faster rate. In the presence of AcrAB-TolC, ethidium bromide accumulates inside the cell very slowly. The assay has been used to determine the substrates binding residues of AcrB.^{122, 123} A comparison of the rate of ethidium bromide accumulation in the presence of different AcrB constructs could be used to evaluate efflux activity.

Figure 4.3 showed the different fluorescence trace of the mutants. The BW25113 Δ *acrB* strains, transformed with pQE70 or pQE70-AcrB_{WT}, were used as the negative and positive controls, respectively. The mutant R780A showed the fastest fluorescence increase, similar to that of the negative control. The mutant R780K had a much slower increasing rate, which was more rapid than WT AcrB but slower than R780A. The ethidium bromide accumulation results were consistent with the result of the MIC assay, indicating that the mutant R780A almost completely lost the activity while R780K maintained partial activity (Table 4.1).

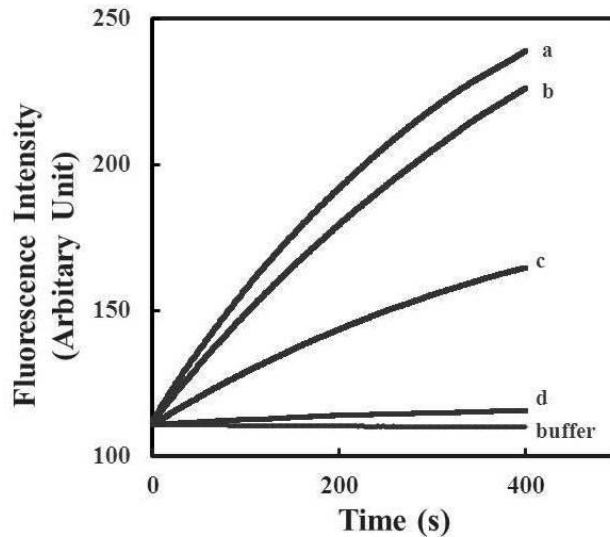


Figure 4.3 Real-time measurement of ethidium bromide accumulation for the intact BW25113 $\Delta acrB$ with different AcrB mutant. BW25113 $\Delta acrB$ (a), R780A (b), R780K (c), and WT AcrB (d).

4.3.4 Structural Characterization of AcrB_{R780A}

The replacement of R780 with other amino acids might possibly change the protein tertiary structure. To determine how R780A affect AcrB function, I chose R780A for further structure characterization *in vitro* and *in vivo*. The secondary structure of the mutant was characterized with circular dichroism (CD) spectroscopy. In Figure 4.4A, the CD spectrum in the far UV range of the mutant overlapped well with that of the WT, which indicated that the mutant still remained well folded secondary structure. Thermal denaturation experiments were also performed to test the stability of the purified mutant. The melting curves of the mutant and WT AcrB were similar (figure 4.4B), which was consistent with our previous report and confirmed that the conformations of the proteins were close.

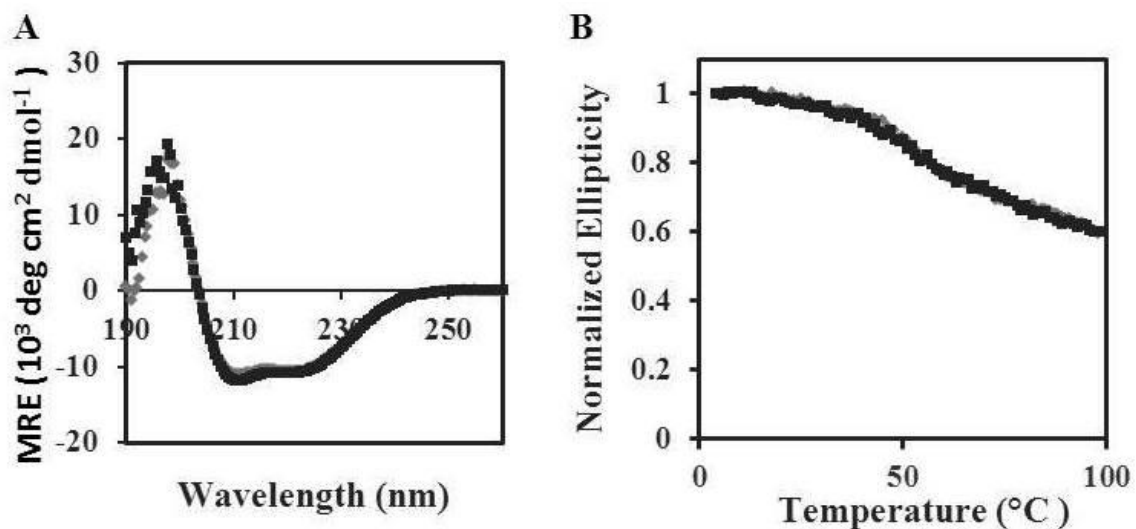


Figure 4.4 A. UV CD spectra of wild type AcrB (black) and AcrB_{R780A} (grey) superimposed well onto each other, indicating the two proteins had similar secondary structure contents. B. Temperature denaturation curves of wild-type (black) and AcrB_{R780A} (grey). The ellipticity values monitored at 222 nm were normalized to the reading at 4 °C. The thermal stabilities of the two proteins were very similar.

To probe whether the R780A mutation change the tertiary structure, the disulfide-trapping method was used to characterize R780A as described in section 2.3.3. As shown in Figure 4.5, similar to P223G structure characterization, a series of Cys pairs were introduced in the R780A mutant as reporters, which covered different parts of the protein in the periplasm domain of AcrB. The drug susceptibility assay had been used to confirm that these mutations did not affect the protein activity. All five Cys-pairs formed disulfide bonds at similar levels in the mutant as in the wild type background. Specifically, the 184-771 Cys pair was close to R780 and the formation of disulfide bond between them was not affected by the R780 to Ala mutation, which was a good indication that

AcrB_{R780A} maintained a similar tertiary structure as AcrB_{WT} and the mutation R780A did not alter the protein tertiary structure.

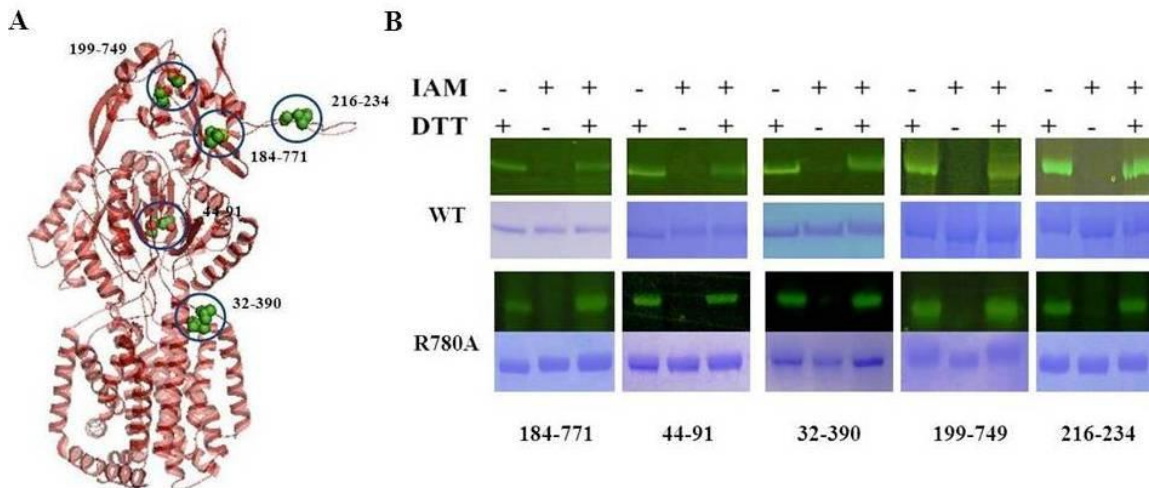


Figure 4.5 Disulfide trapping analysis of AcrB tertiary structure. A. The locations of reporter Cys pairs in the structure of AcrB were highlighted using black circles and blue ball-and-stick models. Residue numbers of the Cys mutations were marked. B. AcrB tertiary structure as revealed by the disulfide trapping method. The extents of disulfide bond formation for each reporter Cys pair were very similar in AcrB_{R780A} as compared to AcrB_{WT}. Therefore, the overall conformation, or tertiary structure, of AcrB_{R780A} was very similar to that of AcrB_{WT}.

The quaternary structure of AcrB_{R780A} was characterized with a modified BN-PAGE method as described in section 4.2.4. The oligomer state of the wild type and the mutant P223G were also quantified with BN-PAGE for comparison. The AcrB_{WT} migrated as a trimer as expected while most AcrB_{P223G} and AcrB_{R780A} as monomers (Figure 4.6A),

which indicated that the R780 is also involved in the oligomerization of the protein. In addition, AcrB_{R780A} has less trimer content than AcrB_{P223G} (Figure 4.6B).

To qualify the *in vivo* oligomer state of the mutant AcrB_{R780A}, two cysteines mutation were introduced to AcrB_{R780A}, V225C and A777C. Those two cysteines could form inter-subunit disulfide bond, covalently linked AcrB monomers into a trimer *in vivo* but did not affect its function as described in chapter 2.¹¹² The extracted membrane from BW25112 Δ *acrB* expressing *CL*AcrB_{R780A/V225C/A777C} was analyzed by Western blot (Figure 4.7). In the absence of DTT, a clear band migrated at high molecule weight in the SDS-PAGE, indicating that the mutant AcrB_{R780A} still formed a trimer *in vivo*. The disulfide crosslinking result of AcrB_{R780A} was the same as the result observed for AcrB_{P223G} as reported before.¹⁷³ However, the inter-subunit Cys pair (V225C and A777C) could partly restore the pump activity of AcrB_{P223G} but did not have such an effect on AcrB_{R780}. That is, AcrB_{R780A} has the same MIC values as *CL*AcrB_{R780A/V225C/A777C} (Table 4.1), implying that R780 might play other roles in addition to stabilizing the trimer.

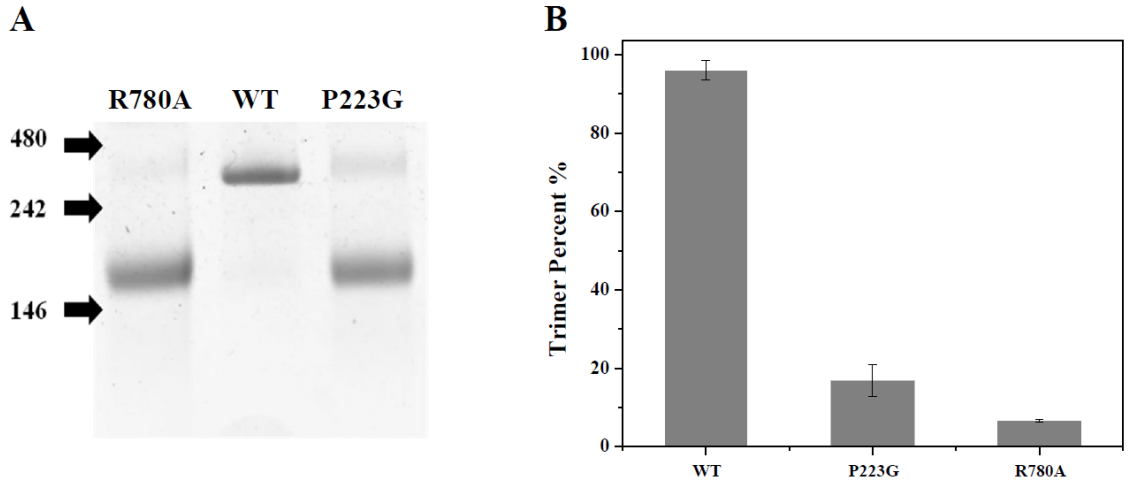


Figure 4.6 Quaternary structure analysis. A. BN-PAGE analyses of freshly purified AcrB_{WT}, AcrB_{R780A}, and AcrB_{P223G}. B. The AcrB trimer content percent is calculated from BN-PAGE (ImageJ).

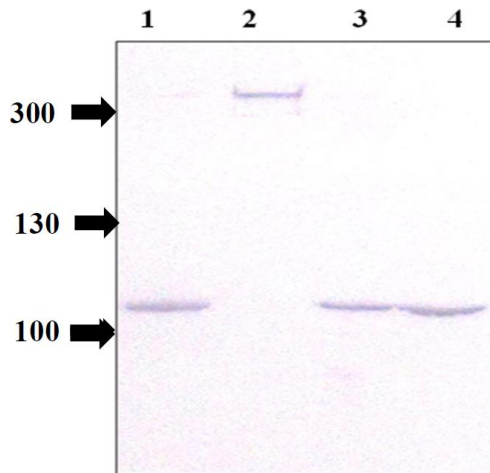


Figure 4.7 Western blot analysis of membrane vesicles extracted from BW25113 Δ *acrB* expressing wild type AcrB (lane 1 and lane 3), AcrB_{R780A/V225C/A777C} (lane 2 and lane 4) with or without 4 mM DTT in LB medium.

4.3.5 Fluorescence Labeling Assay

One possibility is that the mutant R780A affects the AcrAB-TolC activity through changing the conformation of the drug transport pathway. To explore this possibility, a fluorescence-based whole cell assay was used to determine the accessibility of residues lining up the drug translocation pathway.¹²⁶ In this method, the two intrinsic Cys residues in the sequence of AcrB were first replaced with Ala to create a cysless AcrB ($_{CL}AcrB$). Next, the residues along the substrate pathway in the AcrB are replaced with cysteine one at a time, and those mutated residues are labeled with a low concentration of Bodipy FL maleimide which is the substrate of AcrB. The labeling reagent travels through the AcrB channel and covalently reacted with cysteines lining up the translocation pathway. The intensity of fluorescence due to the labeling could be quantified to determine whether the residues could be accessed by the substrate. Experimental details could be found in Materials and Methods. This reaction is specific to residues involved in drug binding.

As shown in Figure 4.8, each SDS-PAGE gel was first imaged under fluorescence light, and then stained with Coomassie blue dye. Coomassie blue staining was used to reveal the concentration of protein in each lane and fluorescence image reflected the efficiency of fluorescence substrate labeling. If the mutant R780A alters the interaction with the substrate, then the fluorescence labeling efficiency of residues lining up the drug transport pathway will reduce and band intensity will decrease. Four such residues were chosen for this study, including T676, S134, F617 and D276. T676 is located in the external cleft; S134, F617 and D276 are in the binding pocket of AcrB. Those residues were mutated to cysteine one at a time in $_{CL}AcrB_{WT}$, $_{CL}AcrB_{P223G}$ and $_{CL}AcrB_{R780A}$ for

labeling assay. As shown in Figure 4.8, the fluorescence band intensity of $_{CL}AcrB_{WT/T676C}$, $_{CL}AcrB_{P223G/T676C}$ and $_{CL}AcrB_{R780A/T676C}$ were close, indicating that the labeling efficiency of Bodipy FL maleimide to sites at the external cleft was similar among those mutants. For S134C, F617C, and D276C, the fluorescence band intensity of $_{CL}AcrB_{P223G}$ and $_{CL}AcrB_{R780A}$ were similar, which were much lower than that of $_{CL}AcrB_{WT}$. This result indicates that the fluorescence dye could easily label the external cleft of the residues either $AcrB_{WT}$ or mutants. However, for the binding pocket, the labeling efficiency was low for $_{CL}AcrB_{P223G}$ and $_{CL}AcrB_{R780A}$. Those results suggest that the substrate could still enter from the external cleft to binding pocket in mutants $AcrB_{P223G}$ and $AcrB_{R780A}$ but could not reach the deep binding pocket.

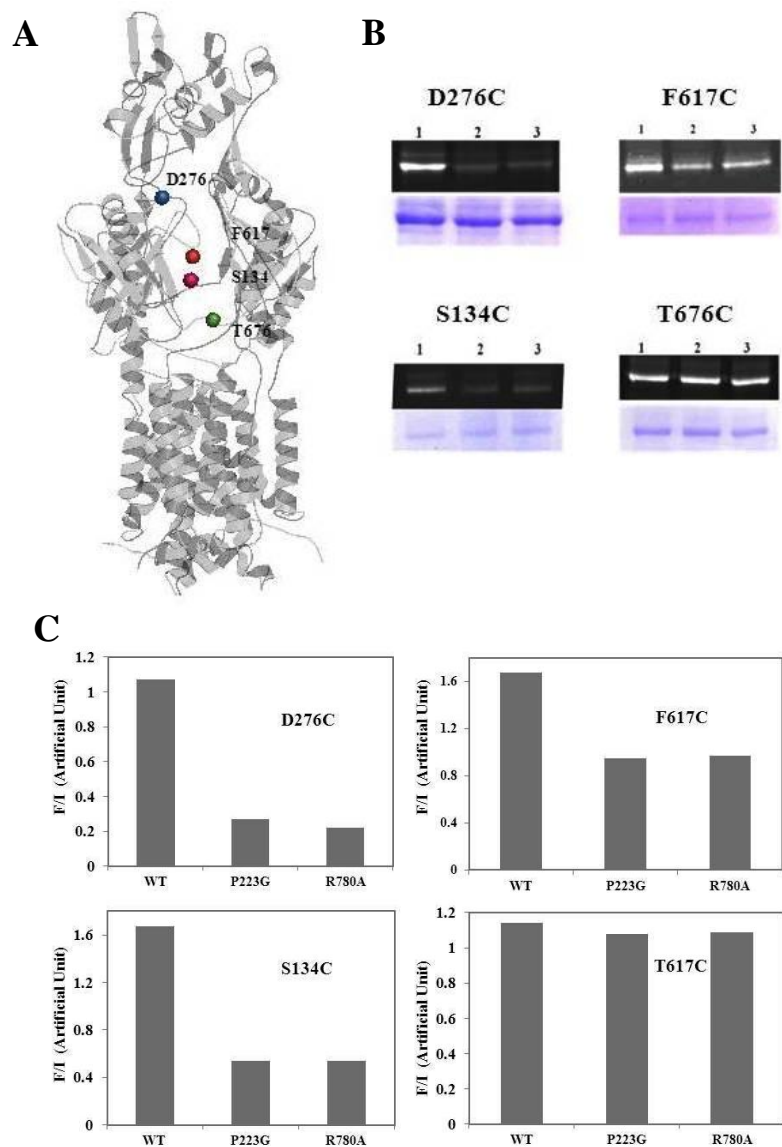


Figure 4.8 Fluorescent substrate labeling assay. A. The selected residues along the substrate transport pathway of AcrB. The residue was shown in a colored ball sphere model B. The labeling results. 1, 2, and 3 represents AcrB_{WT}, AcrB_{P223G}, and AcrB_{R780A}, respectively. For each labeling data, the upper panel is the fluorescence image before staining and the lower panel is the same gel after Coomassie blue stain. C. Quantitative analysis of labeling. The extent of labeling (F/I) was calculated by dividing the band fluorescence intensity with the amount of protein from the Coomassie staining.

4.3.6 *In Vivo* Chemical Cross-linking

It is also possible that the mutant R780A affects AcrB docking with AcrA or TolC. To probe *in vivo* interactions between components of AcrAB-TolC efflux pump, a chemical cross-linking experiment was performed. The chemical cross-linker dithiobis succinimidyl propionate (DSP) contains an amine active *N*-hydroxysuccinimide ester which reacts with primary amine to form stable amide bonds, and a disulfide bond which could be cleaved under reducing conditions. Thus the fixed 12 Å spacer arm of DSP could connect primary amine groups of target proteins in close proximity to study the protein-protein interactions. Live cells were treated with DSP and lysed. Cell membrane was solubilized, and protein complexes were isolated by Ni-NTA resin. The isolated complexes were reduced with DTT to release the conjugated complexes. The reduced components were resolved by 10% SDS-PAGE and detected by immunoblotting. In Figure 4.9, AcrB_{WT}, AcrB_{P223G} and AcrB_{R780A} could cross-link with both AcrA and TolC. There are no obvious differences in band intensities of AcrA or TolC cross-linking among AcrB_{WT}, AcrB_{P223G} and AcrB_{R780A}. Those results suggest that the mutant AcrB_{R780A} could interact with AcrA and TolC as AcrB_{WT} and AcrB_{P223G} did. The efflux pump could still form in AcrB_{R780A}.

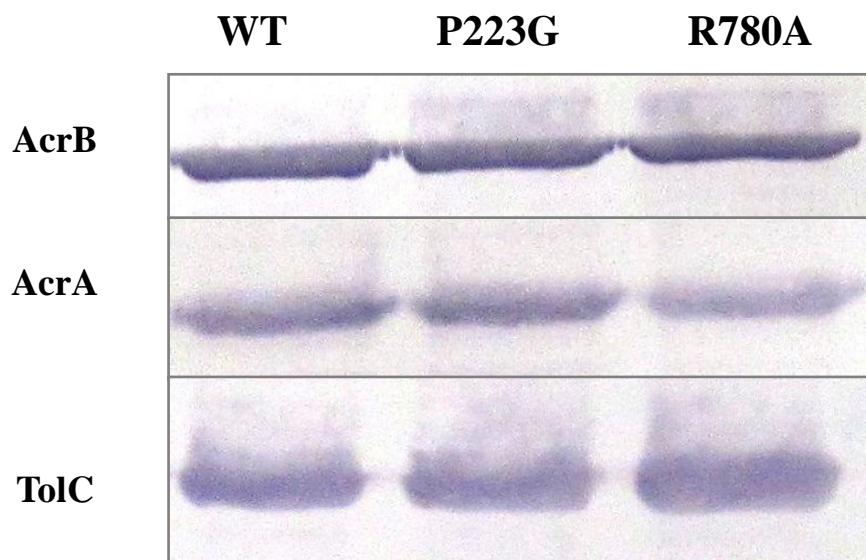


Figure 4.9 *In vivo* chemical cross-linking of the AcrAB-TolC efflux pump. The complex was purified from membrane fractions of lysed cells with Ni⁺-agarose. The cross-linked proteins were reduced by DTT, resolved by 10% SDS-PAGE and identified by immunoblotting.

4.3.7 *In Vivo* AcrB-TolC Disulfide Cross-Linking Assay

AcrB has a tip-to-tip contact with TolC. The AcrB_{D256C} and AcrB_{D795C} could form disulfide bonds with TolC_{G147C} and TolC_{G365C}, respectively, which provided evidence for direct interaction between AcrB and TolC. (Figure 4.10)¹³⁷ Since R780 is close to D795, the mutation R780A might change the conformation of the TolC docking domain in AcrB and prevent correct docking between AcrB and TolC. To test this hypothesis, D256 or D795 were mutated to cysteines in pBAD-AcrB (WT, P223G, and R780A) plasmid; G147 and G365 were mutated to cysteines in pAC5-TolC plasmid. The AcrB and TolC mutants were co-expressed in a Δ *acrABtolC* strain and disulfide bond formation between

AcrB and TolC were tested with Western blot. The disulfide bond might not form if the mutants R780A change the TolC docking domain. As shown in Figure 4.11, the purified proteins (AcrB_{D256C}/TolC_{G147C} and AcrB_{D795C}/TolC_{G365C}) were analyzed by SDS-PAGE and immunblotting. There are three major bands (110, 260 and 330 kDa) on the SDS-PAGE when anti-AcrB antibody was used for detection. In the presence of reducing agent DTT, the 260 and 330 kDa bands disappeared. The 260 kDa bands also appeared when anti-TolC antibody was used in detection. Based on the molecular weight of AcrB (110 kDa) and TolC (50 kDa), the 260 kDa band could be a complex for the trimeric TolC with monomeric AcrB which are consistent with the previous report.¹³⁷ It was found that mutants P223G or R780A both formed disulfide bond with engineered TolC, similar as the WT AcrB. It is possible that the mutants R780A and P223G did not affect the TolC docking domain.

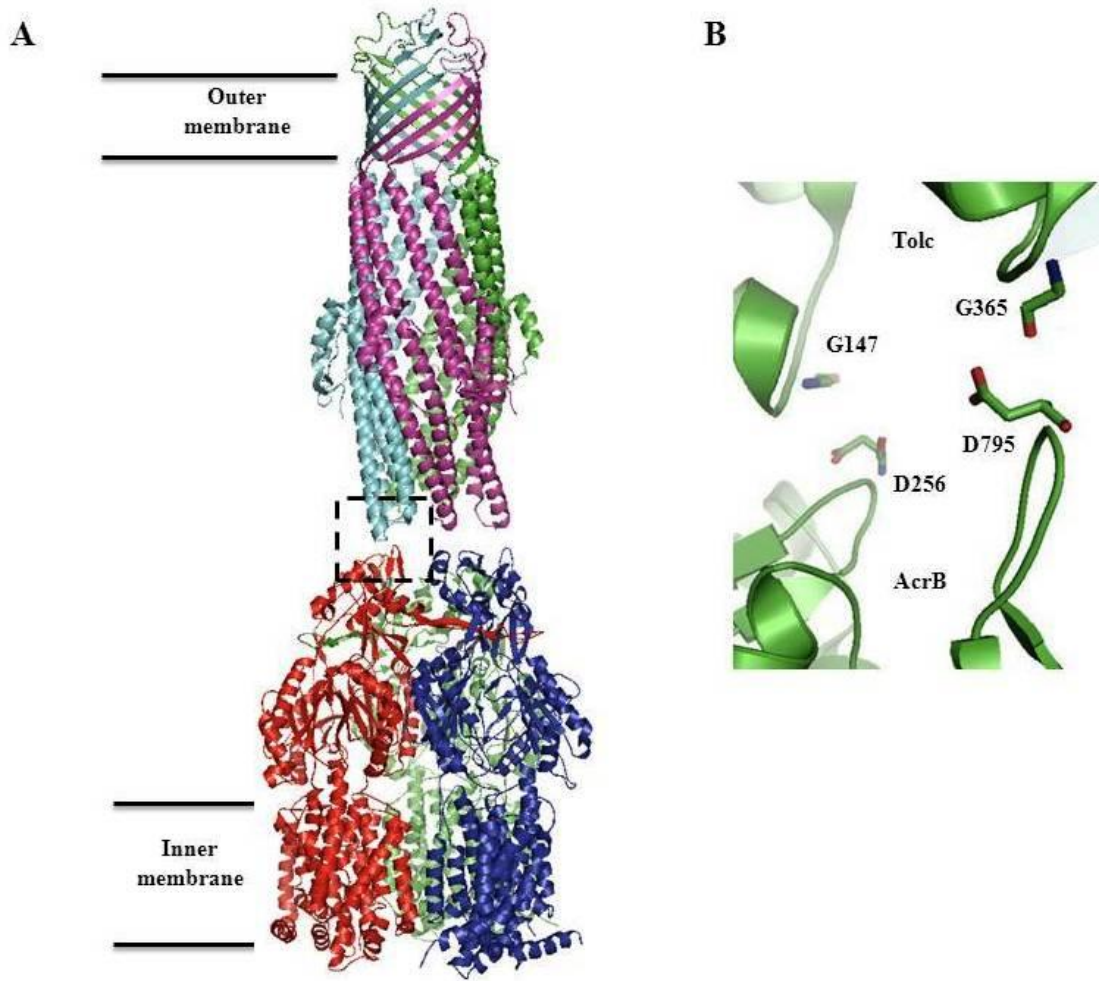


Figure 4.10 A. The direct interaction of AcrB and TolC model. (Protein Data Bank ID 2DRD and 1EK9)^{61, 135} B. Zoom in picture of the residues which are involved in the tip-to-tip contacts between AcrB and TolC.

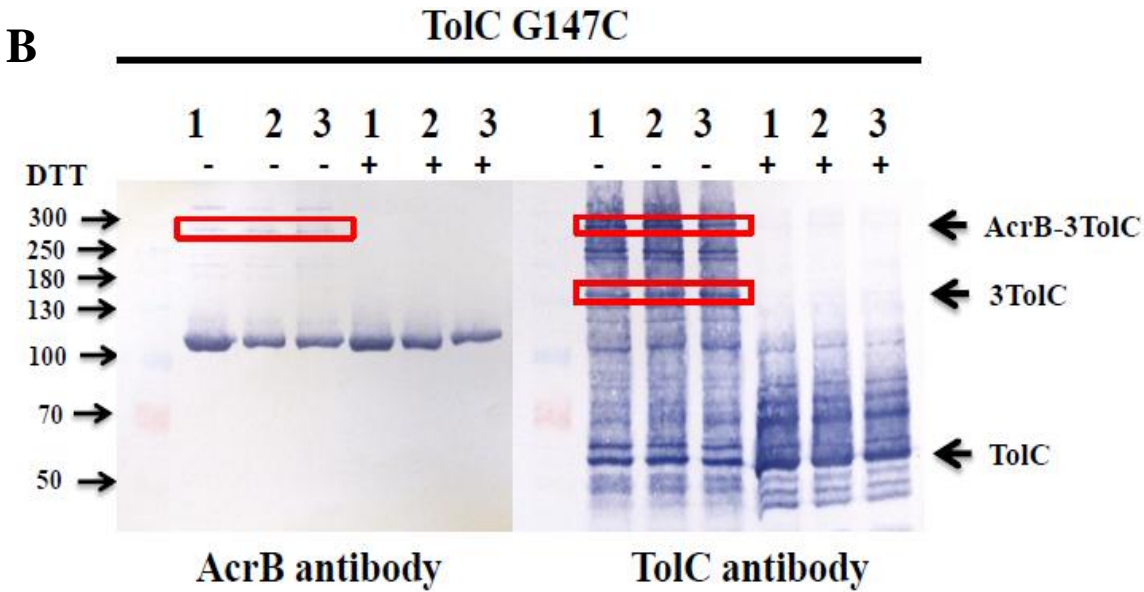
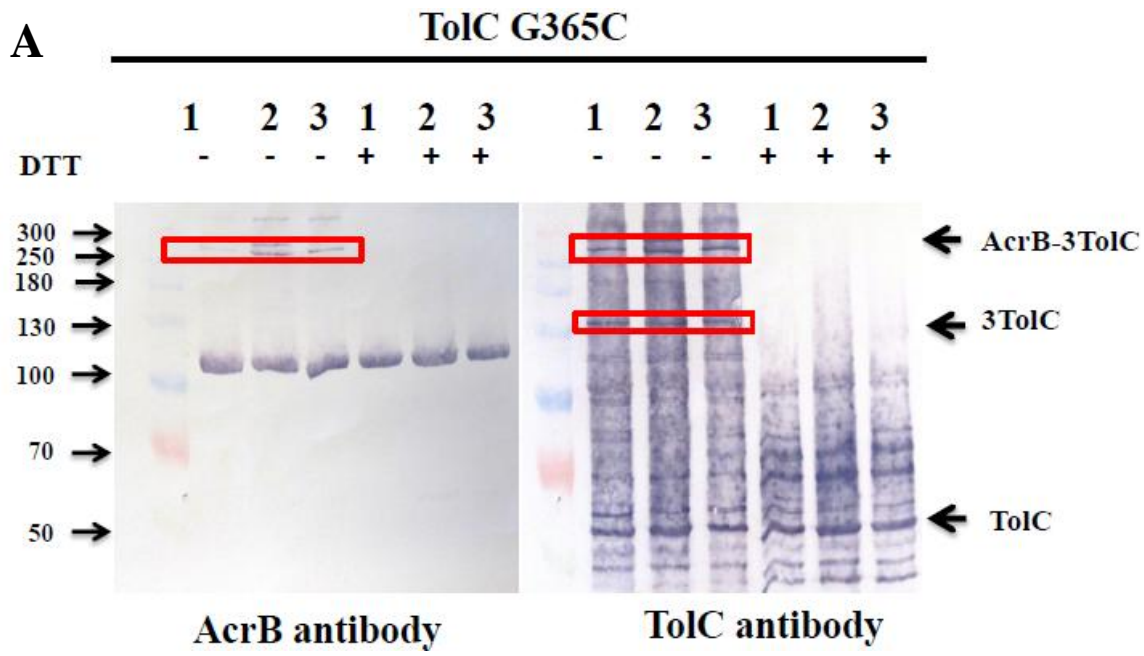


Figure 4.11 *In vivo* disulfide cross-linking between AcrB and TolC. 1, 2, and 3 represents WT, P223G and R780A of AcrB, respectively.

4.4 Discussion and Conclusion

To understand the oligomerization process and inter-subunit interaction of AcrB, structures and function of AcrB mutants were characterized in chapter 2 and 3. Our results identified a conserved residue P223 in the protruding loop, which helped the loop to form a “wedge”-like structure and stabilized the trimeric state. And the protruding loop is important for the trimerization and function of AcrB. In this study, to further illustrate the interaction between the loop-and-tunnel interactions in neighboring subunits of AcrB, I performed Ala scanning study of the proposed binding pocket of P223 and identified a critical residue R780 in the tunnel. Mutation of R780 had a drastic impact on AcrB function. The side chain of R780 could form a hydrogen bond to backbone carbonyl oxygen of P223. CD spectrum and disulfide bond trapping method were used to characterize the secondary and tertiary structure of the mutant AcrB_{R780A}, which were similar to AcrB_{WT}. The purified AcrB_{R780A} was a monomer with BN-PAGE but a trimer *in vivo* with intra-disulfide bond cross-linking, which implied that R780A weakened oligomeric state of AcrB and trimeric AcrB_{R780A} dissociated easily during purification.

However, the inter-subunit disulfide bond cross-linking could not restore the activity of the mutant AcrB_{R780A}, which was different from that of AcrB_{P223G}. Based on the crystal structure (Figure 4.12), the backbone carbonyl oxygen of P223 is within H-bonding distance with the side chain of R780 from the neighboring subunit. When P223 was replaced with another amino acid, the flexibility of the loop increases but the backbone oxygen still exists. The inter-subunit disulfide bond between C225 and C777 helped to stabilize AcrB trimer and partially restores its activity.

In R780 mutants including R780A, R780M and R780Q, the guanidinium group at the end of the Arg side chain was replaced, which eliminated the possibility of forming hydrogen bond with P223 backbone oxygen. Lys could potentially form hydrogen bond with P223 backbone oxygen, therefore the R780K retained partial activity. Compared with lysine, the side chain guanidinium group in arginine might be positioned at a more favorable location to interaction with backbone carbonyl oxygen. R780K did not have the same level of stability as WT AcrB, but maintained partially its function. Moreover, the side chain of R780 underwent conformation change while the protein operate, which led to the switching of hydrogen bond partners with the backbone carbonyl oxygen of P223 (Figure 4.12). The side chain of Lys might not be able to support the structure transition as well as Arg did at position 780.

It was proposed that energy from derived from the proton translocation across in the transmembrane domain of AcrB drove the structural conversion in the periplasm domain of each monomer.⁶¹ The dynamic conformation change of R780 during the pump rotating cycle could be critical to conformational coupling among monomers and might provide an elastic network between the neighboring subunits interaction. Without R780, the inter-subunit disulfide bond cross-linking could link the subunits to each other to form a trimer but not fully function for the lack of a dynamic hinge to provide the flexibility. Therefore, the inter-subunit disulfide bond cross-linking could partially restore the activity of the mutant AcrB_{P223G} but not AcrB_{R780A}.

In this study, the stabilizing of AcrB oligomer for its functionality was further clarified. In an earlier study,¹⁷³ it was suggested that the loop kept rigid structure during the

trimerization. Combined with the finding in this study, the rigid structure of the loop, especially P223 in the tip, help to form an important hydrogen bond to the R780 in the tunnel. During the asymmetric rotation function of AcrB *in vivo*, R780 also altered its conformation to well maintain the hydrogen bond formation and kinetic stabilize the trimer of AcrB.

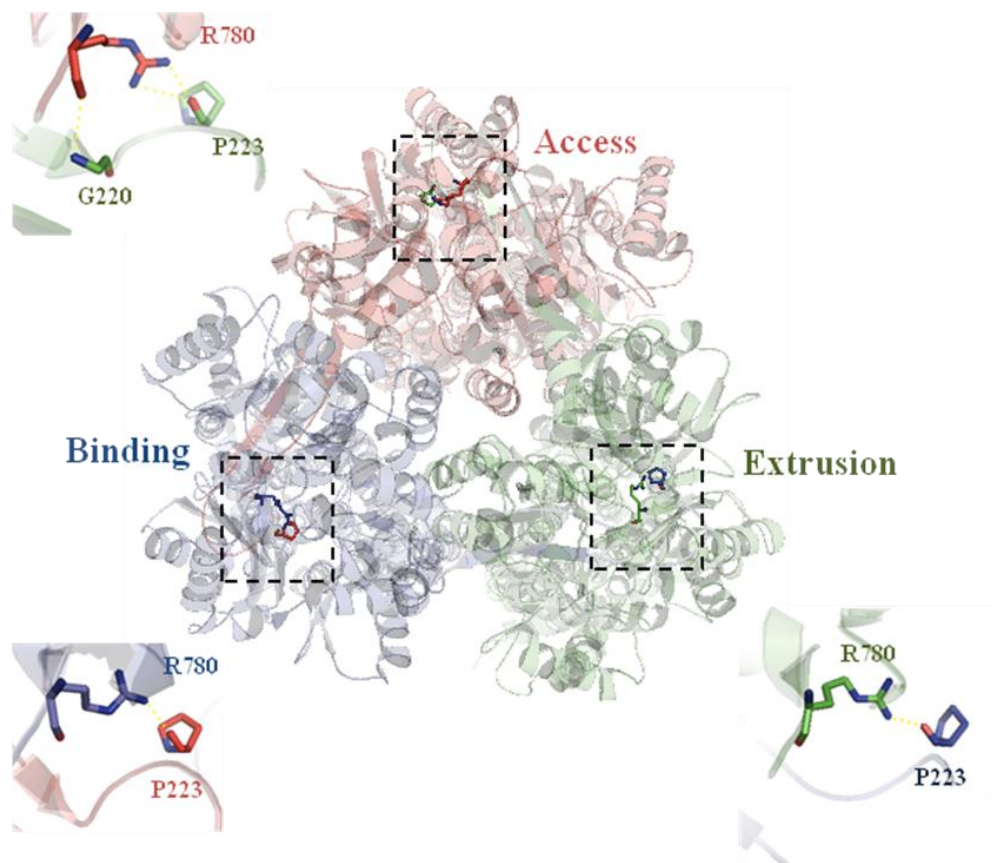


Figure 4.12 The overlook picture of asymmetric AcrB (Protein Data Bank ID 2DRD). Each monomer state was color coded. The zoom-in picture about the hydrogen bond (indicated with a yellow dash line) between R780 and P223 during different states.

Chapter 5 Characterization of Ligand Binding of a Putative Archaeal Regulator Protein ST1710

5.1 Introduction

Transcriptional regulators are proteins involved in regulating transcription of mRNA level. Those usually bind to a DNA binding site to control gene expression. Based on its mechanism, regulators could be divided as an activator and repressor. A transcriptional activator is a protein that increases gene transcription level while a repressor prevents the gene transcription. Multiple antibiotic resistance regulators (MarR) family is an important regulator family to regulate cellular function in response to aromatic catabolic pathways, virulence factors and environmental stress.¹⁸² It was first identified by George and Levy in multidrug resistant strains of *E. coli* in 1983.^{183, 184} Now homologues of MarR can be found throughout the domains of bacteria and archaeon.^{185, 186} The bacteria MarR family has been studied extensively.

MarR regulators bind to their cognate dsDNA sequences as homodimers. The interaction between MarR and DNA is modulated by specific lipophilic compounds, including salicylate, ethidium, and CCCP (Figure 5.1). Crystal structures of several MarR regulators have been obtained, either as apoproteins (MexR from *Pseudomonas aeruginosa*,¹⁸⁷ SlyA from *Enterococcus faecalis*,¹⁸⁸ and MTH313 from *Methanobacterium thermoautotrophicum*¹⁸⁹), in complex with the cognate dsDNA oligonucleotide fragment (OhrR from *Bacillus subtilis*¹⁹⁰), or in complex with salicylate (MarR from *E. coli*¹⁹¹ and MTH313 from *M. thermoautotrophicum*¹⁸⁹). However, the DNA-complexed and ligand-complexed structures are not yet available simultaneously for the same protein to facilitate direct comparison. An allosteric regulation mechanism

has been proposed on the basis of the observation that the four dimers in the crystallographic asymmetric unit of MexR had different conformations, in which an open state (presumably DNA binding) and a closed state (presumably drug binding) could be identified.¹⁸⁷ Recently, crystal structures of MTH313 were determined both in the apo state and in complex with salicylate.¹⁸⁹ A comparison of these two structures illustrated a large conformational change in the DNA binding lobe, further supporting the notion that protein conformational changes are involved in the mechanism of regulation. However, much less is known about the MarR-like regulators in archaea. ST1710 from *Sulfolobus tokodaii* (found in hot springs of Kyushu Island, Japan) is a putative MarR-like regulator. Crystallographic structure of ST1710 has been determined in its apo form (Figure 5.1 A).^{192, 193} The structure of ST1710 superimposes well with the MarR regulators, with a ligand binding site and a DNA binding site that share some common key residues. Based on the similarity in structure, the mechanism of function is expected to resemble that of the bacterial MarR proteins. While the majority of the MarR regulators studied are repressors, there are also some members that act as activators. The repressors bind to their target DNA site to block the transcription of the cognate genes in the absence of the effector (a small molecule that binds to the protein and alters protein activity). When its cytoplasmic concentration reaches a critical level, the effector would bind at the ligand binding site of the repressor and generate a conformational change. The effector binding and conformational changes disrupt the binding between the protein and the DNA, and subsequently RNA polymerase could initiate the transcription of the genes. On the contrary, for activators the effector binding promotes interaction with the target DNA.

The effector binding has been characterized for a couple of bacterial MarR family regulators. These effectors are usually lipophilic compounds with planar structures, such as ethidium, salicylate, and CCCP (Figure 5.1 B). However, no detailed biophysical characterization of the ligand binding to archaeal MarR-like regulators has been reported. In this study, I characterize the binding of the above-mentioned ligands to ST1710. The binding affinity, stoichiometry, and resultant protein conformational change were examined. The effect of ligand binding on the interaction between ST1710 and a double-stranded DNA oligonucleotide containing the putative ST1710 binding site were investigated. The recombinant ST1710 was found to bind to all three ligands, and this binding disrupted the interaction between the protein and DNA.

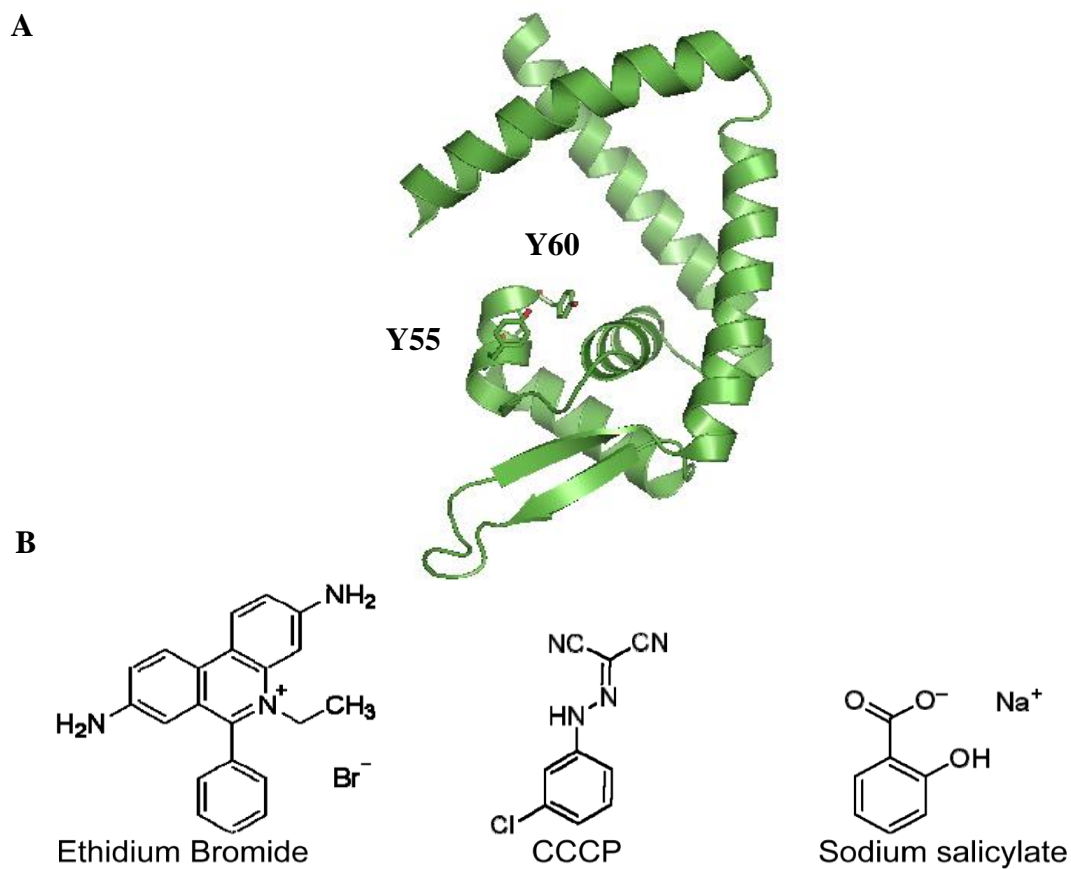


Figure 5.1 Structure of ST1710 and its ligands. A. Crystal structure of apo-form ST1710 (Protein Data Bank ID 2EB7).¹⁹² B. Chemical structure of three ligands used in this study.

5.2 Material and Methods

5.2.1 Cloning, Expression and Purification of ST1710

The gene of ST1710 was amplified by the polymerase chain reaction (PCR) from plasmid STLGR15159 (National Institute of Technology and Evaluation, Japan). Primer pairs used for the PCR are: forward 5'-CACCATGTTAGAAAGTAATGAAAACAGAAT AC, reverse 5'-TCACTGACTAATTTCTCAATTCTTTTC. Next the PCR product was inserted into the TOPO TA expression vector following the manufacturer's instruction (Invitrogen, Carlsbad, CA) to generate plasmid pTOPO-ST1710, which introduced a poly-histidine tag at the N terminus of the protein. pTOPO-ST1710 was transformed into *E coli*. strain Rosetta2 (EMD Biosciences, San Diego, CA) for protein expression. The cells were grown in Luria Bertani (LB) media containing 100 g/mL ampicillin and 34 g/mL chloramphenicol to an OD₆₀₀ of 0.6, and then induced by adding 1 mM of isopropyl-beta-D-thiogalactopyranoside (IPTG). Sixteen hours after the induction, the cells were harvested by centrifugation at 6,000 g for 10 min. The cell pellet was resuspended in buffer A (50 mM HEPES buffer, 200 mM NaCl, pH 7.5), and lysed by sonicating on ice for 5 min with 10 s on/off intervals. Then, the cell debris was separated from the supernatant by centrifugation at 10,000 g for 15 min. The same centrifugation condition was used throughout the purification steps unless otherwise indicated. The supernatant was first incubated at 70 °C for 45 min, followed by centrifugation to remove the heat-denatured impurities. Next, the supernatant was incubated with the Ni-NTA resin (Qiagen, Huntsville, Alabama) with shaking for 1 hour, then washed with buffer B (50 mM HEPES buffer, 200 mM NaCl, 35 mM imidazole, pH 7.5), and finally eluted with buffer C (50 mM HEPES buffer, 200 mM NaCl, 500 mM imidazole, pH 7.5).

Purified ST1710 was dialyzed extensively against buffer A to remove the excess imidazole. The purity of the protein was analyzed with sodium dodecyl sulfate polyacrylamide gel electrophoresis (SDS-PAGE). Protein samples were separated on a 20% homogenous polyacrylamide Phast gel (Phast System, GE healthcare, Waukesha, WI) and visualized by Coomassie Blue stain. Molecular weight standards (Benchmark Protein Markers) were obtained from Invitrogen. Protein concentrations were determined by UV absorbance at 280 nm using an extinction coefficient of $8940 \text{ M}^{-1}\text{cm}^{-1}$.

5.2.2 Circular Dichroism (CD) Spectroscopy

CD was performed on a JASCO J-810 spectrometer (JASCO, United Kingdom) with 1 nm bandwidth and a 0.1 cm path length cuvette. ST1710 was dialyzed overnight into a low salt buffer (20 mM Tris buffer, pH 8.0) before the CD measurement. Blank scans were performed with the exterior dialysis buffer and subtracted from the measured data.

5.2.3 Fluorescent spectroscopy

Fluorescent polarization experiment and wavelength scans were performed with a Perkin Elmer LS-55 fluorescence spectrometer (Perkin Elmer, Waltham, MA). For the fluorescent polarization studies of FITC labeled ST1, the excitation and emission wavelengths are 492 and 515 nm, respectively. The forward oligonucleotide (5'-AATGAAAACAGAATACAAATAATGTCAACAATAGCAAAAATATACAG-3')

was labeled with FITC at the 5' (all DNA oligonucleotides, including FITC labeled ones, are obtained from Operon, Huntsville, Alabama). The forward and reverse oligonucleotides was mixed at a 1 to 1 ratio at 100 μM in 500 μl reaction buffer (10 mM HEPES, pH 7.5, 50 mM NaCl). The sample was protected from light and incubated in 2

L of boiling water bath for 10 minutes, then cooled slowly in the water bath to room temperature. The annealed double stranded DNA was used throughout the binding experiment. The reaction buffer was supplemented with 1 µg/ml calf thymus DNA to eliminate non-specific binding. For measuring the binding of ethidium to ST1710, the excitation and emission wavelengths for the fluorescent polarization experiment are 520 and 600 nm, respectively. The same excitation wavelength was used for the emission spectra.

Two models were used to fit for the binding dissociation constants from the concentration dependent curves. The Hill equation was used when the concentration of the ligand (ST1 or ethidium), which is kept constant during the titration, is much smaller than the concentration of the ST1710. In such circumstances, the concentration of the protein-ligand complex is very small compared to the total protein concentration, so the total protein concentration can be treated as [S] during the fitting:

$$\Delta P = \Delta P_{\max} \times \frac{S^n}{K^n + S^n}$$

P is the polarization increment upon the addition of ST1710, P_{\max} is the maximum polarization increment when the protein concentration [S] approaches infinity, and n is the hill coefficient, with $n > 1$ indicate positive coordination and $n < 1$ indicate negative coordination.

A non-cooperative one to one binding model was used when the concentration of the complex cannot be ignored, as in the case of binding between ST1710 and CCCP:

$$\begin{aligned}
PL &\rightarrow P + L \\
K_d &= \frac{[P_f][L_f]}{[PL]} \\
[P_f] &= [P_T] - [PL], [L_f] = [L_T] - [PL] \\
K_d &= \frac{([P_T] - [PL])([L_T] - [PL])}{[PL]}
\end{aligned}$$

$[P_T]$, $[P_f]$, $[L_T]$, $[L_f]$ and $[PL]$ are concentrations of the total protein, free protein, total ligand, free ligand, and protein-ligand complex, respectively. Solving for $[PL]$:

$$\begin{aligned}
[PL]^2 - ([P_T] + [L_T] + K_d)[PL] + [P_T][L_T] &= 0 \\
[PL] &= \frac{([P_T] + [L_T] + K_d) - \sqrt{([P_T] + [L_T] + K_d)^2 - 4[P_T][L_T]}}{2}
\end{aligned}$$

For CCCP binding, the ellipticity at 325 nm (y) is proportional to the concentration of protein-CCCP complex $[PL]$. The change of y as a function of the total ligand concentration x ($x=[L_T]$) can be represented as:

$$\begin{aligned}
\frac{y - Y_{\min}}{Y_{\max} - Y_{\min}} &= \frac{[PL]}{[P_T]} = \frac{([P_T] + x + K_d) - \sqrt{([P_T] + x + K_d)^2 - 4[P_T]x}}{2[P_T]} \\
y &= \frac{(Y_{\max} - Y_{\min})([P_T] + x + K_d) - \sqrt{([P_T] + x + K_d)^2 - 4[P_T]x}}{2[P_T]} + Y_{\min}
\end{aligned}$$

In the experiment, small aliquot of CCCP was titrated into ST1710. The dilution effect was kept to be less than 2%, so $[P_T]$ can be treated as a constant without causing significant error in fitting. Y_{\min} and Y_{\max} correspond to the theoretical ellipticities at CCCP concentrations of 0 and infinity, respectively. The y vs. x curve was fitted to derive three parameters, K_d , Y_{\min} and Y_{\max} .

5.2.4 Tetranitromethane (TNM) Nitration

The TNM nitration procedure was performed following the published method.¹⁹⁴ Briefly, TNM was added to a reaction buffer (0.5 M Tris-HCl (pH 8.0)) containing 62.5 μM ST1710 at a final concentration of 750 μM . Ethidium bromide was added when indicated to the reaction mixture at a final concentration of 100 μM before the addition of TNM. The reaction mixture was incubated at 35 $^{\circ}\text{C}$ for 1 hour and then passed through desalting columns twice to remove the excess TNM and ethidium. The nitrated Tyr was quantified using the absorbance at 428 nm with an extinction coefficient of $4200\text{ cm}^{-1}\text{ M}^{-1}$.¹⁹⁵ The concentration of the protein was determined using the Bradford assay. The number of nitrated Tyr residues per protein molecule was estimated by the ratio of these two concentrations.

5.3 Results and Discussion

5.3.1 Ligands binding to ST1710

Capacity to bind with effectors is shared by all MarR type regulators characterized thus far. Several small molecules have been shown to bind to the MarR family regulators. Three representative ligands were chosen to study effector binding to ST1710, including a cationic molecule ethidium, an anionic molecule salicylate, and a neutral molecule CCCP (Figure 5.1 B).

The binding of ethidium to ST1710 was studied directly using the intrinsic fluorescence of ethidium. After binding with the protein, the fluorescent emission peak was blue shifted by 5 nm and increased in intensity by 2 folds at 10°C (Figure 5.2 A, red traces). Since *S. tokodaii* is a thermophile living at 80°C, the effect of temperature was examined on ethidium binding with 10°C intervals from 10 to 50°C (Figure 5.2 A). The interaction between ethidium and ST1710 becomes weaker at higher temperature. At 10°C, fitting the binding curve with the Hill equation yields a dissociation constant of $19.1 \pm 4.6 \mu\text{M}$. The n value was found to be 0.88 ± 0.07 , indicating the lack of binding coordination.

To evaluate the potential contribution of the protein structural change on the observed temperature effect on binding, CD spectra of ST1710 was collected at 10 and 50°C, respectively. The structural stability of a helical protein is usually monitored by the disappearance of the helical structure at the far UV region. The far UV CD spectra at 190-260 nm was collected (Figure 5.3). The protein is highly α -helical, consistent with the crystal structure. The two spectra show very little differences, indicating the protein is quite stable at 50°C.

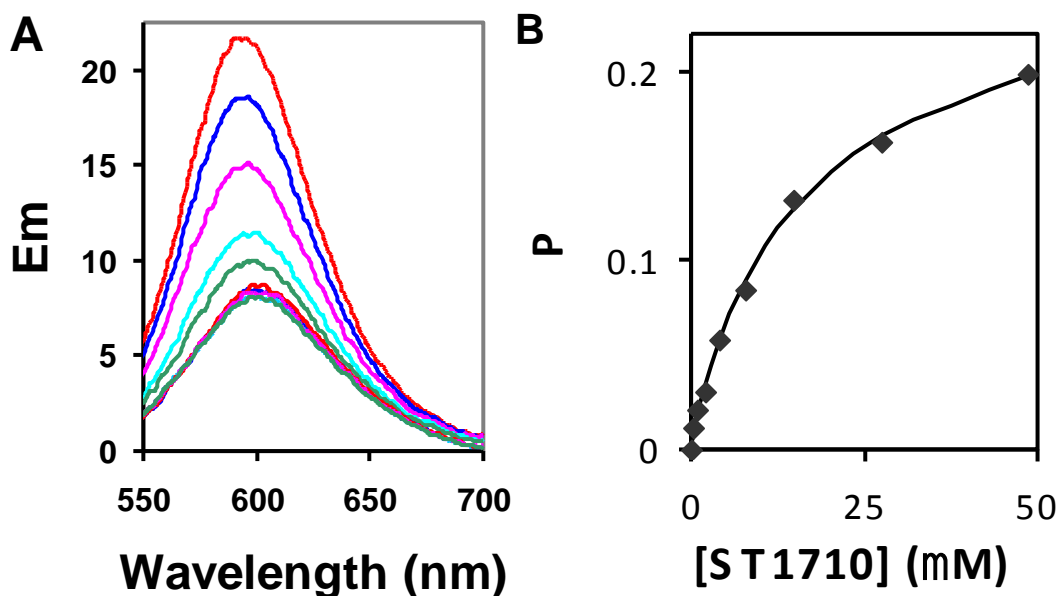


Figure 5.2 Binding of ethidium with ST1710. The intrinsic fluorescence of ethidium was used to monitor its binding to ST1710 at 10°C (red), 20°C (blue), 30°C (magenta), 40°C (cyan), and 50°C (green). Two traces were collected at each temperature, one is ethidium alone and the other is ethidium (1 μM) plus protein (20 μM). The effect of temperature on the fluorescent emission of free ethidium is very small, so traces from all 5 temperatures superimpose onto each other at the bottom of the figure. However, the increase of temperature drastically decreased the binding affinity of ethidium with ST1710. At 10°C, the binding to ST1710 causes the fluorescent emission of ethidium to increase by 2 folds and blue shift (A, first red line from the top). With the rising of the temperature, the binding becomes weaker, and the fluorescent enhancement decreases as a consequence. At 10°C, the fluorescent polarization changes of an ethidium solution upon the addition of ST1710 were recorded and fitted with the Hill equation (B).

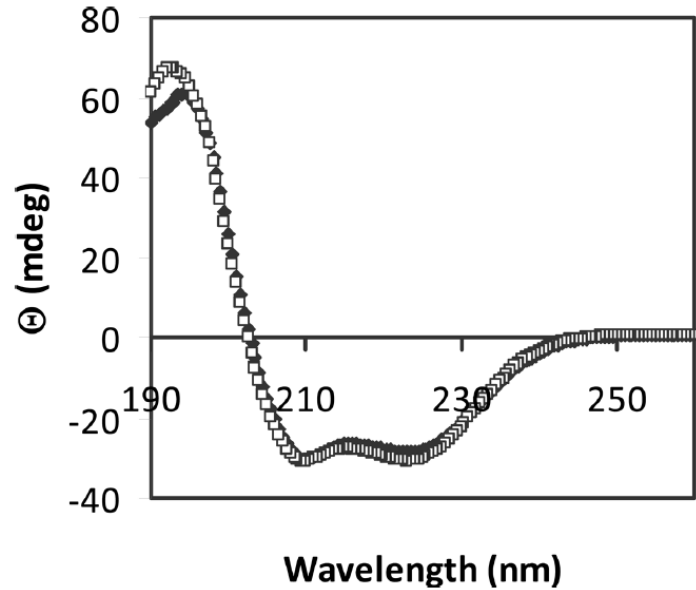


Figure 5.3 Circular Dichroism characterization of ST1710. The secondary structure of ST1710 is highly alpha-helical, consistent with its crystal structure. The conformation of the protein has very slight change when the temperature increased from 10°C (□) to 50°C (◆).

CD spectroscopy also was used to evaluate the ST1710 structural change associated with ligand binding. The near UV CD spectra (260-350 nm) which reveal information about a protein's tertiary structure were collected for the free protein, free ligands, and the protein-ligand complexes (Figure 5.3). Aromatic residues, especially tryptophan, are major contributors to the near UV CD signal. Since ST1710 has no intrinsic tryptophan, high protein concentration has to be used (300 μM) to achieve decent signal to noise level for the spectrum. The ligand concentration need to be high enough to form significant amount of protein complex to facilitate detection, while at the same time not too high so its absorbance won't significant deteriorate the signal. In the case of ethidium, its absorption at 300 μM (to achieve a 1:1 molar ratio to the protein) causes poor signal to

noise, so the spectrum shown in figure 5.3 was acquired with 150 μ M ethidium. At a ligand to protein ratio of 0.5:1, only a portion of the protein would bind with ethidium. However, a clear difference can still be observed between the CD traces of the apo-protein (open square) and the protein-ethidium mixture (filled diamond) at the wavelength region between 260 to 275 nm, indicating protein conformational change accompanied ethidium binding (Figure 5.4).

Salicylate absorbs much less in the wavelength range studied, and can be used at 2 mM to achieve a ligand to protein ratio of 20:3 (Figure 5.4). The differences between the protein (open square) and protein-salicylate mixture (filled diamond) traces are apparent, with the major positive peak shifted from 275 nm to 280 nm, and the minor positive peak at 300 nm became more predominant. The binding of salicylate clearly causes protein conformational change.

Due to the limitations of experimental conditions as discussed above, the near-UV CD spectra exhibited only minor changes after the addition of ethidium (Figure 5.4). To further evaluate the effect of ethidium binding, Trp fluorescence spectrum was monitored. The Trp fluorescence is very sensitive to the environment and thus has been used broadly as a reporter for protein conformational change. Ethidium has no significant fluorescence emission under the experimental condition used for this study. Site-directed mutagenesis experiments were performed to introduce a single Trp into the protein sequence, as ST1710 has no intrinsic Trp. Ideally, the reporter Trp should be placed at a location that experiences the most dramatic structural change following ligand binding. In an effort to identify the proper position for the mutation, the structures of apo ST1710 with apo and

salicylate-bound MTH313 were superimposed (Figure 5.5 A). As expected, the overall structure of ST1710 was very similar to that of MTH313. In the structure of ST1710, two tyrosines (Y55 and Y60) were found to be close to the corresponding ligand binding site in MTH313. Therefore, these two tyrosines were chosen to be replaced with Trp. Two single Tyr to Trp mutants (Y55W and Y60W) were constructed to monitor their Trp fluorescence changes following ethidium binding (Figure 6.5 B,C). The fluorescence of wild-type ST1710 was also acquired under the same experimental condition as a reference (Figure 5.5 B). The fluorescence intensity of wild-type ST1710 was very small in the wavelength region examined, as expected for a protein without intrinsic Trp. As a control experiment, the effect of the presence of ethidium on the fluorescence emission of the free amino acid was also examined. Ethidium quenched the fluorescence of both the ST1710 mutants and the free amino acid Trp. However, in the latter case, the quenching involved an intensity drop of only approximately 30%, with very little wavelength shift of the emission peak. For mutants Y55W and Y60W, the intensities dropped by approximately 35 and 40%, respectively, and the emission maxima also red-shifted. In addition, the changes caused by ethidium binding on the fluorescence spectra of Y55W and Y60W were different, supporting the notion that protein conformational changes were associated with ethidium binding. However, the potential contributions from the direct Trp-ethidium interactions could not be completely excluded. The bound ethidium might be in the proximity of W55 and W60, and thus, the binding of ethidium might have changed the chemical environment of the reporter Trp and therefore produced the observed changes in fluorescence emission.

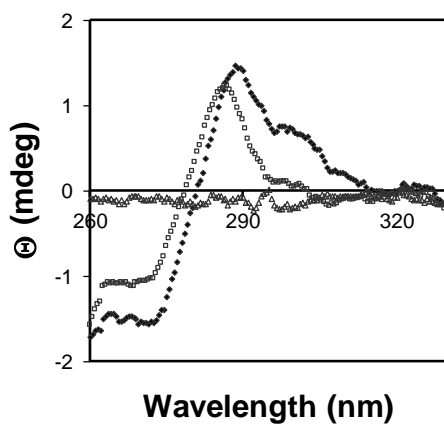
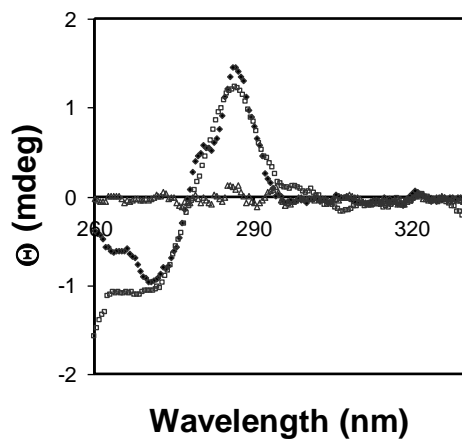


Figure 5.4 Circular Dichroism characterization of ST1710 conformation change. ST1710 conformational change induced by the binding of ethidium (top) and salicylate (bottom) at 50 °C. CD spectra of ST1710 (\square), ligand (Δ), and ST1710 bound with ligand (\blacklozenge).

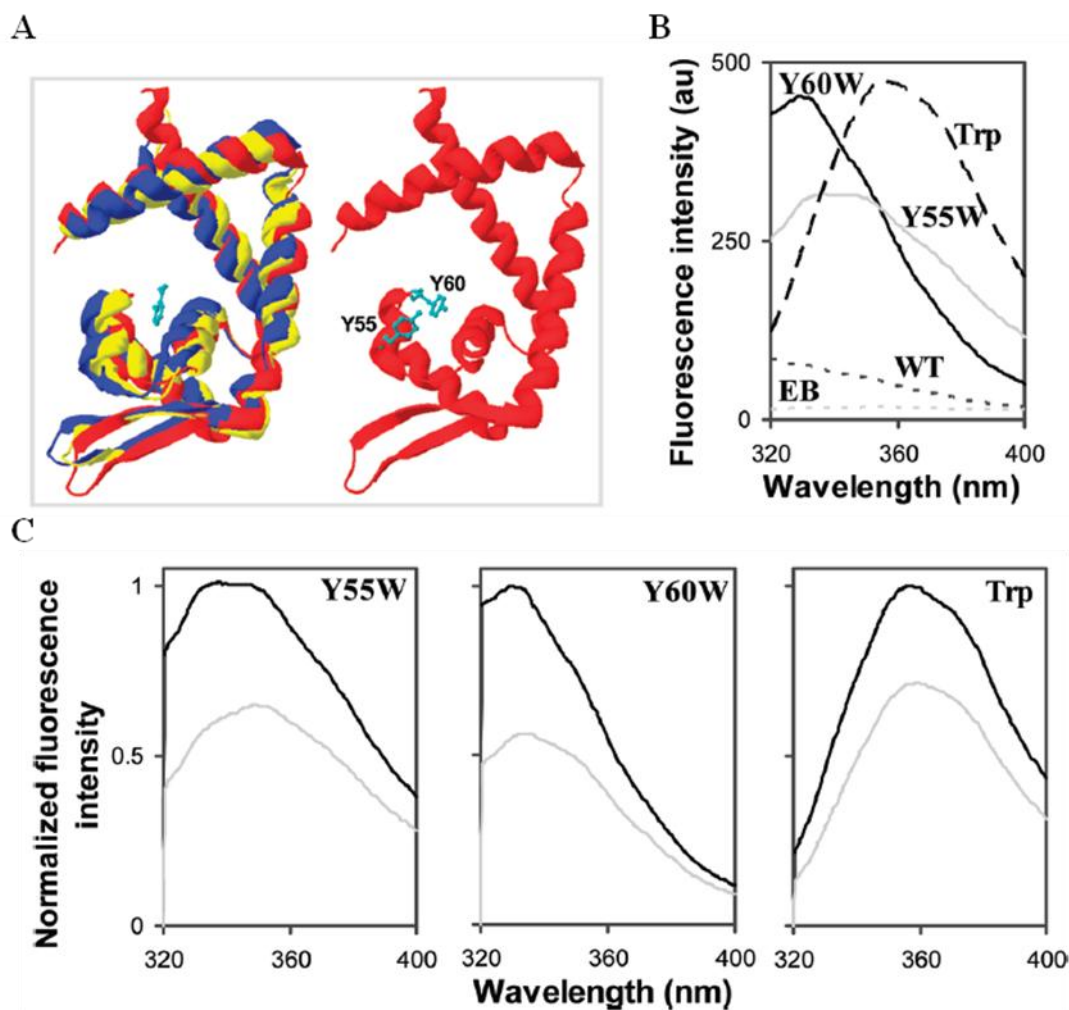


Figure 5.5 Effect of ethidium binding on the Trp fluorescence emission. (A) The left panel shows the superimposition of the crystal structures of apo MTH313 (blue), MT313 in complex with salicylate (yellow, with salicylate shown as a cyan ball-and-stick model), and ST1710 (red). Protein Data Bank entries 3BPV (apo MTH313), 3BPX (MTH313-salicylate complex), and 2EB7 (ST1710) were used to create this figure. The right panel shows the structure of ST1710, with residues Y55 and Y60 shown as cyan ball-and-stick models. (B) Fluorescence emission spectra of mutants Y60W (solid black line), Y55W (solid gray line), wild-type ST1710 (dotted black line), Trp (dashed black line), and

ethidium bromide (dotted gray line). The excitation wavelength was 280 nm. The concentrations of the proteins, Trp, and ethidium were 1, 1, and 5 μ M, respectively. (C) Normalized fluorescence emission spectra of mutants Y55W and Y60W and Trp in the absence (black) and presence (gray) of ethidium bromide. The experimental condition was the same as described above. The spectra in each panel were normalized to the maximum emission intensity of the sample in the absence of ethidium.

Additional experiments were performed to further confirm that protein conformational change occurred. TNM specifically nitrates Tyr to form 3'-nitrotyrosine.^{195, 196} The susceptibility of a specific Tyr in a protein sequence to the TNM nitration has been exploited to assess the solvent accessibility of the corresponding residue.^{194, 196} Wild type ST1710 was treated with TNM in the presence or absence of 100 μ M ethidium bromide. The modified protein was separated from the excess TNM and ethidium bromide by passing the reaction mixture through a desalting column. Finally, the number of Tyr residues nitrated per protein was estimated as described in Materials and Methods. ST1710 has five tyrosines. A 12-fold TNM-to-protein molar excess (2.4-fold molar excess vs Tyr) was used during the experiment. In the absence of ethidium, approximately two tyrosines per protein molecule were nitrated. The presence of ethidium in the nitration step reduced the efficiency of nitration by approximately 30%, with 1.4 tyrosines modified per protein. To identify the exact site of modification, I submitted TNM-modified ST1710 to the University of Kentucky Mass Spectrometry Facility for MS analysis. Gel pieces containing the modified protein were digested with trypsin and then subjected to LC-ESI-MS/MS analysis. Resulting MS/MS spectra were searched against archaeobacteria proteins in the NCBI database using the Mascot search

engine (Matrix Science) allowing nitrotyrosine modification. ST1710 was identified as the top hit. ST1710 contains five tyrosines: Y19, Y37, Y55, Y60, and Y111.

Peptide fragments containing four of them (Y37, Y55, Y60, and Y111) were identified in the MS/MS spectra. Y55 only presented in the nitrated form, suggesting that this Tyr was nitrated to a very high extent. Y37, Y60, and Y111 presented in both the unmodified and nitrated forms. Due to the limited quantification capability of MS, the extent of nitration could not be reliably derived for Y37, Y60, and Y111. The nitration state of Y19 was also unknown, as the peptide fragment containing Y19 could not be observed in the spectra. As a summary, at least four tyrosines (Y37, Y55, Y60, and Y111) were nitrated in ST1710, with Y55 modified to a very high extent. Nitration was not localized to two specific tyrosines, although statistically two tyrosines were modified per protein. The extent of modification was 30% lower in the presence of ethidium. Due to the limited quantification capability of the experiment, it would be difficult to attribute the 30% decrease in nitration to any specific Tyr. Most likely, it was a combined effect of all the modified tyrosines.

The CD spectra for CCCP binding are very intriguing (Figure 5.6). Neither 1 mM CCCP alone (grey) nor the ST1710 alone (black, first line from the top, overlaps partially with the grey line) had significant signal at around 325 nm (Figure 5.6 A). However, a negative peak emerged at 325 nm with the addition of CCCP into ST1710, which grew with the increase of CCCP concentration and finally reached saturation. The near UV CD profiles of proteins have been well characterized, and the signals are attributed to aromatic residues (Tryptophan, Tyrosine and Phenylalanine) and disulfide bond.^{197, 198}

There is no intrinsic tryptophan or cysteine in ST1710. Tyrosine usually has a peak

between 275 and 282 nm, and phenylalanine shows sharp fine structures between 255 and 270 nm.¹⁹⁹ The small change upon the addition of CCCP at the area between 260 to 270 nm might come from the protein conformational change. However, the negative peak at 325 nm most likely came from the protein bound CCCP, which gained a certain degree of chirality in the asymmetric binding pocket. Such observation is well documented for certain ligands and cofactors, that have little CD signal in their free form, while produce large signals once bound with protein.²⁰⁰⁻²⁰³ To further verify if the drastic signal change came from the specific binding of CCCP to ST1710, effect of CCCP on the CD ellipticity of the amino acid Tyrosine was examined (Figure 5.6b). There are five tyrosine residues in ST1710, so 1.5 mM of free Tyrosine was used in this study. The sample with Tyrosine alone had a peak at 270~280 nm, which does not change upon the addition of CCCP, indicating that the peak observed at 325 nm in figure 5.6 A did result from the interaction of CCCP with the protein binding pocket. The ellipticity at 325 nm in figure 5.6 A was plotted versus the molar ratio between CCCP and ST1710 (Figure 5.6 B). A clear inflection point can be observed at a CCCP to ST1710 molar ratio of 1:1, strongly suggesting a binding stoichiometry of one CCCP per ST1710 monomer. The one to one binding model was then used to fit the binding curve, yielding a dissociation constant of $57.0 \pm 7.0 \mu\text{M}$ (Figure 5.6 C).

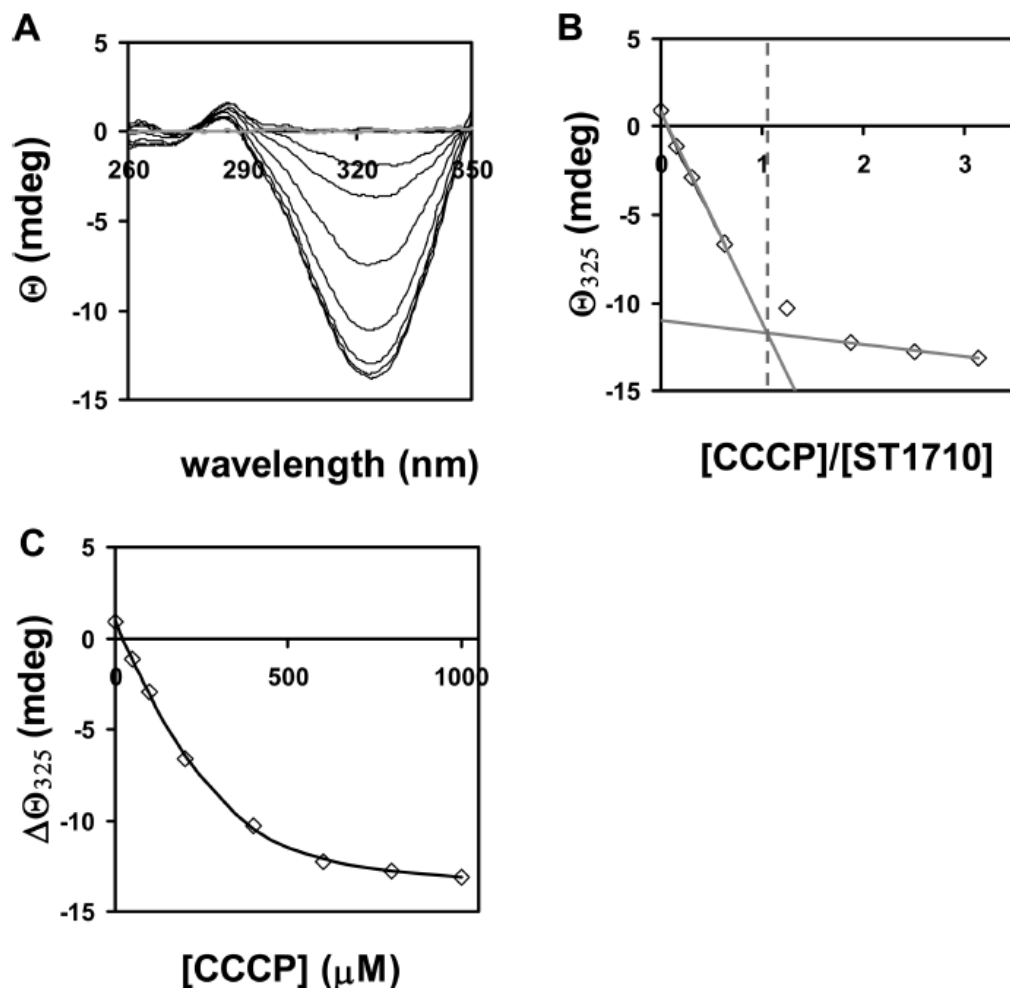


Figure 5.6 Binding study of CCCP and ST1710 with CD spectroscopy. (A) Black traces from top to bottom are for 300 μM ST1710 with 0, 50, 100, 200, 400, 600, 800, and 1000 μM CCCP, respectively. The gray trace is for 1000 μM CCCP alone. (B) The ellipticity at 325nm in panel A was plotted vs the molar ratio of CCCP to ST1710 to determine the stoichiometry of binding. Linear regressions of the data points from the first four (0, 50, 100, and 200 μM) and last three (600, 800, and 1000 μM) concentrations crossed at a ligand-to-protein ratio of $\sim 1:1$ (dotted gray line). (C) The ellipticity at 325 nm was plotted vs the concentration of CCCP and fitted with the 1:1 binding model

The information obtained from the binding of three ligands, it was found that ST1710 binds to the ligands at affinities close to those of the bacterial MarR proteins (Table 5.1). ST1710 forms homodimers in solution, characteristic to MarR family members. Each ST1710 subunit in the dimer binds with one CCCP, However no coordination can be observed between the two binding sites in a ST1710 dimer. Similarly, no coordination can be observed for the binding of ethidium either.

Table 5.1 Fitting parameters of binding property between ST1710 and its ligands.

Ligand binding				
Ligand	protein	Kd (apparent)	N	ref
Salicylate	MarR	2 mM		204
	ST1710	~1 mM*		This study
Ethidium	ST1710	19.1 ± 4.6 μM	0.88 ± 0.07	This study
CCCP	EmrR	5~25 μM		205
	EmrR	2 μM		206
	ST1710	57.0 ± 7.0 μM		This study

DNA binding		
	N	Kd (nM)
10 °C	1.12 ± 0.05	618 ± 34
30 °C	1.13 ± 0.05	334 ± 15
50 °C	1.06 ± 0.04	189 ± 9

* Estimated from its inhibitory effect in Figure 5.8 B.

5.3.2 Temperature effect of ligand binding on ST1710-DNA interaction

A MarR transcriptional regulator can be either a repressor or activator. ST1710 is expected to be a repressor, based on its homology with the *E. coli* MarR repressor EmrR.¹⁹³ Kumarevel et al. identified a putative DNA binding sequence (ST1) for ST1710 through scanning the local sequence of *S. tokodaii* genome for homology with the *ohrA* promoter sequence, the binding site for a MarR regulator OhrR.¹⁹⁰ The binding constant between ST1 and ST1710 was estimated to be ~15 μ M using gel-mobility shift assay by the authors. Because of the low binding affinity, the authors suggested that the observed binding might be non-specific. One factor that was not taken into consideration during the study is the temperature. ST1710 normally operates at 80°C, and temperature is known to affect the interactions between DNA and protein.²⁰⁷⁻²⁰⁹ Binding constant determined at room temperature may not accurately reflect the real physiological value at 80°C. In this study, binding between ST1 and ST1710 with a different method (fluorescent polarization) at three temperatures, 10, 30, and 50°C was investigated. The highest temperature for this study is limited by the instrumentation, and the melting temperature of the double stranded oligonucleotide that contains the binding sequence. Since the *Sulfolobus tokodaii* is cultured in the *Sulfolobus* medium, which has an ionic strength around 0.04 M (calculated based on the composition of the *Sulfolobus* medium), 50 mM NaCl was included in the binding buffer (10 mM HEPES, pH 7.5, 50 mM NaCl, 1 μ g/ml Calf Thymus DNA). The forward sequence was labeled with FITC at the 5' end, before annealed with the reverse sequence to generate FITC labeled double stranded sequence (F-ST1). Small aliquots of concentrated ST1710 were titrated into 5 nM of F-ST1, and the change of the fluorescent polarization (P) with the addition of protein was

monitored at all three temperatures (Figure 5.7). To evaluate the potential contribution of FITC to binding, ST1710 was titrated into free FITC solution, and no increase of fluorescent polarization can be observed. The dissociation constant K_d and the Hill coefficient were derived by fitting the binding curves with the Hill equation as described in the material and method section (Table 5.1). Two conclusions can be made based on the fitting results. Number one, the binding affinity increases with the rise of temperature. It almost doubled from 10°C to 30°C, and then doubled again from 30°C to 50°C. Number two, the Hill coefficient n is close to 1 for all three temperatures, indicating no coordination in binding can be observed. The melting temperature of the oligonucleotide prevented us from doing binding studies at even higher temperature. The increase of binding affinity with the rise of temperature is encouraging, suggesting that at 80°C the dissociation constant may further decrease to a value less than 100 nM. However, the lack of binding coordination is different from what had been observed with the bacterial MarR regulators, which clearly should positive coordination between the two subunits in a protein dimer.²¹⁰

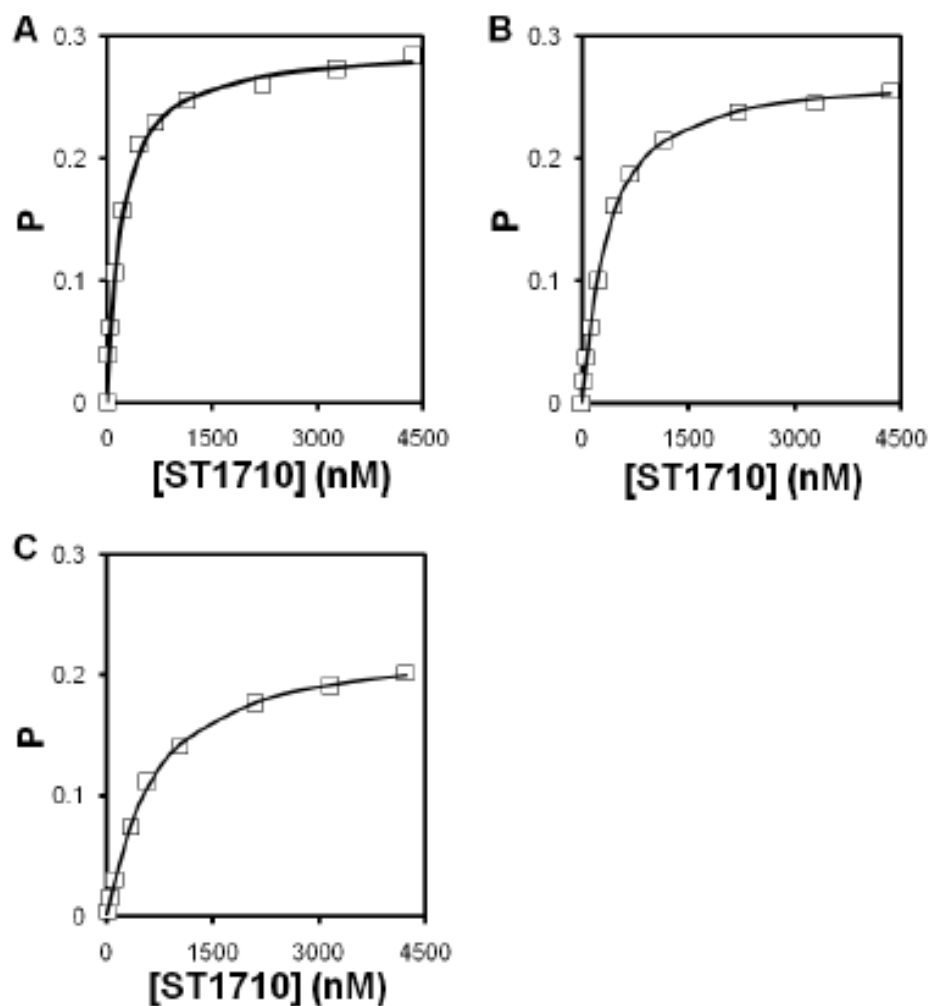


Figure 5.7 Effect of temperature on the binding between ST1710 and ST1. ST1710 was titrated into a binding buffer (10mM HEPES, 50 mM NaCl, pH 7.2) containing F-ST1 at 5 nM at 50°C (A), 30°C (B) and 10°C (C). Fluorescent polarization was monitored with the excitation wavelength of 492 nm and emission wavelength of 515 nm. The binding curves were fitted with the Hill equation for the dissociate constant K_d and Hill coefficient n (summarized in Table 5.1).

5.3.3 Small ligands repress the binding between ST1710 and ST1.

Using the complex of ST1710-ST1 as a model system, the inhibitory effect of CCCP and salicylate on the protein-DNA binding at 50°C was examined (Figure 5.8). Ethidium was excluded from this study due to its capability to intercalate into dsDNA. The fluorescent polarization value of the ST1710-ST1 mixture was monitored while small aliquots of concentrated ligands were titrated into the system. For both CCCP and salicylate, the addition of ligand induced the dissociation of ST1710 and ST1, resulting in decreased polarization. No such effect can be observed when the ligands were titrated into free ST1 solution. To further investigate the specificity of this inhibitory effect, I checked the effect of the amino acid Tyr on ST1710-ST1 binding. Tyr contains a phenyl moiety, resembles the structure of salicylate. The concentration range was limited by the poor solubility of Tyr in the binding buffer, but no repression could be observed at the highest concentration I used in this study (Figure 5.8 C).

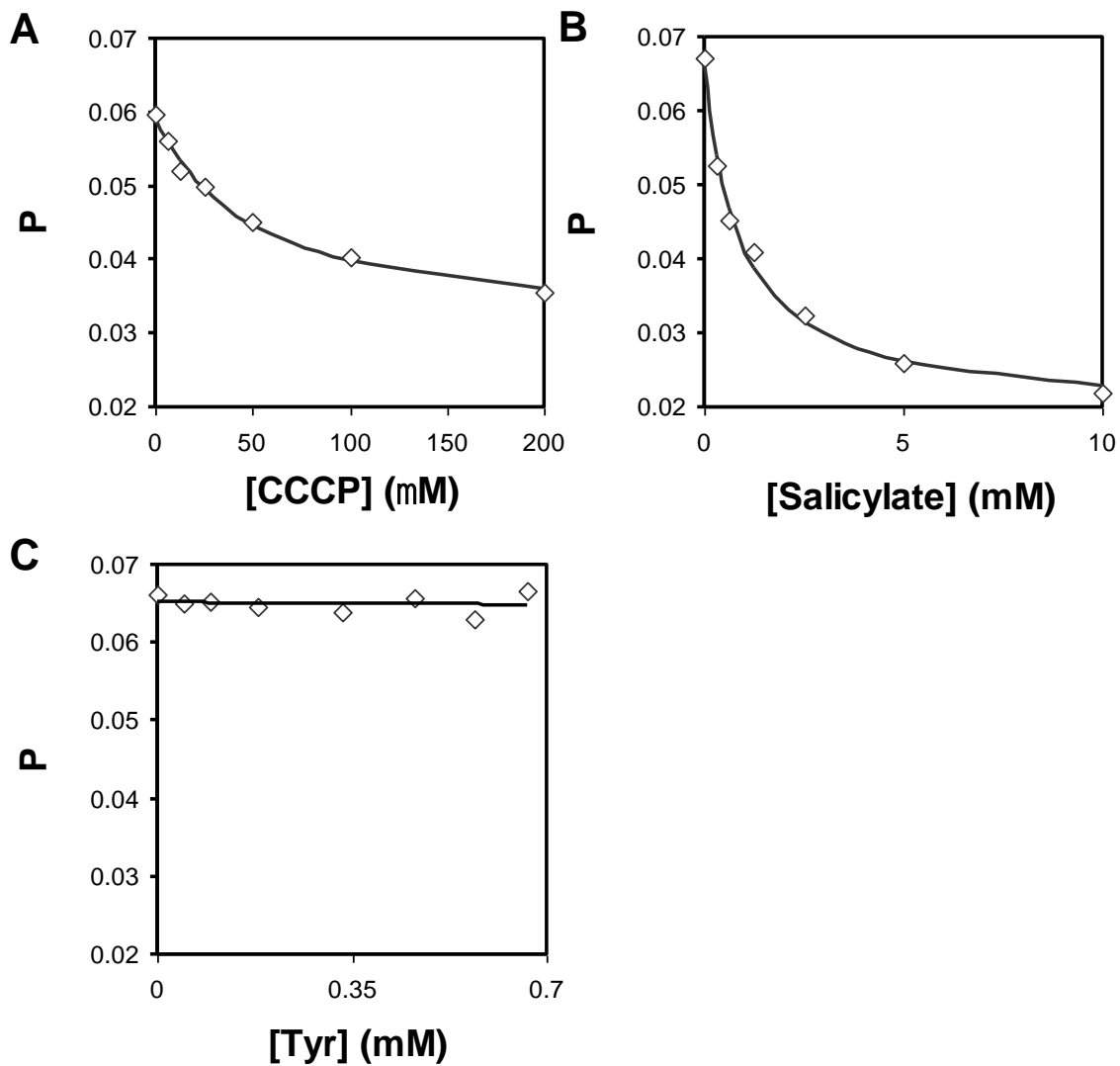


Figure 5.8 Effects of small molecule ligands salicylate (A), CCCP (B) and Tyr (C) on ST1710-DNA binding. The ligand was titrated into a buffer solution (10mM HEPES, 50 mM NaCl, pH 7.5, 1 μ g/ml calf thymus DNA) containing 20 nM F-ST1 with 50 nM ST1710. Solid lines shows the trend of the data.

In summary, I characterized the effector binding property of an archaeal MarR-type repressor, ST1710, to three representative bacterial MarR ligands, a cation, an anion, and a neutral molecule. These bindings cause conformational changes of the protein, as

revealed by the change of the protein tertiary structure. The binding affinities of the ligands were comparable to their bacterial homologs. For CCCP, one ligand binds to one ST1710 monomeric subunit, and no coordination of binding can be observed. Intriguingly, no coordination can be observed for ST1710 binding to ST1 either, different from the bacterial MarR type repressor. Although it is possibility that the archaeal MarR has a difference mechanism of function, the high degree of structural and sequence homology with the bacterial MarR argues against it. Since ST1 was identified by sequence homology, not the more thorough study with DNA footprinting coupled with mutational experiments, there remains a possibility that ST1 does not contain the real promoter sequence of ST1710. The MarR regulators bind to (pseudo) palindromic sequences. No clear base pair symmetry can be found in ST1. It is possible that part of the ST1 resembles half of the palindromic binding sequence, to which only one subunit of the protein dimer bind efficiently. This may explain the less than expected binding constant for a real promoter sequence, and the lack of binding coordination. Nonetheless, the binding of CCCP and salicylate clearly disrupted the ST1710 to DNA binding. Gene encoding ST1710 is just downstream of gene ST1709, forming part of a bacteria like operon. ST1709 is a putative multiple drug resistant transporter protein that belongs to the Major Facilitator Superfamily. It is likely that both proteins are involved in functions such as detoxification or response to environmental stress, with ST1710 regulating the expression level of ST1709. The MarR is one of the few regulator families that exist broadly in both the kingdoms of bacterium and archaea. As many archaea species are found in extremely hostile environments, it is not surprising that the MarR type regulators would be critical for the survival of such organisms. An archaeal MarR activator, BldR,

have been shown to play important roles of detoxification of aromatic aldehyde. The exact cellular function of ST1709 is still waiting to be determined.

Chapter 6 Development of a Direct Fluorescence Polarization Assay for the Detection of Glycopeptide Antibiotics

6.1 Introduction

Glycopeptide antibiotics are cyclic peptides that bind to the peptide precursor acyl-D-alanyl-D-alanine in peptidoglycan to inhibit the biosynthesis of bacterial cell walls. Vancomycin, teicoplanin and telavancin are three main glycopeptides antibiotics used widely in clinical settings.²¹¹⁻²¹³ The ability to precisely monitoring of the serum level of those glycopeptides antibiotics would help to minimize their toxicities and side effects,^{214, 215} provide important pharmacokinetic and pharmacodynamic parameters for clinical studies,²¹⁶⁻²²⁰ and thus optimize therapy for patients.²²¹⁻²²³

Various assays have been developed to measure the concentration of glycopeptide antibiotics, including immunoassay,²²⁴⁻²²⁶ HPLC,²²⁷⁻²²⁹ bioassay,^{230, 231} and solid phase enzyme receptor assay (SPERA).^{232, 233} These existing methods suffer from various drawbacks including the lack of selectivity, the requirement of large amount of samples, or the cumbersome pretreatment processes. For example, fluorescence polarization immunoassay (FPIA) is a traditional method for the determination of glycopeptide antibiotics in human serum.^{226, 230} The fluorescent-labeled vancomycin binds to an anti-vancomycin antibody and leads to an increase of the fluorescence polarization signal. Free vancomycin in the clinical samples competitively binds to the antibody, release the labeled one, decrease the fluorescence polarization signal and allow the quantification of the analyte (Figure 6.1).^{234, 235}

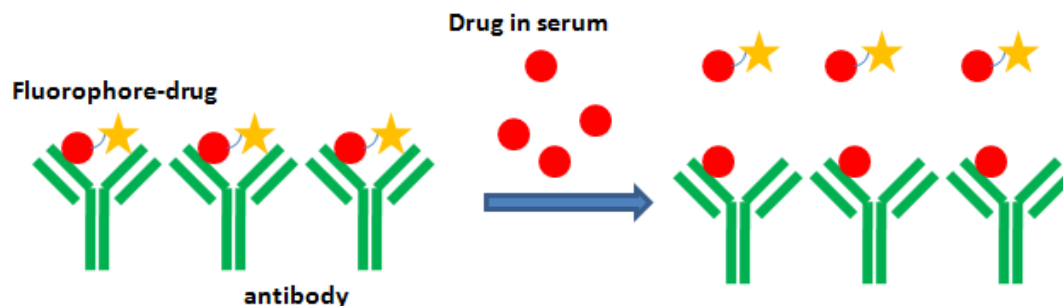


Figure 6.1 The mechanism of fluorescence polarization immunoassay

In this study I developed a direct fluorescence polarization (FP) based assay, taking advantage of the specific interaction between glycopeptide antibiotics and their therapeutic target, the D-alanyl-D-alanine. Fluorescence polarization is an intrinsically powerful tool for analysis of molecule interaction. These interactions include protein-protein interaction, protein-DNA interaction, and protein-RNA interaction. And also the fluorescence polarization technology has been successfully applied to monitoring of medicine level, detection of enzyme activity and even to high-throughput screening during for the drug discovery.²³⁶

The theory of fluorescence polarization is based on that when a small fluorescent molecule is excited with plane-polarized light, the emitted light is depolarized because molecules tumble and rotate rapidly in solution. However, when the small fluorescent molecule binds with a large molecule, the complex moves much slower and thus is not as efficient at depolarizing the light. The free fluorescent molecule and bound complex each has an intrinsic fluorescence polarization value: the free molecule has a low value while the bound has a higher one. The fluorescence polarization value of a fluorescent molecule

is proportional to the molecule's rotational relaxation time (t), which depends on molecule volume (V), temperature (T), and viscosity (η). The relationship is as follow,

$$t = \frac{3\eta V}{RT}$$

R is the gas constant. From the equation, decreasing temperature or increasing viscosity will increase fluorescence polarization value. On the other hand, if temperature and viscosity are kept constant, increasing the molecule volume will also increase fluorescence polarization value. Change of molecule volume can result from binding or dissociation of two molecules.

Experimentally, the degree of polarization is monitored by measurements of fluorescence intensities parallel and perpendicular with respect to the plane of linearly polarized excitation light, and is expressed in terms of fluorescence polarization (P) or anisotropy (r)

$$P = \frac{(I_v - I_h)}{(I_v + I_h)} \quad r = \frac{(I_v - I_h)}{(I_v + 2I_h)}$$

P is the polarization, r is anisotropy, I_v is the vertical component of the emitted light and I_h is the horizontal component of the emitted light. From the equation, both P and r are independent of the fluorophore concentration.²³⁷

Here, the acetylated L-Lys-D-Ala-D-Ala was labeled with a fluorephore and the increase of FP of the labeled peptide in the presence of antibiotics was monitored. Compared to the existing fluorescence polarization immunoassay, our method has the advantages of being more simple and cost-efficient. In addition, since no protein (such as the anti-

vancomycin antibody) is used in the assay, the shelf-life and stability of the assay is expected to greatly exceed those of the immunoassay. The simplicity and low-cost of our direct fluorescence polarization assay hold a promise for the application of clinical use to determine the concentration of glycopeptide antibiotics.

6.2 Materials and Methods

6.2.1 Materials

The acetylated L-Lys-D-Ala-D-Ala peptide, teicoplanin, fluorescein isothiocyanate (FITC), High-performance-liquid-chromatography (HPLC) grade acetonitrile, and heat inactivated, sterile-filtered fetal bovine serum (FBS) were from Sigma-Aldrich (St. Louis, MO). Vancomycin hydrochloride was from Duchefa (Haarlem, the Netherlands). Telavancin was from Astellas (Deerfield, IL). AlexaFluor 680 (AF680) was from Invitrogen (Eugene, OR). Teicoplanin FPIA kit was from LABfx (Portland, OR). All other reagents were of analytical grade and purchased from Sigma-Aldrich.

6.2.2 Labeling the Fluorophore to the Peptide

The acetylated peptide L-Lys-D-Ala-D-Ala (3 mM) was incubated with FITC (4.5 mM) in a PBS buffer (10 mM Na₂HPO₄, 2 mM KH₂PO₄, 2.7 mM KCl, 137 mM NaCl, pH 7.4) at room temperature overnight. Tris-HCl buffer (5 mM, pH 7.4) was added to the reaction mixture and incubated for 2 h at room temperature to terminate the reaction. The FITC - labeled peptide was purified using a reverse-phase HPLC (Waters, Milford, MA) on a C18 column (Waters, Milford, MA). The purified FITC-labeled peptide was dried under vacuum and then resuspended in water. The molecule weight of the labeled peptide was confirmed by mass spectroscopy analysis. The concentration of the peptide was determined based on the absorption at 515 nm. Labeling with AlexaFluor 680 was performed similarly. The peptide probe concentration was determined by absorption at 680 nm. The molecule weight of the labeled peptide was also confirmed by mass spectroscopy analysis.

6.2.3 Fluorescence Polarization Measurements

Fluorescence polarization measurements were performed using a Perkin Elmer LS-55 fluorescence spectrometer (Perkin Elmer, Waltham, MA). The temperature was kept at 20°C. Fluorophore-conjugated peptide (FITC-peptide or AF680-peptide) was added into 400 µl PBS buffer or FBS to a final concentration of 1 µM. The excitation and emission wavelengths were 479 nm and 515 nm for FITC-peptide, and 679 nm and 702 nm for AF680-peptide. Teicoplanin FPIA assay system was also performed on the Perkin Elmer LS-55 fluorescence spectrometer (Perkin Elmer, Waltham, MA) and followed the product instruction.

6.2.4 Titration and Data Fitting

For titration experiments, fluorophore-conjugated peptide (FITC-peptide or AF680-peptide) was added into 400 µl PBS buffer to a final concentration of 1 µM, and then small aliquots of glycopeptide antibiotics (vancomycin, teicoplanin or telavancin) were titrated into the sample. The increases of FP upon the formation of drug-peptide complex were recorded.

The titration curve was simulated with the non-cooperative one to one binding model.

²³⁸[Eq. (1)]

$$Y = (Y_{\max} - Y_{\min}) \left(\frac{([P] + x + Kd) - \sqrt{([P] + x + Kd)^2 - 4[P]x}}{2[P]} \right) + Y_{\min} \quad (1)$$

Y is the fluorescence polarization at the specific emission wavelength. (Y_{max}-Y_{min}) is the maximum change of the fluorescence polarization at the specific emission wavelength.

[P] is the peptide probe concentration. K_d is the dissociation constant between the probe and the glycopeptide antibiotic. x is the concentration of the glycopeptides antibiotics added into the buffer. The titration curve is fitted using Origin (Northampton, MA). The standard deviation of the calculated dissociation constant is from the fitting.

6.2.5 Binding Selectivity Assay

For the selectivity measurement, AF680-peptide was added into 400 μ l FBS to a final concentration of 1 μ M. Different antibiotics (ampicillin, gentamicin, tetracycline, nalidixic acid, chloramphenicol, vancomycin and teicoplanin) were added into the FBS at a concentration of 8 μ M.

6.2.6 Determination of Drug Concentration in Test Samples

For tests in serum, AF680-peptide was added to 400 μ l of FBS to a final concentration of 1 μ M. Then, known quantities of antibiotics were added into the sample. The concentrations of the drugs were determined based on the calibration curves derived in FBS. For tests in blood, three human blood samples were spiked with teicoplanin in the therapeutic range by a person not involved in this project. The exact values were kept blind to the authors during the analysis. The blood samples were centrifuged at 2000g for 10min. The supernatant (serum) was collected and analyzed together with a series of teicoplanin standards in FBS as described above. For each serum sample, two sets of dilutions were prepared. So the final concentration of teicoplanin would be in the working concentration range of the assay. The first sets of three test samples contain 10 μ l of serum and 390 μ l of FBS with 1 μ M of AF680-peptide. The second sets of three test samples contain 20 μ L of serum and 380 μ l of FBS with 1 μ M of AF680-peptide. The

teicoplanin concentration in each set of samples was determined. The original teicoplanin concentration calculated from the set of samples falls in the working concentration range. The same serum samples were analyzed using the teicoplanin FPIA kit following the instruction of the manufacturer.

6.3 Results and Discussions

6.3.1 The Design and Synthesis of Peptide Probes.

I used amine-reactive fluorophores to label the peptide acetylated L-Lys-D-Ala-D-Ala. I chose this peptide for three reasons. First, glycopeptide antibiotics are known to bind specifically to D-Ala-D-Ala. Second, L-lys is naturally occurring in the peptidylglycan precursor peptide L-Ala-D-Glu-L-Lys-D-Ala-D-Ala. I expect the incorporation of the L-lys will not affect the interaction between the peptide and the antibiotics. Third, the side chain of Lys contains a primary amine group, which is far from the binding site judged by the crystal structure of the vancomycin and di-acetyl-L-Lys-D-Ala-D-Ala complex.²³⁹ As expected, I found that the binding affinity between the labeled peptide and vancomycin is consistent with the value reported for the binding between the free peptide and the tested glycopeptide antibiotics, indicating that the modification did not affect the interaction (Table 6.1).

Table 6.1 Fitting parameters of labeled peptide and drug interaction

Probe	Glycopeptide	Test System	Binding Constant
	Antibiotics		Kd (μM)
FITC-peptide	Vancomycin	PBS	0.91 ± 0.06
	Teicoplanin	PBS	0.14 ± 0.07
	Telavancin	PBS	3.22 ± 0.38
AF680-peptide	Vancomycin	PBS	1.07 ± 0.19
		FBS	1.81 ± 0.13
	Teicoplanin	PBS	0.29 ± 0.02
		FBS	0.87 ± 0.08
	Telavancin	PBS	1.81 ± 0.13
		FBS	5.36 ± 0.35

6.3.2 Effect of Different Fluorephores

The change of fluorescence polarization signal follows the Perrin Equation ²⁴⁰[Eq. (2)].

$$\left(\frac{1}{P} - \frac{1}{3}\right) = \left(\frac{1}{P_0} - \frac{1}{3}\right) \left(1 + \frac{kT}{\eta V} \tau\right) \quad (2)$$

τ is the fluorescence lifetime (average time the molecule stays in its excited state before emitting a photon), P_0 is the limiting polarization, k is the Boltzman constant, T is the absolute temperature, η the viscosity and V the molecular volume (molecule weight). The fluorescence polarization is reversely proportional to the lifetime of fluorophore, and proportional to the molecule volume (molecule weight). In order to maximize the observed change of polarization upon antibiotic binding, I tested two fluorephores with different lifetimes, FITC (4 ns) and AF680 (1 ns). I found that AF680-peptide yielded a larger change of signal upon drug binding (Figure 6.2), as expected based on their small sizes.

To examine if the fluorophores (FITC or AF680) themselves associate non-specifically with the glycopeptide antibiotics, I first measured the FP of 1 μ M solutions of each fluorescent molecules, FITC, AF680, FITC-peptide, or AF680-peptide. Then glycopeptides antibiotics were added into the solutions to final concentrations of 8 μ M. The final FP signals were recorded (Figure 6.3). No significant fluorescence polarization changes were observed in the solutions with the free fluorophores, suggesting that there is no significant interaction between the drugs and the peptide probes.

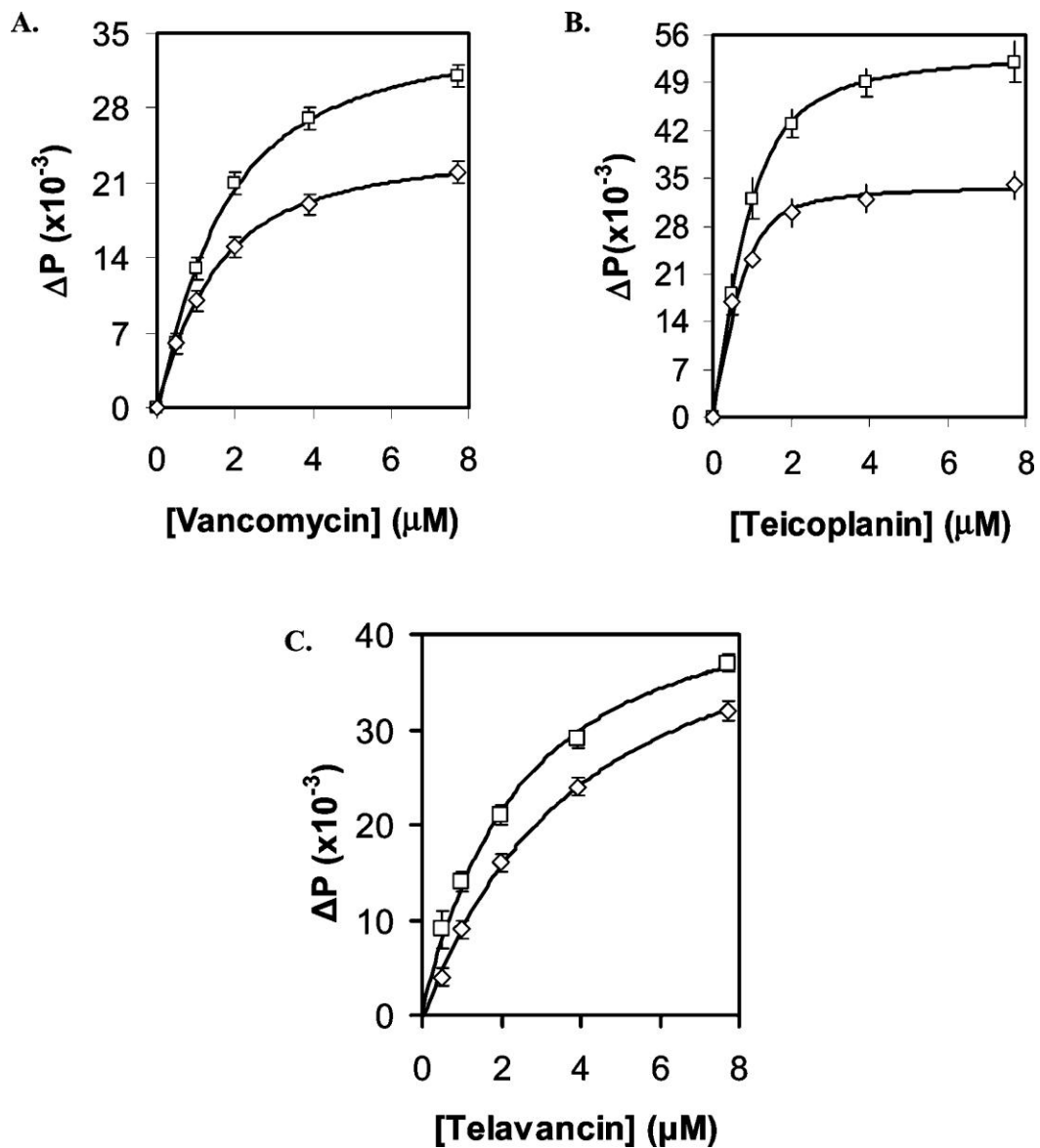


Figure 6.2 Calibration curves of two different peptide probes (FITC-peptide-diamond and AF680-peptide-squares) with vancomycin, teicoplanin, and telavancin in PBS buffer. The concentration of the peptide probes were 1 μM . The concentrations of the glycopeptides antibiotics were increased from 0 to 8 μM during the titration.

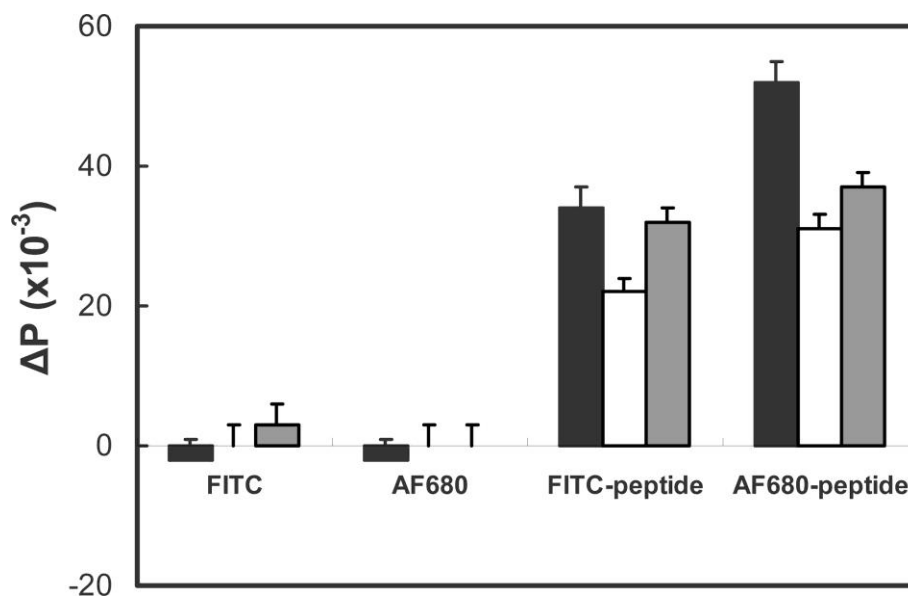


Figure 6.3 The free fluorophores do not interact with glycopeptide antibiotics. The fluorescence polarization changed when the vancomycin (black), teicoplanin (white) or telavancin (gray) was added into PBS buffer containing peptide probes (FITC-peptide or AF680-peptide). However, no change was observed when the drugs were added into solution of the free fluorophores (FITC or AF680). The free fluorophores (FITC or AF680) were first deactivated using Tris-HCl buffer (5 mM, pH 7.4). The concentration of fluorophores or peptide probes was 1 μ M. The concentration of the drugs is 8 μ M.

6.3.3 Titration Curves of Glycopeptide Antibiotics.

The binding between the antibiotics and peptide probes were monitored following the increase of fluorescence polarization of the samples upon addition of an increasing concentration of the antibiotics (Figure 6.1). The dissociation constants (K_d) between the drugs and peptide probes were estimated to be approximately 1 μ M, 0.2 μ M, and 1.8 μ M, respectively, for vancomycin, teicoplanin, and telavancin (Table 6.1). The nature of the fluorophores did not have a drastic effect on the binding affinity, indicating they are not directly involved in the interaction. The determined affinities are similar to the values reported for the bindings between those antibiotics and the ligand di-acetyl-L-Lys-D-Ala-D-Ala.²⁴¹⁻²⁴⁴ Compared with the FITC-peptide probe, the AF680-peptide yielded larger changes in fluorescence polarization signals when it bound to the antibiotics, as expected from its shorter lifetime.

6.3.4 Selectivity Study

In many situations, several antibiotics may be used together as a cocktail in research or clinical applications. It is desirable to have a method that can selectively detect a specific one or specific class of antibiotics. The interaction between the peptide probe and glycopeptide antibiotics is highly specific. The binding selectivity of the AF680-peptide probe toward different antibiotics were tested in FBS (Figure 6.4). The assay was highly selective toward the three glycopeptides. No significant change of fluorescence polarization was observed for other antibiotics tested.

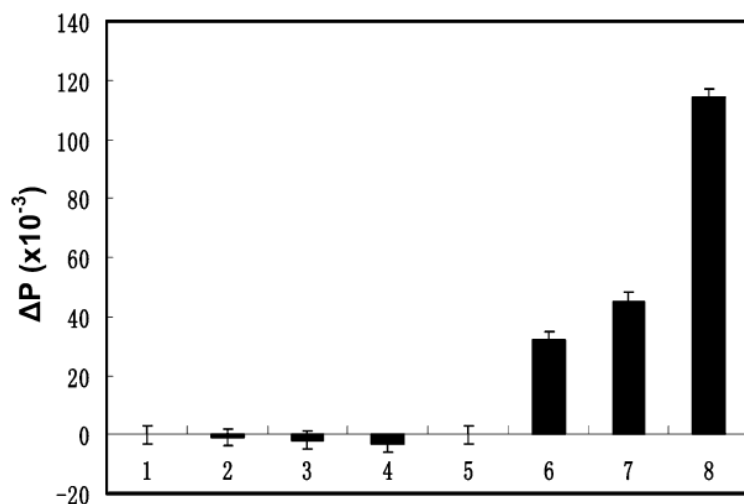


Figure 6.4 Selectivity of the assay. Different antibiotics (8 μM) were added into solutions containing AF680-peptide (1 μM). Antibiotics tested were ampicillin (1), gentamicin (2), tetracycline (3), nalidixic acid (4), chloramphenicol (5), vancomycin (6), telavancin (7), and teicoplanin (8). Error bars indicate the standard deviations from three independent measurements.

6.3.5 Drugs Detection in Serum

To further examine the usefulness of the current method in the detection of glycopeptide antibiotics in clinical samples, such as serum, I measured the calibration curve using AF680-peptide for the detection of vancomycin, teicoplanin, and telavancin in fetal bovine serum (Figure 6.5). The potential influence of serum on the assay is in two fold. First, according to the Eq 2, increasing viscosity will slow down the tumbling of the fluorophores, and thus increase fluorescence polarization. Second, certain species in the serum may interact with the peptide probe or the drugs to prevent accurate detection. As expected, since the viscosity of fetal bovine serum is higher than that of the PBS buffer, the fluorescence polarization measured in serum increased both for the free peptide

probes and the drug-peptide complex. The increase is more dramatic for the complex, which resulted in an increase in the ΔP . The binding affinity of both drugs decreased slightly compared to the affinities measured in PBS buffer (Table 6.1). I speculate this change of affinity is due to the interaction between certain components in the serum with either the peptide probe or glycopeptides antibiotics, which weakened their affinity for each other through competition mechanism.

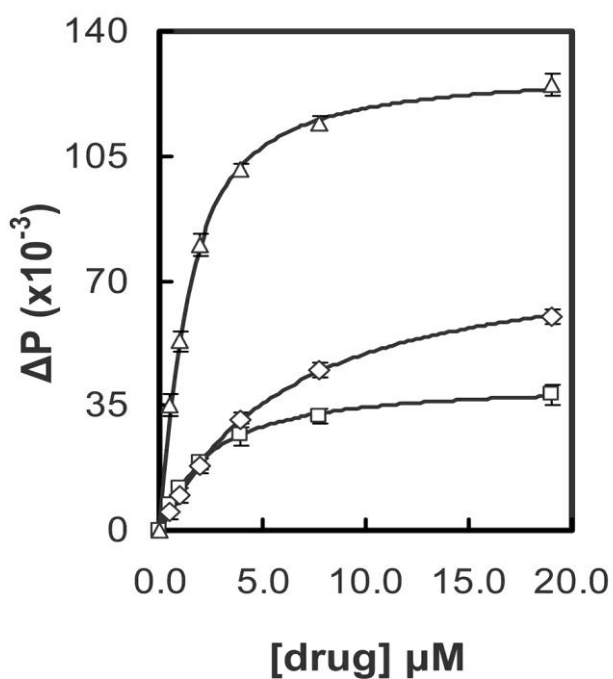


Figure 6.5 Calibration curves of detection for vancomycin, teicoplanin and telavancin in FBS. AF680-peptide (1 μM) was used in the assay.

6.3.5 Recovery Test in Human Blood

Finally, I used human blood samples spiked with known amounts of teicoplanin and compared our assay with a commercial FPIA kit. Human blood samples were spiked with different concentrations of teicoplanin based on the therapeutic concentration window of the drug. The same sample was tested with our assay side by side with a commercial FPIA teicoplanin detection kit. Each blood sample spiked with the teicoplanin was first centrifuge to remove the blood cells. The supernatant plasma was collected and diluted to the working concentration range. The working concentration range of teicoplanin ranges from 0.47 to 3.8 $\mu\text{g/ml}$ while teicoplanin therapeutic window approximately is about 10-30 $\mu\text{g/ml}$.^{222, 245} Therefore, each plasma sample was diluted to 20 fold and 40 fold. At least one of the diluted final concentrations would be in the working concentration range. The concentrations in the diluted serum solution were determined based on the calibration curve in the fetal bovine serum. In the meantime, each plasma sample was also tested with a commercial FPIA kit. The results of spiked human blood were listed in (Table 6.2). The accuracy and precision of the designed assay is comparable to the commercial kit.

Table 6.2 The recovery of teicoplanin with designed method and commercial kit

Detection of teicoplanin in human blood with designed assay or a commercial FPIA kit				
Spiked ($\mu\text{g/mL}$)	Designed Assay	Recovery (%)	FPIA	Recovery (%)
9.5	9.2 ± 0.2	97	9.8 ± 0.6	103
19	19.6 ± 0.4	103	18.5 ± 0.6	97
38	39.0 ± 1.0	103	37.8 ± 4.4	99

In conclusion, a simple analytical assay was developed for the quantitative analysis of glycopeptides antibiotics in various samples. The method is highly selective toward glycopeptide antibiotics. Due to its high specificity, no pre-treatment is necessary for the assay, which greatly reduced the time and cost of the analysis. The therapeutic window for the glycopeptides antibiotics is very narrow. While the therapeutic range of vancomycin in human serum is 10 to 30 μM .^{214, 220} The toxicity effect occurs when the drug concentration is above 30 μM .²¹⁴ This range is much higher than the detection limit of our method, indicating our assay can be useful for such detections after sample dilution. Since fluorescence polarization immunoassay are already commercially available and widely used in research and clinical laboratories, our assay method could be used with the same instrumental setting with minimal modifications.

Reference

1. Wallin E, von Heijne G (1998) Genome-wide analysis of integral membrane proteins from eubacterial, archaean, and eukaryotic organisms. *Protein Science* 7: 1029-1038.
2. Daley DO, Rapp M, Granseth E, Melen K, Drew D, von Heijne G (2005) Global topology analysis of the Escherichia coli inner membrane proteome. *Science* 308: 1321-1323.
3. Casadio R, Fariselli P, Finocchiaro G, Martelli PL (2003) Fishing new proteins in the twilight zone of genomes: The test case of outer membrane proteins in Escherichia coli K12, Escherichia coli O157 : H7, and other Gram-negative bacteria. *Protein Science* 12: 1158-1168.
4. Meng G, Fronzes R, Chandran V, Remaut H, Waksman G (2009) Protein oligomerization in the bacterial outer membrane (Review). *Molecular Membrane Biology* 26: 136-145.
5. Lynch M (2012) The evolution of multimeric protein assemblages. *Molecular Biology and Evolution* 29: 1353-1366.
6. Halic M, Beckmann R (2005) The signal recognition particle and its interactions during protein targeting. *Current Opinion in Structural Biology* 15: 116-125.
7. Nagai K, Oubridge C, Kuglstatter A, Menichelli E, Isel C, Jovine L (2003) Structure, function and evolution of the signal recognition particle. *EMBO Journal* 22: 3479-3485.
8. Seluanov A, Bibi E (1997) FtsY, the prokaryotic signal recognition particle receptor homologue, is essential for biogenesis of membrane proteins. *Journal of Biological Chemistry* 272: 2053-2055.
9. Reyes CL, Rutenber E, Walter P, Stroud RM (2007) X-ray Structures of the Signal Recognition Particle Receptor Reveal Targeting Cycle Intermediates. *Plos One* 2:e607
10. Ulbrandt ND, Newitt JA, Bernstein HD (1997) The E-coli signal recognition particle is required for the insertion of a subset of inner membrane proteins. *Cell* 88: 187-196.
11. Veenendaal AK, van der Does C, Driessen AJ (2004) The protein-conducting channel SecYEG. *Biochimica et Biophysica Acta* 1694: 81-95.
12. van den Berg B, Clemons WM, Collinson I, Modis Y, Hartmann E, Harrison SC, Rapoport TA (2004) X-ray structure of a protein-conducting channel. *Nature* 427: 36-44.
13. Pogliano JA, Beckwith J (1994) SecD and SecF facilitate protein export in Escherichia coli. *EMBO Journal* 13: 554-561.
14. Tsukazaki T, Mori H, Echizen Y, Ishitani R, Fukai S, Tanaka T, Perederina A, Vassilyev DG, Kohno T, Maturana AD, Ito K, Nureki O (2011) Structure and function of a membrane component SecDF that enhances protein export. *Nature* 474: 235-238.
15. Vrontou E, Economou A (2004) Structure and function of SecA, the preprotein translocase nanomotor. *Biochimica et Biophysica Acta* 1694: 67-80.

16. Wu ZC, de Keyzer J, Kedrov A, Driessen AJ (2012) Competitive binding of the SecA ATPase and ribosomes to the SecYEG translocon. *Journal of Biological Chemistry* 287: 7885-7895.
17. Neugebauer SA, Baulig A, Kuhn A, Facey SJ (2012) Membrane Protein Insertion of Variant MscL Proteins Occurs at YidC and SecYEG of *Escherichia coli*. *Journal of Molecular Biology* 417: 375-386.
18. Samuelson JC, Chen MY, Jiang FL, Moller I, Wiedmann M, Kuhn A, Phillips GJ, Dalbey RE (2000) YidC mediates membrane protein insertion in bacteria. *Nature* 406: 637-641.
19. Popot JL, Engelman DM (1990) Membrane protein folding and oligomerization: the two-stage model. *Biochemistry* 29: 4031-4037.
20. Green WN, Claudio T (1993) Acetylcholine-Receptor Assembly - Subunit Folding and Oligomerization Occur Sequentially. *Cell* 74: 57-69.
21. Kennedy KA, Gachelet EG, Traxler B (2004) Evidence for multiple pathways in the assembly of the *Escherichia coli* maltose transport complex. *Journal of Biological Chemistry* 279: 33290-33297.
22. Traxler B, Beckwith J (1992) Assembly of a hetero-oligomeric membrane protein complex. *Proceedings of the National Academy of Sciences of the United States of America* 89: 10852-10856.
23. Kennedy KA, Traxler B (1999) MalK forms a dimer independent of its assembly into the MalFGK(2) ATP-binding cassette transporter of *Escherichia coli*. *Journal of Biological Chemistry* 274: 6259-6264.
24. Xu D, Tsai CJ, Nussinov R (1998) Mechanism and evolution of protein dimerization. *Protein science* 7: 533-544.
25. Yin CC, Aldema-Ramos ML, Borges-Walmsley MI, Taylor RW, Walmsley AR, Levy SB, Bullough PA (2000) The quarternary molecular architecture of TetA, a secondary tetracycline transporter from *Escherichia coli*. *Molecular microbiology* 38: 482-492.
26. Safferling M, Griffith H, Jin J, Sharp J, De Jesus M, Ng C, Krulwich TA, Wang DN (2003) TetL tetracycline efflux protein from *Bacillus subtilis* is a dimer in the membrane and in detergent solution. *Biochemistry* 42: 13969-13976.
27. Hong H, Joh NH, Bowie JU, Tamm LK (2009) Methods for Measuring the Thermodynamic Stability of Membrane Proteins. *Methods in Enzymology: Biothermodynamics, Vol 455, Part A 455*: 213-236.
28. Hong H, Blois TM, Cao Z, Bowie JU (2010) Method to measure strong protein-protein interactions in lipid bilayers using a steric trap. *Proceedings of the National Academy of Sciences of the United States of America* 107: 19802-19807.
29. Fleming KG, Engelman DM (2001) Specificity in transmembrane helix-helix interactions can define a hierarchy of stability for sequence variants. *Proceedings of the National Academy of Sciences of the United States of America* 98: 14340-14344.
30. Russ WP, Engelman DM (1999) TOXCAT: A measure of transmembrane helix association in a biological membrane. *Proceedings of the National Academy of Sciences of the United States of America* 96: 863-868.

31. Schneider D, Engelman DM (2003) GALLEX, a measurement of heterologous association of transmembrane helices in a biological membrane. *The Journal of biological chemistry* 278: 3105-3111.
32. Jentsch TJ, Friedrich T, Schriever A, Yamada H (1999) The CLC chloride channel family. *Pflugers Archiv-European Journal of Physiology* 437: 783-795.
33. Simon DB, Bindra RS, Mansfield TA, NelsonWilliams C, Mendonca E, Stone R, Schurman S, Nayir A, Alpay H, Bakkaloglu A, RodriguezSoriano J, Morales JM, Sanjad SA, Taylor CM, Pilz D, Brem A, Trachtman H, Griswold W, Richard GA, John E, Lifton RP (1997) Mutations in the chloride channel gene, *CLCNKB*, cause Bartter's syndrome type III. *Nature Genetics* 17: 171-178.
34. Scheel O, Zdebik AA, Lourdel S, Jentsch TJ (2005) Voltage-dependent electrogenic chloride/proton exchange by endosomal CLC proteins. *Nature* 436: 424-427.
35. Maduke M, Pheasant DJ, Miller C (1999) High-level expression, functional reconstitution, and quaternary structure of a prokaryotic ClC-type chloride channel. *Journal of General Physiology* 114: 713-722.
36. Mindell JA, Maduke M, Miller C, Grigorieff N (2001) Projection structure of a ClC-type chloride channel at 6.5 Å resolution. *Nature* 409: 219-223.
37. Dutzler R, Campbell EB, Cadene M, Chait BT, MacKinnon R (2002) X-ray structure of a ClC chloride channel at 3.0 Å reveals the molecular basis of anion selectivity. *Nature* 415: 287-294.
38. Robertson JL, Kolmakova-Partensky L, Miller C (2010) Design, function and structure of a monomeric ClC transporter. *Nature* 468: 844-847.
39. Devuyst O, Thakker RV (2010) Dent's disease. *Orphanet journal of rare diseases* 5: 28.
40. Wu F, Roche P, Christie PT, Loh NY, Reed AAC, Esnouf RM, Thakker RV (2003) Modeling study of human renal chloride channel (hCLC-5) mutations suggests a structural-functional relationship. *Kidney International* 63: 1426-1432.
41. Lourdel S, Grand T, Burgos J, Gonzalez W, Sepulveda FV, Teulon J (2012) ClC-5 mutations associated with Dent's disease: a major role of the dimer interface. *Pflugers Archiv-European Journal of Physiology* 463: 247-256.
42. Duffield M RG, Bretag A, Roberts M (2003) Involvement of helices at the dimer interface in ClC-1 common gating. *Journal of General Physiology* 121: 149-161.
43. Chen TY, Hwang TC (2008) CLC-0 and CFTR: Chloride channels evolved from transporters. *Physiological Reviews* 88: 351-387.
44. Slepko ER, Rainey JK, Sykes BD, Fliegel L (2007) Structural and functional analysis of the Na⁺/H⁺ exchanger. *Biochemical Journal* 401: 623-633.
45. Brett CL, Donowitz M, Rao R (2005) Evolutionary origins of eukaryotic sodium/proton exchangers. *American Journal of Physiology-Cell Physiology* 288: C223-C239.
46. Apse MP, Blumwald E (2007) Na⁺ transport in plants. *FEBS Letters* 581: 2247-2254.
47. Padan E, Bibi E, Ito M, Krulwich TA (2005) Alkaline pH homeostasis in bacteria: New insights. *Biochimica Et Biophysica Acta-Biomembranes* 1717: 67-88.

48. Hunte C, Screpanti E, Venturi M, Rimon A, Padan E, Michel H (2005) Structure of a Na⁺/H⁺ antiporter and insights into mechanism of action and regulation by pH. *Nature* 435: 1197-1202.
49. Williams KA (2000) Three-dimensional structure of the ion-coupled transport protein NhaA. *Nature* 403: 112-115.
50. Hilger D, Jung H, Padan E, Wegener C, Vogel KP, Steinhoff HJ, Jeschke G (2005) Assessing oligomerization of membrane proteins by four-pulse DEER: pH-dependent dimerization of NhaA Na⁺/H⁺ antiporter of *E. coli*. *Biophysical Journal* 89: 1328-1338.
51. Williams KA, Geldmacher-Kaufer U, Padan E, Schuldiner S, Kuhlbrandt W (1999) Projection structure of NhaA, a secondary transporter from *Escherichia coli*, at 4.0 angstrom resolution. *The EMBO journal* 18: 3558-3563.
52. Hilger D, Polyhach Y, Padan E, Jung H, Jeschke G (2007) High-resolution structure of a Na⁺/H⁺ antiporter dimer obtained by pulsed electron paramagnetic resonance distance measurements. *Biophysical Journal* 93: 3675-3683.
53. Rimon A, Tzuberly T, Padan E (2007) Monomers of the NhaA Na⁺/H⁺ antiporter of *Escherichia coli* are fully functional yet dimers are beneficial under extreme stress conditions at alkaline pH in the presence of Na⁺ or Li⁺. *Journal of Biological Chemistry* 282: 26810-26821.
54. Herz K, Rimon A, Jeschke G, Padan E (2009) Beta-sheet-dependent dimerization is essential for the stability of NhaA Na⁺/H⁺ antiporter. *Journal of Biological Chemistry* 284: 6337-6347.
55. Karasawa A, Mitsui K, Matsushita M, Kanazawa H (2010) Intermolecular cross-linking of monomers in *Helicobacter pylori* Na⁺/H⁺ antiporter NhaA at the dimer interface inhibits antiporter activity. *Biochemical Journal* 426: 99-108.
56. Rosgen J, Pettitt BM, Bolen DW (2005) Protein folding, stability, and solvation structure in osmolyte solutions. *Biophysical Journal* 89: 2988-2997.
57. Arakawa T, Timasheff SN (1985) The Stabilization of Proteins by Osmolytes. *Biophysical Journal* 47: 411-414.
58. Ressler S, van Scheltinga ACT, Vorrhein C, Ott V, Ziegler C (2009) Molecular basis of transport and regulation in the Na⁺/betaine symporter BetP. *Nature* 458: 47-U41.
59. Tsai CJ, Khafizov K, Hakulinen J, Forrest LR, Kramer R, Kuhlbrandt W, Ziegler C (2011) Structural asymmetry in a trimeric Na⁺/betaine symporter, BetP, from *Corynebacterium glutamicum*. *Journal of Molecular Biology* 407: 368-381.
60. Perez C, Koshy C, Yildiz O, Ziegler C (2012) Alternating-access mechanism in conformationally asymmetric trimers of the betaine transporter BetP. *Nature* 490: 126-130.
61. Murakami S, Nakashima R, Yamashita E, Matsumoto T, Yamaguchi A (2006) Crystal structures of a multidrug transporter reveal a functionally rotating mechanism. *Nature* 443: 173-179.
62. Perez C, Khafizov K, Forrest LR, Kramer R, Ziegler C (2011) The role of trimerization in the osmoregulated betaine transporter BetP. *EMBO Reports* 12: 804-810.

63. Borgnia M, Nielsen S, Engel A, Agre P (1999) Cellular and molecular biology of the aquaporin water channels. *Annual Review of Biochemistry* 68: 425-458.
64. Fu DX, Libson A, Miercke LJW, Weitzman C, Nollert P, Krucinski J, Stroud RM (2000) Structure of a glycerol-conducting channel and the basis for its selectivity. *Science* 290: 481-486.
65. Cymer F, Schneider D (2010) A Single Glutamate Residue Controls the Oligomerization, Function, and Stability of the Aquaglyceroporin GlpF. *Biochemistry* 49: 279-286.
66. Veerappan A, Cymer F, Klein N, Schneider D (2011) The Tetrameric alpha-Helical Membrane Protein GlpF Unfolds via a Dimeric Folding Intermediate. *Biochemistry* 50: 10223-10230.
67. Yellen G (2002) The voltage-gated potassium channels and their relatives. *Nature* 419: 35-42.
68. Doyle DA, Cabral JM, Pfuetzner RA, Kuo AL, Gulbis JM, Cohen SL, Chait BT, MacKinnon R (1998) The structure of the potassium channel: Molecular basis of K⁺ conduction and selectivity. *Science* 280: 69-77.
69. Cortes DM, Cuello LG, Perozo E (2001) Molecular architecture of full-length KcsA - Role of cytoplasmic domains in ion permeation and activation gating. *Journal of General Physiology* 117: 165-180.
70. Krishnan MN, Bingham JP, Lee SH, Trombley P, Moczydlowski E (2005) Functional role and affinity of inorganic cations in stabilizing the tetrameric structure of the KcsA K⁺ channel. *Journal of General Physiology* 126: 271-283.
71. Splitt H, Meuser D, Borovok I, Betzler M, Schrempf H (2000) Pore mutations affecting tetrameric assembly and functioning of the potassium channel KcsA from *Streptomyces lividans*. *FEBS Letters* 472: 83-87.
72. van Dalen A, Schrempf H, Killian JA, de Kruijff B (2000) Efficient membrane assembly of the KcsA potassium channel in *Escherichia coli* requires the protonmotive force. *EMBO Reports* 1: 340-346.
73. Molina ML, Encinar JA, Barrera FN, Fernandez-Ballester G, Riquelme G, Gonzalez-Ros JM (2004) Influence of C-terminal protein domains and protein-lipid interactions on tetramerization and stability of the potassium channel KcsA. *Biochemistry* 43: 14924-14931.
74. Van Dort HM, Knowles DW, Chasis JA, Lee G, Mohandas N, Low PS (2001) Analysis of integral membrane protein contributions to the deformability and stability of the human erythrocyte membrane. *The Journal of biological chemistry* 276: 46968-46974.
75. Marianayagam NJ, Sunde M, Matthews JM (2004) The power of two: protein dimerization in biology. *Trends in Biochemical Sciences* 29: 618-625.
76. Hashimoto K, Madej T, Bryant SH, Panchenko AR (2010) Functional States of Homooligomers: Insights from the Evolution of Glycosyltransferases. *Journal of Molecular Biology* 399: 196-206.
77. Hashimoto K, Nishi H, Bryant S, Panchenko AR (2011) Caught in self-interaction: evolutionary and functional mechanisms of protein homooligomerization. *Physical Biology* 8: 035007.

78. Paulsen IT (2003) Multidrug efflux pumps and resistance: regulation and evolution. *Current Opinion in Microbiology* 6: 446-451.
79. Poole K (2005) Efflux-mediated antimicrobial resistance. *Journal of Antimicrobial Chemotherapy* 56: 20-51.
80. Hirakata Y, Srikumar R, Poole K, Gotoh N, Suematsu T, Kohno S, Kamihira S, Hancock RE, Speert DP (2002) Multidrug efflux systems play an important role in the invasiveness of *Pseudomonas aeruginosa*. *Journal of Experimental Medicine* 196: 109-118.
81. Yang S, Lopez CR, Zechiedrich EL (2006) Quorum sensing and multidrug transporters in *Escherichia coli*. *Proceedings of the National Academy of Sciences of the United States of America* 103: 2386-2391.
82. Su CC, Long F, Zimmermann MT, Rajashankar KR, Jernigan RL, Yu EW (2011) Crystal structure of the CusBA heavy-metal efflux complex of *Escherichia coli*. *Nature* 470: 558-U153.
83. Rouch DA, Cram DS, DiBerardino D, Littlejohn TG, Skurray RA (1990) Efflux-mediated antiseptic resistance gene *qacA* from *Staphylococcus aureus*: common ancestry with tetracycline- and sugar-transport proteins. *Molecular Microbiology* 4: 2051-2062.
84. Nikaido H (2009) Multidrug resistance in bacteria. *Annual Review of Biochemistry* 78: 119-146.
85. Yin Y, He X, Szewczyk P, Nguyen T, Chang G (2006) Structure of the multidrug transporter EmrD from *Escherichia coli*. *Science* 312: 741-744.
86. Bay DC, Rommens KL, Turner RJ (2008) Small multidrug resistance proteins: A multidrug transporter family that continues to grow. *Biochimica Et Biophysica Acta-Biomembranes* 1778: 1814-1838.
87. Tal N, Schuldiner S (2009) A coordinated network of transporters with overlapping specificities provides a robust survival strategy. *Proceedings of the National Academy of Sciences of the United States of America* 106: 9051-9056.
88. Chen YJ, Pornillos O, Lieu S, Ma C, Chen AP, Chang G (2007) X-ray structure of EmrE supports dual topology model. *Proceedings of the National Academy of Sciences of the United States of America* 104: 18999-19004.
89. Morrison EA, DeKoster GT, Dutta S, Vafabakhsh R, Clarkson MW, Bahl A, Kern D, Ha T, Henzler-Wildman KA (2012) Antiparallel EmrE exports drugs by exchanging between asymmetric structures. *Nature* 481: 45-U50.
90. Lloris-Garcera P, Bianchi F, Slusky JSG, Seppala S, Daley DO, von Heijne G (2012) Antiparallel Dimers of the Small Multidrug Resistance Protein EmrE Are More Stable Than Parallel Dimers. *Journal of Biological Chemistry* 287: 26052-26059.
91. Kuroda T, Tsuchiya T (2009) Multidrug efflux transporters in the MATE family. *Biochimica Et Biophysica Acta-Proteins and Proteomics* 1794: 763-768.
92. He XA, Szewczyk P, Karyakin A, Evin M, Hong WX, Zhang QH, Chang G (2010) Structure of a cation-bound multidrug and toxic compound extrusion transporter. *Nature* 467: 991-U139.
93. Linton KJ, Higgins CF (1998) The *Escherichia coli* ATP-binding cassette (ABC) proteins. *Molecular Microbiology* 28: 5-13.

94. Aller SG, Yu J, Ward A, Weng Y, Chittaboina S, Zhuo R, Harrell PM, Trinh YT, Zhang Q, Urbatsch IL, Chang G (2009) Structure of P-glycoprotein reveals a molecular basis for poly-specific drug binding. *Science* 323: 1718-1722.
95. Konings WN, Poelarends GJ (2002) Bacterial multidrug resistance mediated by a homologue of the human multidrug transporter P-glycoprotein. *IUBMB life* 53: 213-218.
96. Putman M, Van Veen HW, Degener JE, Konings WN (2000) Antibiotic resistance: era of the multidrug pump. *Molecular Microbiology* 36: 772-773.
97. Dawson RJ, Locher KP (2006) Structure of a bacterial multidrug ABC transporter. *Nature* 443: 180-185.
98. Modali SD, Zgurskaya HI (2011) The periplasmic membrane proximal domain of MacA acts as a switch in stimulation of ATP hydrolysis by MacB transporter. *Molecular Microbiology* 81: 937-951.
99. Lu S, Zgurskaya HI (2012) Role of ATP binding and hydrolysis in assembly of MacAB-TolC macrolide transporter. *Molecular Microbiology*.
100. Nakamura H (1965) Gene-Controlled Resistance to Acriflavine and Other Basic Dyes in *Escherichia coli*. *Journal of bacteriology* 90: 8-14.
101. Nakamura H (1968) Genetic determination of resistance to acriflavine, phenethyl alcohol, and sodium dodecyl sulfate in *Escherichia coli*. *Journal of bacteriology* 96: 987-996.
102. Ma D, Cook DN, Alberti M, Pon NG, Nikaido H, Hearst JE (1993) Molecular cloning and characterization of *acrA* and *acrE* genes of *Escherichia coli*. *Journal of Bacteriology* 175: 6299-6313.
103. Ma D, Cook DN, Alberti M, Pon NG, Nikaido H, Hearst JE (1995) Genes *acrA* and *acrB* encode a stress-induced efflux system of *Escherichia coli*. *Molecular Microbiology* 16: 45-55.
104. Fralick JA (1996) Evidence that TolC is required for functioning of the Mar/AcrAB efflux pump of *Escherichia coli*. *Journal of Bacteriology* 178: 5803-5805.
105. Ma D, Alberti M, Lynch C, Nikaido H, Hearst JE (1996) The local repressor AcrR plays a modulating role in the regulation of *acrAB* genes of *Escherichia coli* by global stress signals. *Molecular Microbiology* 19: 101-112.
106. White DG, Goldman JD, Demple B, Levy SB (1997) Role of the *acrAB* locus in organic solvent tolerance mediated by expression of *marA*, *soxS*, or *robA* in *Escherichia coli*. *Journal of Bacteriology* 179: 6122-6126.
107. Murakami S, Nakashima R, Yamashita E, Yamaguchi A (2002) Crystal structure of bacterial multidrug efflux transporter AcrB. *Nature* 419: 587-593.
108. Yu EW, McDermott G, Zgurskaya HI, Nikaido H, Koshland DE (2003) Structural basis of multiple drug-binding capacity of the AcrB multidrug efflux pump. *Science* 300: 976-980.
109. Seeger MA, Schiefner A, Eicher T, Verrey F, Diederichs K, Pos KM (2006) Structural asymmetry of AcrB trimer suggests a peristaltic pump mechanism. *Science* 313: 1295-1298.

110. Sennhauser G, Amstutz P, Briand C, Storchenegger O, Grutter MG (2007) Drug export pathway of multidrug exporter AcrB revealed by DARPin inhibitors. *Plos Biology* 5: 106-113.
111. Takatsuka Y, Nikaido H (2007) Site-directed disulfide cross-linking shows that cleft flexibility in the periplasmic domain is needed for the multidrug efflux pump AcrB of *Escherichia coli*. *Journal of Bacteriology* 189: 8677-8684.
112. Seeger MA, von Ballmoos C, Eicher T, Brandstatter L, Verrey F, Diederichs K, Pos KM (2008) Engineered disulfide bonds support the functional rotation mechanism of multidrug efflux pump AcrB. *Nature Structural & Molecular Biology* 15: 199-205.
113. Schulz R, Vargiu AV, Collu F, Kleinekathofer U, Ruggerone P (2010) Functional Rotation of the Transporter AcrB: Insights into Drug Extrusion from Simulations. *Plos Computational Biology* 6.
114. Yao XQ, Kenzaki H, Murakami S, Takada S (2010) Drug export and allosteric coupling in a multidrug transporter revealed by molecular simulations. *Nature Communications* 1.
115. Wang BB, Weng JW, Fan KNA, Wang WN (2011) Elastic network model-based normal mode analysis reveals the conformational couplings in the tripartite AcrAB-TolC multidrug efflux complex. *Proteins-Structure Function and Bioinformatics* 79: 2936-2945.
116. Goldberg M, Pribyl T, Juhnke S, Nies DH (1999) Energetics and topology of CzcA, a cation/proton antiporter of the resistance-nodulation-cell division protein family. *Journal of Biological Chemistry* 274: 26065-26070.
117. Guan L, Nakae T (2001) Identification of essential charged residues in transmembrane segments of the multidrug transporter MexB of *Pseudomonas aeruginosa*. *Journal of bacteriology* 183: 1734-1739.
118. Takatsuka Y, Nikaido H (2006) Threonine-978 in the transmembrane segment of the multidrug efflux pump AcrB of *Escherichia coli* is crucial for drug transport as a probable component of the proton relay network. *Journal of Bacteriology* 188: 7284-7289.
119. Seeger MA, von Ballmoos C, Verrey F, Pos KM (2009) Crucial Role of Asp408 in the Proton Translocation Pathway of Multidrug Transporter AcrB: Evidence from Site-Directed Mutagenesis and Carbodiimide Labeling. *Biochemistry* 48: 5801-5812.
120. Takatsuka Y, Nikaido H (2009) Covalently Linked Trimer of the AcrB Multidrug Efflux Pump Provides Support for the Functional Rotating Mechanism. *Journal of Bacteriology* 191: 1729-1737.
121. Murakami S, Tamura N, Saito A, Hirata T, Yamaguchi A (2004) Extramembrane central pore of multidrug exporter AcrB in *Escherichia coli* plays an important role in drug transport. *Journal of Biological Chemistry* 279: 3743-3748.
122. Yu EW, Aires JR, McDermott G, Nikaido H (2005) A periplasmic drug-binding site of the AcrB multidrug efflux pump: a crystallographic and site-directed mutagenesis study. *Journal of bacteriology* 187: 6804-6815.

123. Bohnert JA, Schuster S, Seeger MA, Fahrnich E, Pos KM, Kern WV (2008) Site-Directed Mutagenesis Reveals Putative Substrate Binding Residues in the Escherichia coli RND Efflux Pump AcrB. *Journal of bacteriology* 190: 8225-8229.
124. Vargiu AV, Collu F, Schulz R, Pos KM, Zacharias M, Kleinekathofer U, Ruggerone P (2011) Effect of the F610A Mutation on Substrate Extrusion in the AcrB Transporter: Explanation and Rationale by Molecular Dynamics Simulations. *Journal of the American Chemical Society* 133: 10704-10707.
125. Takatsuka Y, Chen C, Nikaido H (2010) Mechanism of recognition of compounds of diverse structures by the multidrug efflux pump AcrB of Escherichia coli. *Proceedings of the National Academy of Sciences of the United States of America* 107: 6559-6565.
126. Husain F, Nikaido H (2010) Substrate path in the AcrB multidrug efflux pump of Escherichia coli. *Molecular Microbiology* 78: 320-330.
127. Husain F, Bikhchandani M, Nikaido H (2011) Vestibules Are Part of the Substrate Path in the Multidrug Efflux Transporter AcrB of Escherichia coli. *Journal of Bacteriology* 193: 5847-5849.
128. Ohene-Agyei T, Lea JD, Venter H (2012) Mutations in MexB that affect the efflux of antibiotics with cytoplasmic targets. *FEMS Microbiology Letters* 333: 20-27.
129. Aires JR, Nikaido H (2005) Aminoglycosides are captured from both periplasm and cytoplasm by the AcrD multidrug efflux transporter of Escherichia coli. *Journal of Bacteriology* 187: 1923-1929.
130. Nakashima R, Sakurai K, Yamasaki S, Nishino K, Yamaguchi A (2011) Structures of the multidrug exporter AcrB reveal a proximal multisite drug-binding pocket. *Nature* 480: 565-U199.
131. Eicher T, Cha HJ, Seeger MA, Brandstatter L, El-Delik J, Bohnert JA, Kern WV, Verrey F, Grutter MG, Diederichs K, Pos KM (2012) Transport of drugs by the multidrug transporter AcrB involves an access and a deep binding pocket that are separated by a switch-loop. *Proceedings of the National Academy of Sciences of the United States of America* 109: 5687-5692.
132. Su CC, Yu EW (2007) Ligand-transporter interaction in the AcrB multidrug efflux pump determined by fluorescence polarization assay (vol 581, pg 4972, 2007). *FEBS Letters* 581: 5548-5548.
133. Nagano K, Nikaido H (2009) Kinetic behavior of the major multidrug efflux pump AcrB of Escherichia coli. *Proceedings of the National Academy of Sciences of the United States of America* 106: 5854-5858.
134. Lim SP, Nikaido H (2010) Kinetic Parameters of Efflux of Penicillins by the Multidrug Efflux Transporter AcrAB-TolC of Escherichia coli. *Antimicrobial Agents and Chemotherapy* 54: 1800-1806.
135. V K, Sharff A, Koronakis E, Luisi B, Hughes C (2000) Crystal structure of the bacterial membrane protein TolC central to multidrug efflux and protein export. *Nature* 405: 914-919.
136. Touze T, Eswaran J, Bokma E, Koronakis E, Hughes C, Koronakis V (2004) Interactions underlying assembly of the Escherichia coli AcrAB-TolC multidrug efflux system. *Molecular Microbiology* 53: 697-706.

137. Tamura N, Murakami S, Oyama Y, Ishiguro M, Yamaguchi A (2005) Direct interaction of multidrug efflux transporter AcrB and outer membrane channel TolC detected via site-directed disulfide cross-linking. *Biochemistry* 44: 11115-11121.
138. Tikhonova EB, Yamada Y, Zgurskaya HI (2011) Sequential mechanism of assembly of multidrug efflux pump AcrAB-TolC. *Chemistry & Biology* 18: 454-463.
139. Zgurskaya HI, Nikaido H (2000) Cross-linked complex between oligomeric periplasmic lipoprotein AcrA and the inner-membrane-associated multidrug efflux pump AcrB from *Escherichia coli*. *Journal of Bacteriology* 182: 4264-4267.
140. Kawabe T, Fujihira E, Yamaguchi A (2000) Molecular construction of a multidrug exporter system, AcrAB: Molecular interaction between AcrA and AcrB, and cleavage of the N-terminal signal sequence of AcrA. *Journal of Biochemistry* 128: 195-200.
141. Elkins CA, Nikaido H (2003) Chimeric analysis of AcrA function reveals the importance of its c-terminal domain in its interaction with the AcrB multidrug efflux pump. *Journal of bacteriology* 185: 5349-5356.
142. Ge Q, Yamada Y, Zgurskaya H (2009) The C-Terminal Domain of AcrA Is Essential for the Assembly and Function of the Multidrug Efflux Pump AcrAB-TolC. *Journal of Bacteriology* 191: 4365-4371.
143. Mikolosko J, Bobyk K, Zgurskaya HI, Ghosh P (2006) Conformational flexibility in the multidrug efflux system protein AcrA. *Structure* 14: 577-587.
144. Symmons MF, Bokma E, Koronakis E, Hughes C, Koronakis V (2009) The assembled structure of a complete tripartite bacterial multidrug efflux pump. *Proceedings of the National Academy of Sciences of the United States of America* 106: 7173-7178.
145. Husain F, Humbard M, Misra R (2004) Interaction between the TolC and AcrA proteins of a multidrug efflux system of *Escherichia coli*. *Journal of Bacteriology* 186: 8533-8536.
146. Lobedanz S, Bokma E, Symmons MF, Koronakis E, Hughes C, Koronakis V (2007) A periplasmic coiled-coil interface underlying TolC recruitment and the assembly of bacterial drug efflux pumps. *Proceedings of the National Academy of Sciences of the United States of America* 104: 4612-4617.
147. Kim HM, Xu YB, Lee M, Piao SF, Sim SH, Ha NC, Lee K (2010) Functional Relationships between the AcrA Hairpin Tip Region and the TolC Aperture Tip Region for the Formation of the Bacterial Tripartite Efflux Pump AcrAB-TolC. *Journal of Bacteriology* 192: 4498-4503.
148. Xu Y, Lee M, Moeller A, Song S, Yoon BY, Kim HM, Jun SY, Lee K, Ha NC (2011) Funnel-like Hexameric Assembly of the Periplasmic Adapter Protein in the Tripartite Multidrug Efflux Pump in Gram-negative Bacteria. *Journal of Biological Chemistry* 286: 17910-17920.
149. Tikhonova EB, Zgurskaya HI (2004) AcrA, AcrB, and TolC of *Escherichia coli* form a stable intermembrane multidrug efflux complex. *Journal of Biological Chemistry* 279: 32116-32124.

150. Stroebel D, Sendra V, Cannella D, Helbig K, Nies DH, Coves J (2007) Oligomeric behavior of the RND transporters CusA and AcrB in micellar solution of detergent. *Biochimica Et Biophysica Acta-Biomembranes* 1768: 1567-1573.
151. Lu W, Zhong M, Wei Y (2011) Folding of AcrB Subunit Precedes Trimerization. *Journal of Molecular Biology* 411: 264-274.
152. Lu W, Zhong M, Wei YN (2011) A Reporter Platform for the Monitoring of In Vivo Conformational Changes in AcrB. *Protein and Peptide Letters* 18: 863-871.
153. Klein DC, Pavlicek J, Coon SL, Ganguly S, Weller JL, Hassan SA, Sackett DL (2008) Evidence that proline focuses movement of the floppy loop of arylalkylamine N-acetyltransferase (EC 2.3.1.87). *Journal of Biological Chemistry* 283: 14552-14558.
154. Kay BK, Williamson MP, Sudol P (2000) The importance of being proline: the interaction of proline-rich motifs in signaling proteins with their cognate domains. *FASEB Journal* 14: 231-241.
155. Wallace BA, Charalambous K, O'Reilly AO, Bullough PA (2009) Thermal and chemical unfolding and refolding of a eukaryotic sodium channel. *Biochimica Et Biophysica Acta-Biomembranes* 1788: 1279-1286.
156. Michelle A. O'Malley ANN, Tzventana Lazarova, and Anne S. Robinson (2011) Analysis of Adenosine A2a Receptor Stability: Effects of Ligands and Disulfide Bonds. *Biochemistry* 49: 9181-9189.
157. Bantscheff M, Weiss V, Glocker MO (1999) Identification of linker regions and domain borders of the transcription activator protein NtrC from *Escherichia coli* by limited proteolysis, in-gel digestion, and mass spectrometry. *Biochemistry* 38: 11012-11020.
158. Nouwen N, Stahlberg H, Pugsley AP, Engel A (2000) Domain structure of secretin PulD revealed by limited proteolysis and electron microscopy. *EMBO Journal* 19: 2229-2236.
159. Bakos E, Hegedus T, Hollo Z, Welker E, Tusnady GE, Zaman GJ, Flens MJ, Varadi A, Sarkadi B (1996) Membrane topology and glycosylation of the human multidrug resistance-associated protein. *Journal of Biological Chemistry* 271: 12322-12326.
160. Wei Lu MZ, Yinan Wei (2011) Folding of AcrB Subunit precedes trimerization. *Journal of Molecular Biology*.
161. Lu W, Zhong M, Wei Y (2011) A Reporter Platform for the Monitoring of In vivo Conformational Changes in AcrB. *Protein and peptide letters*.
162. Wittig I, Braun HP, Schagger H (2006) Blue native PAGE. *Nature Protocols* 1: 418-428.
163. Heuberger EH, Veenhoff LM, Duurkens RH, Friesen RH, Poolman B (2002) Oligomeric state of membrane transport proteins analyzed with blue native electrophoresis and analytical ultracentrifugation. *Journal of Molecular Biology* 317: 591-600.
164. Nikaido H, Takatsuka Y (2006) Threonine-978 in the transmembrane segment of the multidrug efflux pump AcrB of *Escherichia coli* is crucial for drug transport as a probable component of the proton relay network. *Journal of Bacteriology* 188: 7284-7289.

165. Pos KM, Seeger MA, von Ballmoos C, Verrey F (2009) Crucial Role of Asp408 in the Proton Translocation Pathway of Multidrug Transporter AcrB: Evidence from Site-Directed Mutagenesis and Carbodiimide Labeling. *Biochemistry* 48: 5801-5812.
166. Nikaido H, Husain F (2010) Substrate path in the AcrB multidrug efflux pump of *Escherichia coli*. *Molecular Microbiology* 78: 320-330.
167. Middlemiss JK, Poole K (2004) Differential impact of MexB mutations on substrate selectivity of the MexAB-OprM multidrug efflux pump of *Pseudomonas aeruginosa*. *Journal of Bacteriology* 186: 1258-1269.
168. Klingenberg M (1981) Membrane protein oligomeric structure and transport function. *Nature* 290: 449-454.
169. Raja M (2011) The potassium channel KcsA: A model protein in studying membrane protein oligomerization and stability of oligomeric assembly? *Archives of Biochemistry and Biophysics* 510: 1-10.
170. Morrison KL, Weiss GA (2001) Combinatorial alanine-scanning. *Current Opinion in Chemical Biology* 5: 302-307.
171. Weiss GA, Watanabe CK, Zhong A, Goddard A, Sidhu SS (2000) Rapid mapping of protein functional epitopes by combinatorial alanine scanning. *Proceedings of the National Academy of Sciences of the United States of America* 97: 8950-8954.
172. Sennhauser G, Bukowska MA, Briand C, Grutter MG (2009) Crystal structure of the multidrug exporter MexB from *Pseudomonas aeruginosa*. *Journal of Molecular Biology* 389: 134-145.
173. Yu L, Lu W, Wei Y (2011) AcrB trimer stability and efflux activity, insight from mutagenesis studies. *Plos One* 6: e28390.
174. Krissinel E, Henrick K (2007) Inference of macromolecular assemblies from crystalline state. *Journal of Molecular Biology* 372: 774-797.
175. Lo Conte L, Chothia C, Janin J (1999) The atomic structure of protein-protein recognition sites. *Journal of Molecular Biology* 285: 2177-2198.
176. Nooren IM, Thornton JM (2003) Structural characterisation and functional significance of transient protein-protein interactions. *Journal of Molecular Biology* 325: 991-1018.
177. Li XZ, Poole K, Nikaido H (2003) Contributions of MexAB-OprM and an EmrE homolog to intrinsic resistance of *Pseudomonas aeruginosa* to aminoglycosides and dyes. *Antimicrobial agents and chemotherapy* 47: 27-33.
178. Husain F, Nikaido H (2010) Substrate path in the AcrB multidrug efflux pump of *Escherichia coli*. *Molecular Microbiology* 78: 320-330.
179. Borders CL, Broadwater JA, Bekeny PA, Salmon JE, Lee AS, Eldridge AM, Pett VB (1994) A Structural Role for Arginine in Proteins - Multiple Hydrogen-Bonds to Backbone Carbonyl Oxygens. *Protein Science* 3: 541-548.
180. Chan VWF, Bjerrum MJ, Borders CL (1990) Evidence That Chemical Modification of a Positively Charged Residue at Position-189 Causes the Loss of Catalytic Activity of Iron-Containing and Manganese-Containing Superoxide Dismutases. *Archives of Biochemistry and Biophysics* 279: 195-201.
181. Winn PJ, Ludemann SK, Gauges R, Lounnas V, Wade RC (2002) Comparison of the dynamics of substrate access channels in three cytochrome P450s reveals

- different opening mechanisms and a novel functional role for a buried arginine. *Proceedings of the National Academy of Sciences of the United States of America* 99: 5361-5366.
182. Wilkinson SP, Grove A (2006) Ligand-responsive transcriptional regulation by members of the MarR family of winged helix proteins. *Current Issues in Molecular Biology* 8: 51-62.
 183. George AM, Levy SB (1983) Amplifiable resistance to tetracycline, chloramphenicol, and other antibiotics in *Escherichia coli*: involvement of a non-plasmid-determined efflux of tetracycline. *Journal of Bacteriology* 155: 531-540.
 184. George AM, Levy SB (1983) Gene in the major cotransduction gap of the *Escherichia coli* K-12 linkage map required for the expression of chromosomal resistance to tetracycline and other antibiotics. *Journal of Bacteriology* 155: 541-548.
 185. Perez-Rueda E, Collado-Vides J (2001) Common history at the origin of the position-function correlation in transcriptional regulators in Archaea and Bacteria. *Journal of Molecular Evolution* 53: 172-179.
 186. Perez-Rueda E, Collado-Vides J, Segovia L (2004) Phylogenetic distribution of DNA-binding transcription factors in bacteria and archaea. *Computational Biology and Chemistry* 28: 341-350.
 187. Lim D, Poole K, Strynadka NC (2002) Crystal structure of the MexR repressor of the mexRAB-oprM multidrug efflux operon of *Pseudomonas aeruginosa*. *Journal of Biological Chemistry* 277: 29253-29259.
 188. Wu RY, Zhang RG, Zagnitko O, Dementieva I, Maltzev N, Watson JD, Laskowski R, Gornicki P, Joachimiak A (2003) Crystal structure of *Enterococcus faecalis* SlyA-like transcriptional factor. *Journal of Biological Chemistry* 278: 20240-20244.
 189. Saridakis V, Shahinas D, Xu X, Christendat D (2008) Structural insight on the mechanism of regulation of the MarR family of proteins: high-resolution crystal structure of a transcriptional repressor from *Methanobacterium thermoautotrophicum*. *Journal of Molecular Biology* 377: 655-667.
 190. Hong M, Fuangthong M, Helmann JD, Brennan RG (2005) Structure of an OhrR-ohrA operator complex reveals the DNA binding mechanism of the MarR family. *Molecular Cell* 20: 131-141.
 191. Alekshun MN, Levy SB, Mealy TR, Seaton BA, Head JF (2001) The crystal structure of MarR, a regulator of multiple antibiotic resistance, at 2.3 Å resolution. *Nature Structural Biology* 8: 710-714.
 192. Kumarevel T, Tanaka T, Nishio M, Gopinath SCB, Takio K, Shinkai A, Kumar PKR, Yokoyama S (2008) Crystal structure of the MarR family regulatory protein, ST 1710, from *Sulfolobus tokodaii* strain 7. *Journal of Structural Biology* 161: 9-17.
 193. Miyazono KI, Tsujimura M, Kawarabayasi Y, Tanokura M (2007) Crystal structure of an archaeal homologue of multidrug resistance repressor protein, EmrR, from hyperthermophilic archaea *Sulfolobus tokodaii* strain 7. *Proteins-Structure Function and Bioinformatics* 67: 1138-1146.

194. Hugli TE, Stein WH (1971) Involvement of a tyrosine residue in the activity of bovine pancreatic deoxyribonuclease A. *Journal of Biological Chemistry* 246: 7191-7200.
195. Riordan JF, Sokolovsky M, Vallee BL (1967) The functional tyrosyl residues of carboxypeptidase A. Nitration with tetranitromethane. *Biochemistry* 6: 3609-3617.
196. Riordan JF, Sokolovsky M, Vallee BL (1967) Environmentally sensitive tyrosyl residues. Nitration with tetranitromethane. *Biochemistry* 6: 358-361.
197. Kahn PC (1979) The interpretation of near-ultraviolet circular dichroism. *Methods in Enzymology* 61: 339-378.
198. Strickland EH, Mercola D (1976) Near-ultraviolet tyrosyl circular dichroism of pig insulin monomers, dimers, and hexamers. Dipole-dipole coupling calculations in the monopole approximation. *Biochemistry* 15: 3875-3884.
199. Kelly SM, Price NC (1997) The application of circular dichroism to studies of protein folding and unfolding. *Biochimica et biophysica acta* 1338: 161-185.
200. Noble MA, Munro AW, Rivers SL, Robledo L, Daff SN, Yellowlees LJ, Shimizu T, Sagami I, Guillemette JG, Chapman SK (1999) Potentiometric analysis of the flavin cofactors of neuronal nitric oxide synthase. *Biochemistry* 38: 16413-16418.
201. Andersson LA, Peterson JA (1995) Active-site analysis of ferric P450 enzymes: hydrogen-bonding effects on the circular dichroism spectra. *Biochemical and Biophysical Research Communications* 211: 389-395.
202. Cogdell RJ, Scheer H (1985) Circular-Dichroism of Light-Harvesting Complexes from Purple Photosynthetic Bacteria. *Photochemistry and Photobiology* 42: 669-678.
203. West SM, Price NC (1990) The Unfolding and Attempted Refolding of Mitochondrial Aspartate-Aminotransferase from Pig-Heart. *Biochemical Journal* 265: 45-50.
204. Alekshun MN, Levy SB (1999) Alteration of the repressor activity of MarR, the negative regulator of the *Escherichia coli* marRAB locus, by multiple chemicals in vitro. *Journal of Bacteriology* 181: 4669-4672.
205. Xiong A, Gottman A, Park C, Baetens M, Pandza S, Matin A (2000) The EmrR protein represses the *Escherichia coli* emrRAB multidrug resistance operon by directly binding to its promoter region. *Antimicrobial Agents and Chemotherapy* 44: 2905-2907.
206. Brooun A, Tomashek JJ, Lewis K (1999) Purification and ligand binding of EmrR, a regulator of a multidrug transporter. *Journal of Bacteriology* 181: 5131-5133.
207. Berezovski M, Krylov SN (2005) Thermochemistry of protein-DNA interaction studied with temperature-controlled nonequilibrium capillary electrophoresis of equilibrium mixtures. *Analytical chemistry* 77: 1526-1529.
208. Liu CC, Richard AJ, Datta K, LiCata VJ (2008) Prevalence of temperature-dependent heat capacity changes in protein-DNA interactions. *Biophysical Journal* 94: 3258-3265.
209. Peters WB, Edmondson SP, Shriver JW (2004) Thermodynamics of DNA binding and distortion by the hyperthermophile chromatin protein Sac7d. *Journal of Molecular Biology* 343: 339-360.

210. Oh SY, Shin JH, Roe JH (2007) Dual role of OhrR as a repressor and an activator in response to organic hydroperoxides in *Streptomyces coelicolor*. *Journal of Bacteriology* 189: 6284-6292.
211. Delalla F, Nicolini R, Rinaldi E, Scarpellini P, Rigoli R, Manfrin V, Tramarin A (1992) Prospective-Study of Oral Teicoplanin Versus Oral Vancomycin for Therapy of Pseudomembranous Colitis and Clostridium-Difficile-Associated Diarrhea. *Antimicrobial agents and chemotherapy* 36: 2192-2196.
212. Higgins DL, Chang R, Debatov DV, Leung J, Wu T, Krause KA, Sandvik E, Hubbard JM, Kaniga K, Schmidt DE, Gao QF, Cass RT, Karr DE, Benton BM, Humphrey PP (2005) Telavancin, a multifunctional lipoglycopeptide, disrupts both cell wall synthesis and cell membrane integrity in methicillin-resistant *Staphylococcus aureus*. *Antimicrobial agents and chemotherapy* 49: 1127-1134.
213. Perkins HR (1982) Vancomycin and Related Antibiotics. *Pharmacology & Therapeutics* 16: 181-197.
214. James CW, Gurk-Turner C (2001) Recommendations for monitoring serum vancomycin concentrations. *Proc (Bayl Univ Med Cent)* 14: 189-190.
215. Williams AH, Gruneberg RN (1984) TEICOPLANIN. *Journal of Antimicrobial Chemotherapy* 14: 441-445.
216. Svetitsky S, Leibovici L, Paul M (2009) Comparative Efficacy and Safety of Vancomycin versus Teicoplanin: Systematic Review and Meta-Analysis. *Antimicrobial Agents and Chemotherapy* 53: 4069-4079.
217. Wood MJ (1997) The comparative efficacy and safety of teicoplanin and vancomycin (vol 37, pg 209, 1996). *Journal of Antimicrobial Chemotherapy* 40: 147-147.
218. Cobo J, Fortun J (1996) The comparative efficacy and safety of teicoplanin and vancomycin. *Journal of Antimicrobial Chemotherapy* 38: 1113-1114.
219. Wood MJ (1996) The comparative efficacy and safety of teicoplanin and vancomycin (vol 37, pg 209, 1996). *Journal of Antimicrobial Chemotherapy* 38: 919-919.
220. Wood MJ (1996) The comparative efficacy and safety of teicoplanin and vancomycin. *Journal of Antimicrobial Chemotherapy* 37: 209-222.
221. Brink AJ, Richards GA, Cummins RR, Lambson J, Teicoplanin GU (2008) Recommendations to achieve rapid therapeutic teicoplanin plasma concentrations in adult hospitalised patients treated for sepsis. *International Journal of Antimicrobial Agents* 32: 455-458.
222. Pea F, Brollo L, Viale P, Pavan F, Furlanut M (2003) Teicoplanin therapeutic drug monitoring in critically ill patients: a retrospective study emphasizing the importance of a loading dose. *Journal of Antimicrobial Chemotherapy* 51: 971-975.
223. Mohammedi I, Descloux E, Argaud L, Le Scanff J, Robert D (2006) Loading dose of vancomycin in critically ill patients: 15 mg/kg is a better choice than 500 mg. *International Journal of Antimicrobial Agents* 27: 259-262.
224. Ackerman BH, Berg HG, Strate RG, Rotschafer JC (1983) Comparison of Radioimmunoassay and Fluorescent Polarization Immunoassay for Quantitative-

- Determination of Vancomycin Concentrations in Serum. *Journal of Clinical Microbiology* 18: 994-995.
225. Cox H, Whitby M, Nimmo G, Williams G (1993) Evaluation of a Novel Fluorescence Polarization Immunoassay for Teicoplanin. *Antimicrobial Agents and Chemotherapy* 37: 1924-1926.
 226. Filburn BH, Shull VH, Tempera YM, Dick JD (1983) Evaluation of an Automated Fluorescence Polarization Immunoassay for Vancomycin. *Antimicrobial Agents and Chemotherapy* 24: 216-220.
 227. Valle MJD, Lopez FG, Navarro AS (2008) Development and validation of an HPLC method for vancomycin and its application to a pharmacokinetic study. *Journal of Pharmaceutical and Biomedical Analysis* 48: 835-839.
 228. Jehl F, Gallion C, Thierry RC, Monteil H (1985) Determination of Vancomycin in Human-Serum by High-Pressure Liquid-Chromatography. *Antimicrobial Agents and Chemotherapy* 27: 503-507.
 229. Farin D, Piva GA, Gozlan I, Kitzes-Cohen R (1998) A modified HPLC method for the determination of vancomycin in plasma and tissues and comparison to FPIA (TDX). *Journal of Pharmaceutical and Biomedical Analysis* 18: 367-372.
 230. Pohlod DJ, Saravolatz LD, Somerville MM (1984) Comparison of Fluorescence Polarization Immunoassay and Bioassay of Vancomycin. *Journal of Clinical Microbiology* 20: 159-161.
 231. Walker CA, Kopp B (1978) Sensitive Bioassay for Vancomycin. *Antimicrobial Agents and Chemotherapy* 13: 30-33.
 232. Corti A, Rurali C, Borghi A, Cassani G (1985) Solid-Phase Enzyme-Receptor Assay (Spera) - a Competitive-Binding Assay for Glycopeptide Antibiotics of the Vancomycin Class. *Clinical Chemistry* 31: 1606-1610.
 233. Cavenaghi L, Corti A, Cassani G (1986) Comparison of the Solid-Phase Enzyme Receptor Assay (Spera) and the Microbiological Assay for Teicoplanin. *Journal of Hospital Infection* 7: 85-89.
 234. Jolley ME, Stroupe SD, Schwenzer KS, Wang CJ, Lusteffes M, Hill HD, Popelka SR, Holen JT, Kelso DM (1981) Fluorescence Polarization Immunoassay .3. An Automated-System for Therapeutic Drug Determination. *Clinical Chemistry* 27: 1575-1579.
 235. Adamczyk M, Grote J, Moore JA, Rege SD, Yu ZG (1999) Structure-binding relationships for the interaction between a vancomycin monoclonal antibody fab fragment and a library of vancomycin analogues and tracers. *Bioconjugate Chemistry* 10: 176-185.
 236. Jameson DM, Ross JA (2010) Fluorescence polarization/anisotropy in diagnostics and imaging. *Chemical Reviews* 110: 2685-2708.
 237. Burke TJ, Loniello KR, Beebe JA, Ervin KM (2003) Development and application of fluorescence polarization assays in drug discovery. *Combinatorial chemistry & high throughput screening* 6: 183-194.
 238. Yu LL, Fang J, Wei YN (2009) Characterization of the Ligand and DNA Binding Properties of a Putative Archaeal Regulator ST1710. *Biochemistry* 48: 2099-2108.

239. Nitnai Y, Kikuchi T, Kakoi K, Hanmaki S, Fujisawa I, Aoki K (2009) Crystal Structures of the Complexes between Vancomycin and Cell-Wall Precursor Analogs. *Journal of Molecular Biology* 385: 1422-1432.
240. Ye BC, Ikebukuro K, Karube I (1998) Quantitative analysis of polymerase chain reaction using anisotropy ratio and relative hydrodynamic volume of fluorescence polarization method. *Nucleic Acids Research* 26: 3614-3615.
241. Popieniek PH, Pratt RF (1987) A Fluorescent Ligand for Binding-Studies with Glycopeptide Antibiotics of the Vancomycin Class. *Analytical Biochemistry* 165: 108-113.
242. Azad M, Hernandez L, Plazas A, Rudolph M, Gomez FA (2003) Determination of binding constants between the antibiotic ristocetin A and D-Ala-D-Ala terminus peptides by affinity capillary electrophoresis. *Chromatographia* 57: 339-343.
243. Rao JH, Yan L, Xu B, Whitesides GM (1999) Using surface plasmon resonance to study the binding of vancomycin and its dimer to self-assembled monolayers presenting D-Ala-D-Ala. *Journal of the American Chemical Society* 121: 2629-2630.
244. van Wageningen AMA, Staroske T, Williams DH (1998) Binding of D-serine-terminating cell-wall analogues to glycopeptide antibiotics. *Chemical Communications*: 1171-1172.
245. Fung FH, Tang JC, Hopkins JP, Dutton JJ, Bailey LM, Davison AS (2012) Measurement of teicoplanin by liquid chromatography-tandem mass spectrometry: development of a novel method. *Annals of Clinical Biochemistry* 49: 475-481.

Vita

PERSONAL INFORMATION

Name **Linliang Yu**

Place of Birth **Shanghai, China**

Nationality **China**

EDUCATION

2004-07 M.S. Medicinal Chemistry Shanghai Institute of Pharmaceutical Industry, Shanghai, China

2000-04 B.S. Pharmaceutical Engineering East China University of Science and Technology, Shanghai, China

Awards and Honors

- ◇ 2009/07, 2011/06 RCTF fellowship, University of Kentucky, Lexington, KY, USA
- ◇ 2010/06, Kentucky Opportunity Fellowship, University of Kentucky, Lexington, KY, USA
- ◇ 2010/07, EPSCoR Travel Fellowship, Oak Ridge National Laboratory, Oak Ridge, TN, USA
- ◇ 2012/06, Presidential fellowship, University of Kentucky, Lexington, KY, USA

Publications

- ◇ Linliang Yu, Jun Fang, Yinan Wei, Characterization of the Ligand and DNA Binding Properties of a Putative Archaeal Regulator ST1710, *Biochemistry*, 2009, 48, 2099-2108.
- ◇ Jun Fang, Linliang Yu, Pei Gao, Yuguang Cai, Yinan Wei, Detection of Protein-DNA Interaction and Regulation Using Gold Nanoparticles, *Anal. Biochem*, 2009, 399, 262-267
- ◇ Linliang Yu, Meng Zhong, Yinan Wei, Direct Fluorescence Polarization Assay for the Detection of Glycopeptide Antibiotics, *Anal.Chem*, 2010, 82, 7044-7048
- ◇ Linliang Yu, Weicheng Zhou, Zhengyu Wang, Synthesis and in vitro Antibacterial Activity of Oxazolidine LBM-415 Analogs as Peptide Deformylase Inhibitors, *Bioorg. Med. Chem. Lett*, 2011, 21, 1541-1544
- ◇ Linliang Yu, Wei Lu, Yinan Wei, AcrB Trimer Stability and Efflux Activity-Insight from Mutagenesis Studies, *PloS One*, 2011, 6, e28390
- ◇ Nehru Neha, Donev Eugenii, Huda Gazi, Linliang Yu, Yinan Wei, Jeffery Todd Hasting, Differentiating Surface and Bulk Interactions using Localized Surface Plasmon Resonances of Gold Nanorods, *Opt Express*, 2012, 26: 6905-6914

- ✧ Wei Lu, Qian Chai, Meng Zhong, Linliang Yu, Jun Fang, Tong Wang, Huilin Li, Haining Zhu, Yanan Wei, Assembling of AcrB Trimer in Cell Membrane, *J. Mol. Biol.*, 2012, 423, 123-134
- ✧ Jun Fang, Linliang Yu, Maria Wu, Yanan Wei, Dissecting the Function of A Protruding Loop in AcrB Trimerization, *J Biomol Struct Dyn* (in publication).

Presentations

- ✧ Yu L., Lu W., and Wei Y. “Stability of AcrB Trimer and Function of AcrAB-Tolc Pump.” Gibbs Conference on Biological Thermodynamics, Carbondale, IL (2011 Sep. 17)
- ✧ Lu W., Chai Q., Yu L., and Wei Y. “Deciphering the role of the transmembrane domain in AcrB trimerization.” Gibbs Conference on Biological Thermodynamics, Carbondale, IL (2011 Sep. 17)
- ✧ Yu L., Lu W., and Wei Y. “The Stability and Functionality of Membrane Transporter”. The American Society for Biochemistry and Molecular Biology Annual Meeting, Washington DC. (2011 Apr. 9)
- ✧ Yu L., Lu W., Zhong M., and Wei Y. “Applying a Reporting Platform to the Study of the Membrane Protein Assembly and Function.” Gibbs Conference on Biological Thermodynamics, Carbondale, IL (2010 Oct. 16)
- ✧ Yu L., Zhong M., and Wei Y. “Detection of Vancomycin with Peptide Probe”. Kentucky Academy of Science Meeting, Highland Heights, KY (2009 November 14)
- ✧ Wei Y., Fang J., Yu L., Gao P., and Cai Y. “Protein-DNA Interaction Mediated Assembly of Gold Nanoparticles for Detection of Effectors”. Gibbs Conference on Biological Thermodynamics, Carbondale, IL (2009 October 3)
- ✧ Fang J., Yu L., Gao P., Cai Y., and Wei Y. “Protein-DNA Interaction Mediated Assembly of Gold Nanoparticles for the Detection of Small Molecule Ligand”. Naff Symposium, Lexington, KY (2009 April 24)
- ✧ Yu L., and Wei Y. “Aptamers with High Affinity for Multi-Drug Resistance (MDR) Regulators”. Naff Symposium, Lexington, KY (2009 April 24)
- ✧ Wei Y., and Yu L. “Aptamers with High Affinity for Multi-Drug Resistance (MDR) Regulators”. Gordon Research Conference, Galveston, TX (2009 March 22)
- ✧ Yu L., and Wei Y. “*In vitro* Selection of Glucose Binding Single-strand DNA”. Kentucky Academy of Science Meeting, Lexington, KY (2008 November 15)
- ✧ Wei Y., and Yu L. “Temperature Dependent DNA and Ligand Binding Study of a Putative Archaeal Regulator Protein ST1710”. Gordon Research Conference, Newport, RI (2008 June 8)